

NOTICE:

The copyright law of the United States (Title 17, United States Code) governs the making of reproductions of copyrighted material. One specified condition is that the reproduction is not to be "used for any purpose other than private study, scholarship, or research." If a user makes a request for, or later uses a reproduction for purposes in excess of "fair use," that user may be liable for copyright infringement.

RESTRICTIONS:

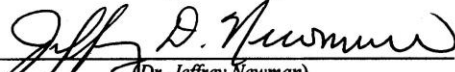
This student work may be read, quoted from, cited, for purposes of research. It may not be published in full except by permission of the author. Per request from author please do not reproduce this work in print.

**Purification and Molecular Structure Determination of Flexirubin Pigments
from *Chryseobacterium***

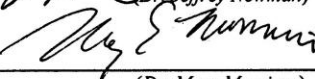
Presented to the faculty of Lycoming College in partial fulfillment
of the requirement for Departmental Honors in
Biology

By
Jordan E. Krebs
Lycoming College
23 April 2013

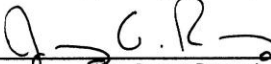
Approved by:



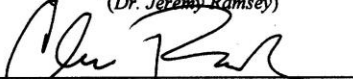
(Dr. Jeffrey Newman)



(Dr. Mary Morrison)



(Dr. Jeremy Ramsey)



(Professor Christopher Reed)

Table of Contents

Abstract	Pg. 3
Ch. 1: Introduction	4
Ch. 2: Method Development	26
Ch. 3: Purification and Structural Determination of <i>C. oranimense</i> peaks	55
Ch. 4: Variation of Flexirubin Pigments	62
Ch. 5: Investigated Flexirubin Characteristics	83
Appendix	89
References	94

Abstract

The taxonomy of bacteria belonging to the *Flavobacteriaceae*, *Cytophagaceae*, and *Chitinophagaceae* families of the *Bacteroidetes* phylum has been widely debated and modified in the past few decades. The presence of flexirubins, a modestly studied class of pigments, has been used to differentiate related genera of the *Bacteroidetes*. The purification and structural determination of forty-two flexirubins isolated from 5 bacterial species has already been accomplished. This project focuses on purifying flexirubins from multiple *Chryseobacterium* species and deducing their chemical structures. Initially, acetone extraction of pigments from *Chryseobacterium oranimense* was performed in methanol for separation of related flexirubin pigments utilizing high performance liquid chromatography (HPLC) at a preparative scale. After nine months of optimization, a longer column, a more extended solvent gradient, and the use of a low pH solvent system, baseline separation of the *C. oranimense* flexirubins was achieved. The collection of preparative fractions is currently underway so that structural analysis can be completed for the two major flexirubin peaks of *C. oranimense*. In addition, the variation of 25 flexirubin producing bacteria was investigated. Some species have unique flexirubin or flexirubin-like peaks while some have many more flexirubin peaks than others. The observed variation in the species chromatographs suggests substantial structural variation as expected. These unique structural variations will be studied in the future with the optimized method designed for this project.

Ch. 1: Introduction

Purpose

Traditional chemical and polyphasic methods of studying bacteria can lead to a somewhat ambiguous taxonomy of closely-related bacteria even with the aid of completed genome sequences. Novel techniques, such as demonstrating chemical structure differences in pigments, to differentiate species that are often shuffled between different genera may offer much needed taxonomic resolution. This study builds upon similar studies of a few species and the characteristics of this novel class of pigments. This type of study is especially beneficial to members of the family *Flavobacteriaceae* and related genera whose taxonomy has been described as a Gordian knot (Bernardet *et al.*, 1996). The target natural products are genus-specific biomarkers for many species within the *Flavobacteriaceae*. This class of pigments is a key biomarker to recognize many of the *Flavobacteriaceae* genera, yet little is known about them, including whether their presence is constitutive for a particular species or induced as a physiological response. The purpose of this study is to purify flexirubins from multiple *Chryseobacterium* species and then determine the molecular structures of purified fractions. No structures have yet to be published from flexirubins extracted from any *Chryseobacteria* and thus may have different variation than already published structures. Initially, an optimized HPLC method will be designed to purify at least the major peak from *C. oranimense*. Once a method has been optimized, flexirubin profiles will be collected for multiple species of the *Chryseobacterium*, *Flavobacterium*, and *Epilithonimonas* genera. In addition, a correlation between colony pigmentation color and flexirubin profile will be investigated. An optimized method to determine a flexirubin profile could be a useful novel technique to characterize

flexirubin-producing bacteria much like FAME, Biolog, and enzyme analysis of closely-related species (Tindall et al., 2010).

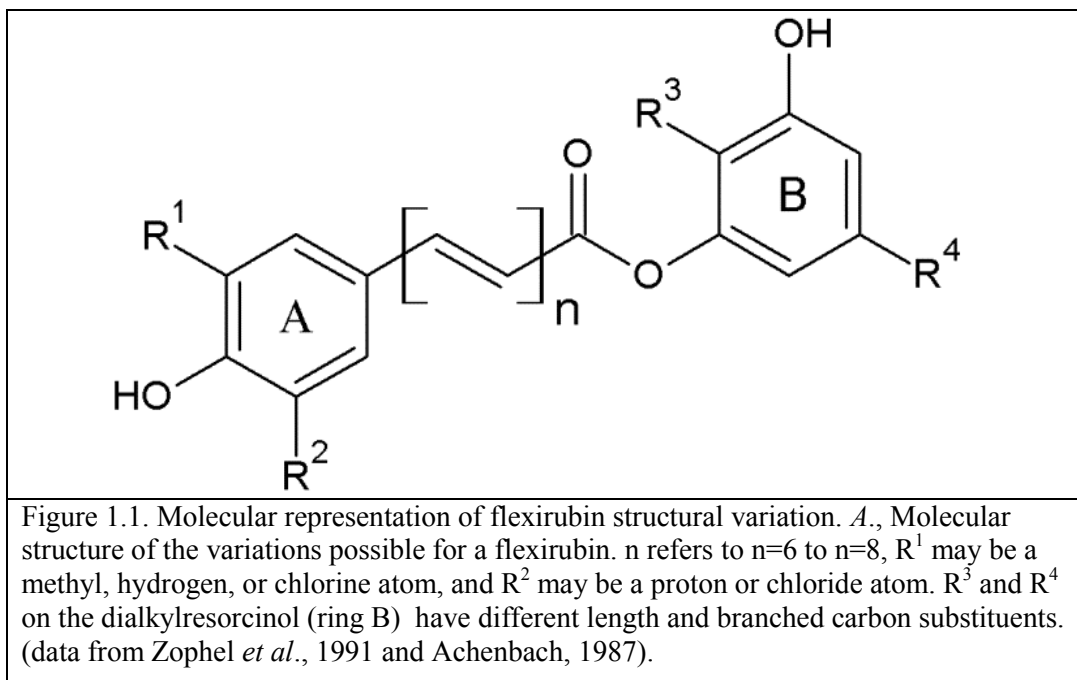
Flexirubins

Flexirubins are present in many, but not all genera of the *Bacteroidetes*. Of the many genera that produce flexirubins, the isolation and the chemical analysis of these pigments has only been completed for 5 species: *Chitinophaga filiformis* Fx e1, *Flavobacterium sp. C 1/2*, *Flavobacterium sp. Samoa*, *Flavobacterium johnsoniae* Cy j1, and an unrelated sulfur-reducing bacterium, *Sulfurospirillum delayianium* 5175. Forty two different flexirubin structures have been elucidated from these 5 species. These pigments have 5 possible structural variations. The number of polyenes may vary from 6 to 8, R¹ may be a methyl, hydrogen, or chlorine atom, and R² may be a proton or chloride atom. R³ and R⁴ on ring B are alkyl substituents of different lengths and branching (Table 1.1 and Figure 1.1). These variations may cluster according to the genus of origin. For example, *Chitinophaga* flexirubins lack a methyl substituent of ring A and also have more variety in alkyl substituents on ring B. Only the *Chintinophaga filiformis* Fx e1 flexirubin had a methyl group in ring A (Fautz and Reichenbach, 1979; Fautz and Reichenbach, 1980). At least one flexirubin with a R³ or R⁴ as a chloride seems to be present in each species.

Two pools of flexirubins are present in each species: the chlorinated-derivative pool and the pool

Table 1.1. Structural Variation of 42 published Flexirubins (data from Zophel et al., 1991 and Achenbach, 1987).

Species	R ¹	R ²	R ³	R ⁴	n	structures
<i>Flavobacterium johnsoniae</i> Cy j1	H or Cl	H	C ₁₀ H ₂₁ or (CH ₂) ₈ CH(CH ₃) ₂	C ₅ H ₁₁ or (CH ₂) ₃ CH(CH ₃) ₂	6, 7, or 8	25
<i>Flavobacterium sp. samoa</i>	H or Cl	H	C ₁₀ H ₂₁ or (CH ₂) ₈ CH(CH ₃) ₃	C ₅ H ₁₁ or (CH ₂) ₃ CH(CH ₃) ₃	8	8
<i>Flavobacterium sp. C1/2</i>	H or Cl	H	C ₁₂ H ₂₅	CH ₃ , C ₃ H ₇ , or CH ₂ CH(CH ₃) ₂	8	5
<i>Chitinophaga filiformis</i> Fx e1	CH ₃	H or Cl	C ₁₂ H ₂₅ or C ₁₃ H ₂₇	CH ₃	8	3
<i>Sulfurospirillum deleyium</i> 5175	CH ₃	H	(CH ₂) ₁₁ CH ₃	CH ₃	8	1



of non-chlorinated analogous structures. The chloride derivative seems to be less abundant. *F. elegans* Fx e1 had a pigment pool of approximately 95% flexirubin and 3% chloroflexirubin (Fautz, and Reichenbach, 1979). Cl as a substituent on Ring A is not an artifact of processing. Some chloride containing pigments were extracted from wet cells with acetone. The residue from the acetone extract was extracted with diethyl ether or dichloromethane. The liquid phase was filtered, evaporated, and stored at -20°C for further purification. The individual pigments were separated from each other using different solvents with an aluminum oxide chromatography column (Archenbach *et al.*, 1982). While a lot of flexirubin data has been compiled for a few species, many key biological aspects of these pigments remain unknown.

A few studies have tried to discover a function for these pigments. The last major flexirubin related study reiterated that the function remained unknown (Zophel *et al.*, 1991). Flexirubins do not seem to have a photoprotective function or involvement in the respiratory chain (Irschik and Reichenbach, 1978). Likewise, cultures grown in the dark contained a slightly greater amount of flexirubin than cultures under light; however, flexirubin biosynthesis was not

stimulated by illumination (Reichenbach *et al.*, 1974). In other possible way to study the function or functions of the pigments is by studying what genes are present in a group of flexirubin producing bacteria.

Flexirubins may aid in the ability to glide although this function may have been lost from related bacteria (Reichenbach *et al.*, 1980). Only a genetics-based study of the genes necessary for gliding motility, such as *Gld* and *spr*, may show a correlation to flexirubin synthesis (Lee *et al.*, 2011). Genes have been shown or predicted to be related to flexirubin biosynthesis and gliding motility. *darA* and *darB* genes encode enzymes involved in the synthesis of 2-hexyl-5-propyl-alkylresorcinol which may be an intermediate of flexirubin biosynthesis; many other genes shared among flexirubin-producing bacteria include lipid synthesis genes that may also be important for flexirubin synthesis. To note, Fjoh_1095 encodes a predicted ABC-2-type transporter component; it is suspected to have a role in flexirubin localization to the outer membrane (McBride *et al.* 2009).

The function of flexirubins is unknown but the characteristics of these pigments may be used to hypothesize possible functions. Flexirubins are non-isoprenoid ω -phenyl-substituted polyene carboxylic acids that are esterified via 2,5-dialkylated resorcinols (Achenbach and Kohl, 1978). Flexirubins are located in the outer membrane and carotenoids, if present, remain in the cytoplasmic membrane (Figure 1.2). Previously, cells were disintegrated to yield two fractions of membranes, heavy (H) and light (L) fractions by the application of lysozyme, EDTA, and the detergent Brij 58 (Irschik and Reichenbach, 1978). Brij 58 has been shown to construct a pool of membrane vesicles while maintaining the asymmetry of the membrane under study (Johansson *et al.*, 1995). The pooled H fraction had a ratio of carbohydrates to proteins that was 3 times higher than the L fraction, and contains 13 times more 2-keto-3-deoxyoctonic acid, a common

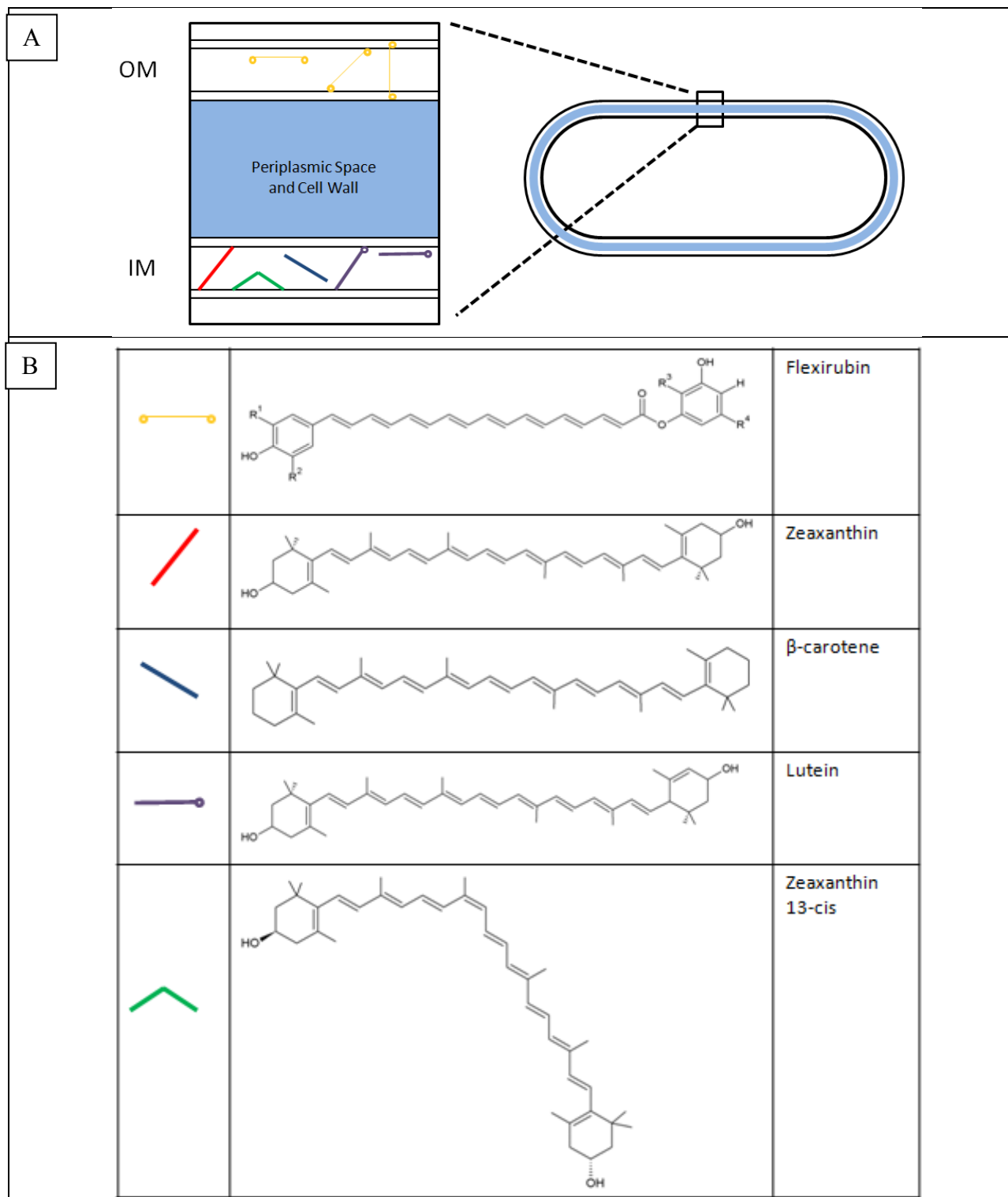
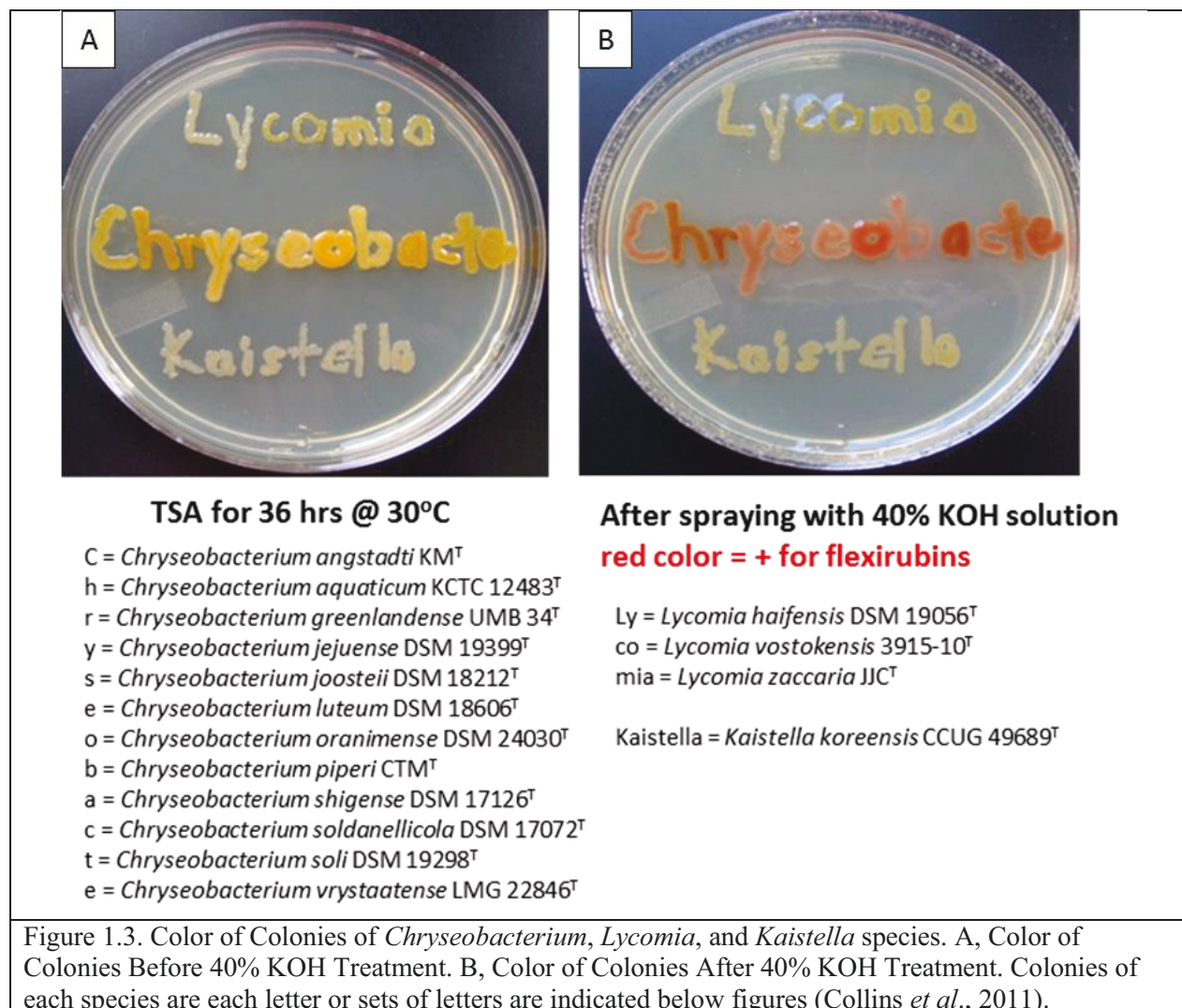


Figure 1.2. Illustration showing the localization of flexirubin and carotenoids in the outer membrane (OM) and inner membrane (IM) of a microbial cell. The colored structures in A correspond to the structures as shown in B (Irschik and Reichenbach, 1978; Gruszecki and Strzałka, 2005).

component of the outer membrane molecule lipopolysaccharide. The latter evidence demonstrates that the H fraction represents the outer membrane and the L fraction contains the cytoplasmic membrane. Flexirubins were mostly in the H fraction while the carotenoids dominated in the L fraction (Irschik and Reichenbach, 1978). Zeaxanthin, β -carotene, lutein, and zeaxanthin 13-cis are some carotenoids that have known orientation in a membrane. The two proposed orientations of lutein are due to its rotational freedom at its one ring not in conjugation with the remainder of the molecule (Gruszecki and Strzałka, 2005). However, the orientation of any flexirubin much like most of the biochemistry of these pigments is unknown.

Some studies have presented studies related to flexirubin biochemistry. Both high phosphate and low pH decrease the specific flexirubin content, but the quantitative amounts of each specific flexirubin did not change in response to changes in the phases of the growth curve. The amount of pigments was nearly constant during logarithmic growth, but the flexirubin amount did decrease a little late during the stationary phase (Reichenbach *et al.*, 1974). Better resolution now available with advances in spectroscopy may yield different results for the latter experiment especially in different organisms, as is proposed by this study. Of all the characteristics of flexirubins, the ability to detect flexirubins in colonies grown on TSA plates with the addition of base is essential to this study.



The color of the molecular shifts from yellowish-orange to purple, red, or brown with the addition of KOH, termed the bathochromic shift, is the key characteristic of flexirubins (Figure 1.3). This reversible shift of the absorption maxima occurs due to the presence of the phenolic hydroxyl group in ring A and the polyene chromophore; this is also the basis for the flexirubin presence test with KOH (Reichenbach *et al.*, 1980). The alcohol groups on the phenol rings are most likely oxidized by the strong base (Bendorf, personal communication) (Figure 1.4). Various shades of the same basic color before and after the chromatic shift have been observed in the genus *Chryseobacterium* (Figure 1.3). This latter observation has led to this study and an initial

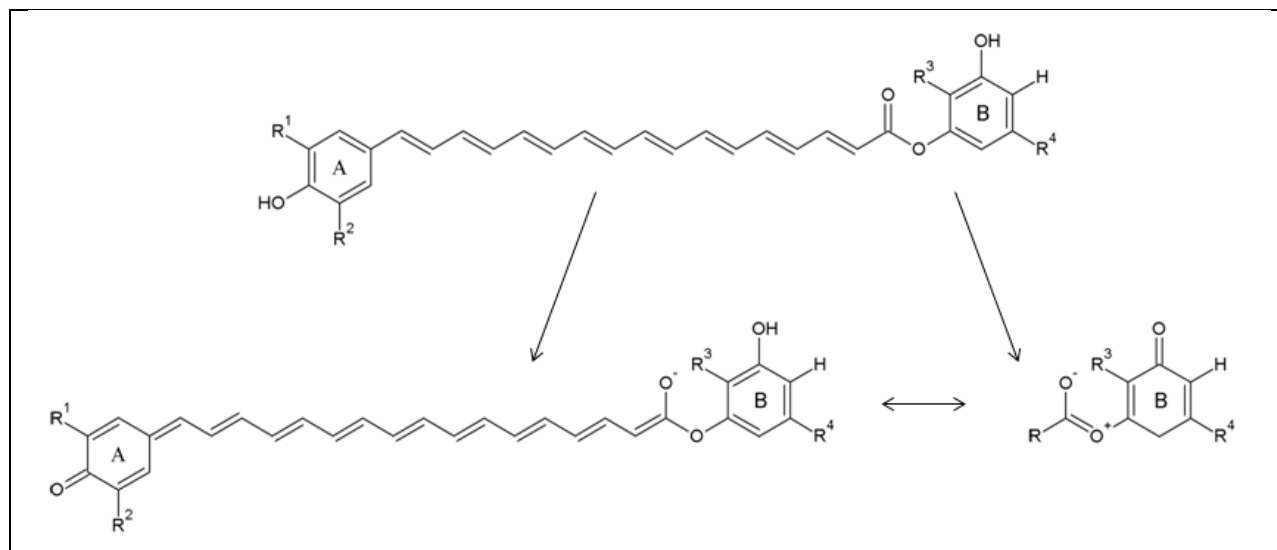
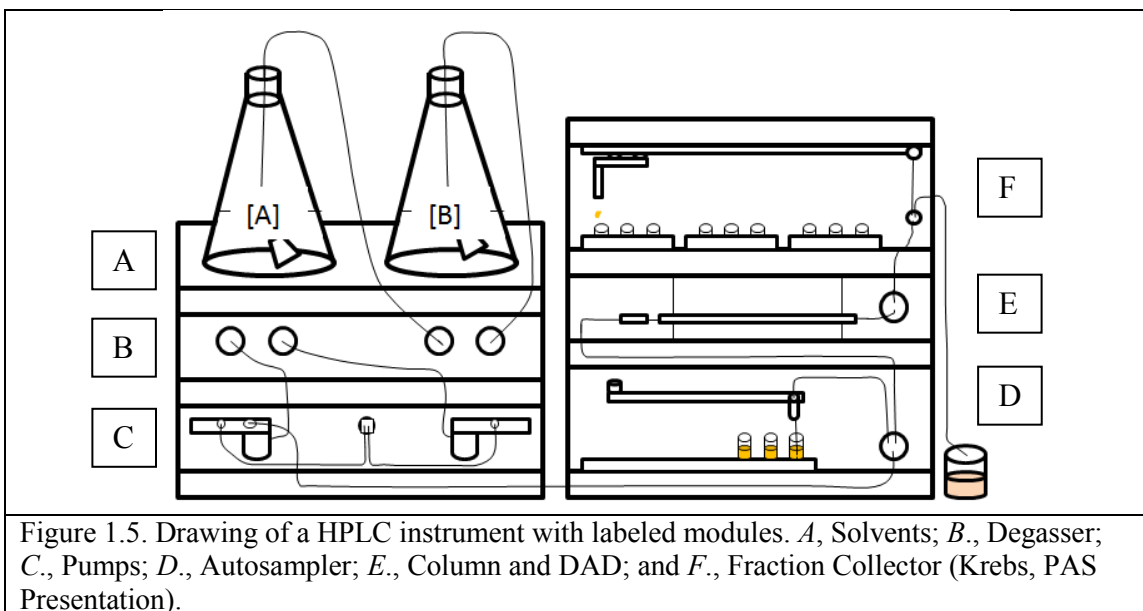


Figure 1.4. Proposed reaction behind the bathochromic shift observed when base is added to flexirubin-producing bacterial colony (Bendorf, personal communication).

hypothesis. My hypothesis is that fractions from *Chryseobacterium* species will yield unique flexirubin structures for each species. Also, the population of *Chryseobacterium* flexirubins will have genus-specific variations.

This interdisciplinary study between natural product chemistry and microbial taxonomy holds much significance for novel microbial research and other applications. Obtaining the chemical structures of flexirubins of *Chryseobacterium* may better differentiate closely related bacteria than previous traditional phenotypic, genetic, and biochemical approaches. Determining additional flexirubin structures from more diverse bacterial species and understanding whether they change in different growth phases may aid in determining the function and biosynthesis of these pigments. Any determined flexirubin structural differences should explain minor color variations of *Chryseobacterium* species when grown on TSBA. A pigment from this study may even more effectively inhibit the growth of *Mycobacterium tuberculosis* than a previously studied flexirubin (Mojib *et al.*, 2010). The data collected from this study will be utilized in upcoming work in correlating possible biosynthetic pathways to structural and genomic data.



High-Pressure Liquid Chromatography

Chromatography is the separation of components of a mixture and is the basis of the separation used for this study. High-Performance Liquid Chromatography (HPLC) is a liquid chromatography technique in which the mobile phase is kept under constant pressure and the stationary phase is made up of very small particles (typically 3-10 μm) (Housecraft and Sharpe, 2012). All aspects of the HPLC from the flow of solvent, the injection of samples, collection of peaks per a designated wavelength, and the collection of fractions can be fully automated depending on the particular instrument utilized. The Agilent 1200 Series HPLC used for this work is fully automated and is run by Chemstation. Multiple modules (Degasser, Pumps, Autosampler, Column and diode array detector (DAD), and Fraction collector) collectively are assembled to form the complete HPLC system (Figure 1.5). The degasser removes all air bubbles from solvents as the pumps push them through the modules. The DAD collects an absorbance reading for every wavelength within the UV-Vis spectrum (200-900nm) every few milliseconds. A full DAD chromatograph is therefore a set of all single wavelength chromatographs aligned in parallel (Figure 1.6). The fraction collector will collect fractions according to predetermined

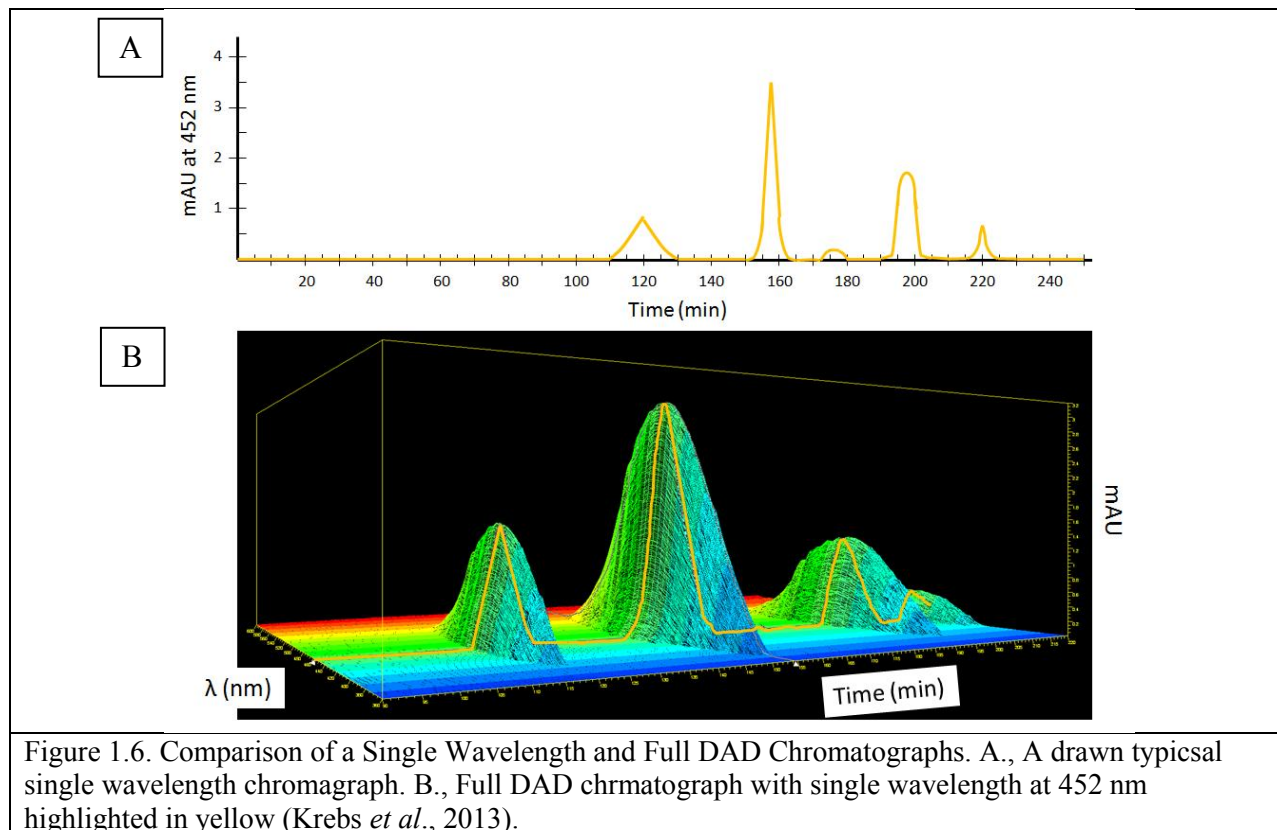


Figure 1.6. Comparison of a Single Wavelength and Full DAD Chromatographs. A., A drawn typical single wavelength chromatograph. B., Full DAD chromatograph with single wavelength at 452 nm highlighted in yellow (Krebs *et al.*, 2013).

parameters designed for each HPLC method.

HPLC Method Development

The ultimate goal of an optimized HPLC method is to be able to collect fractions of baseline separated peaks. The collection of fractions on a large scale makes this method a preparative HPLC method (Huber and Majors, 2007). An optimal method would be one in which less than 15 runs would be necessary to collect the needed 10 mg of sample necessary for structural analysis. However, there are many variables when designing any HPLC method including chromatographic parameters, solvent differences, different solvent gradients, and fraction collection parameters.

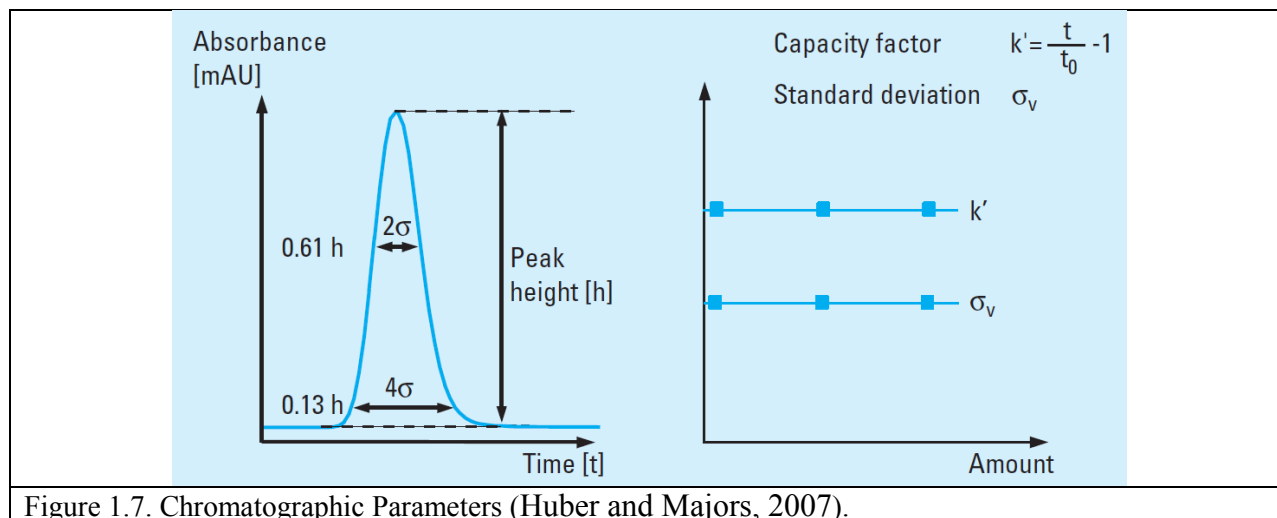
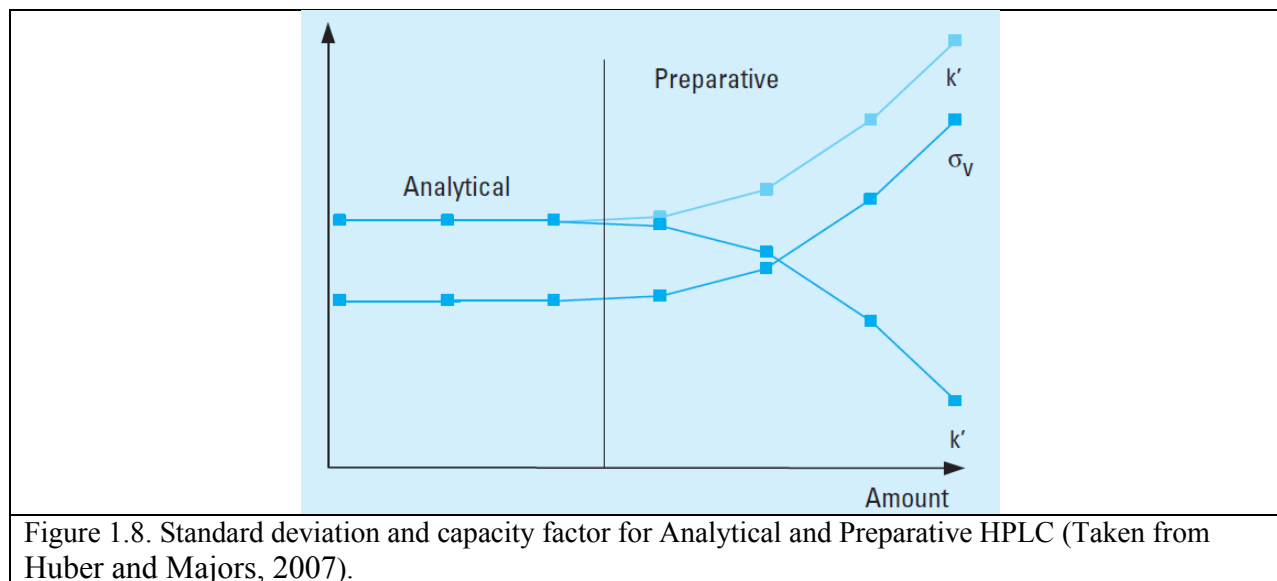


Figure 1.7. Chromatographic Parameters (Huber and Majors, 2007).

Chromatographic Parameters

The three most important chromatographic parameters for reproducible results, especially for analytical HPLC, are peak width, peak symmetry, and resolution. Peak area and height change per sample corresponding to the amount of each compound loaded on the column, but the capacity factor of the column and the symmetry of each peak remain the same (Figure 1.7). Loading greater amounts of sample on to a column will decrease the separation of closely eluting compounds as the height of each peak will change only until the capacity is reached and then the area will increase. Depending on how much area changes, the peaks may overlap each other (Huber and Majors, 2007).

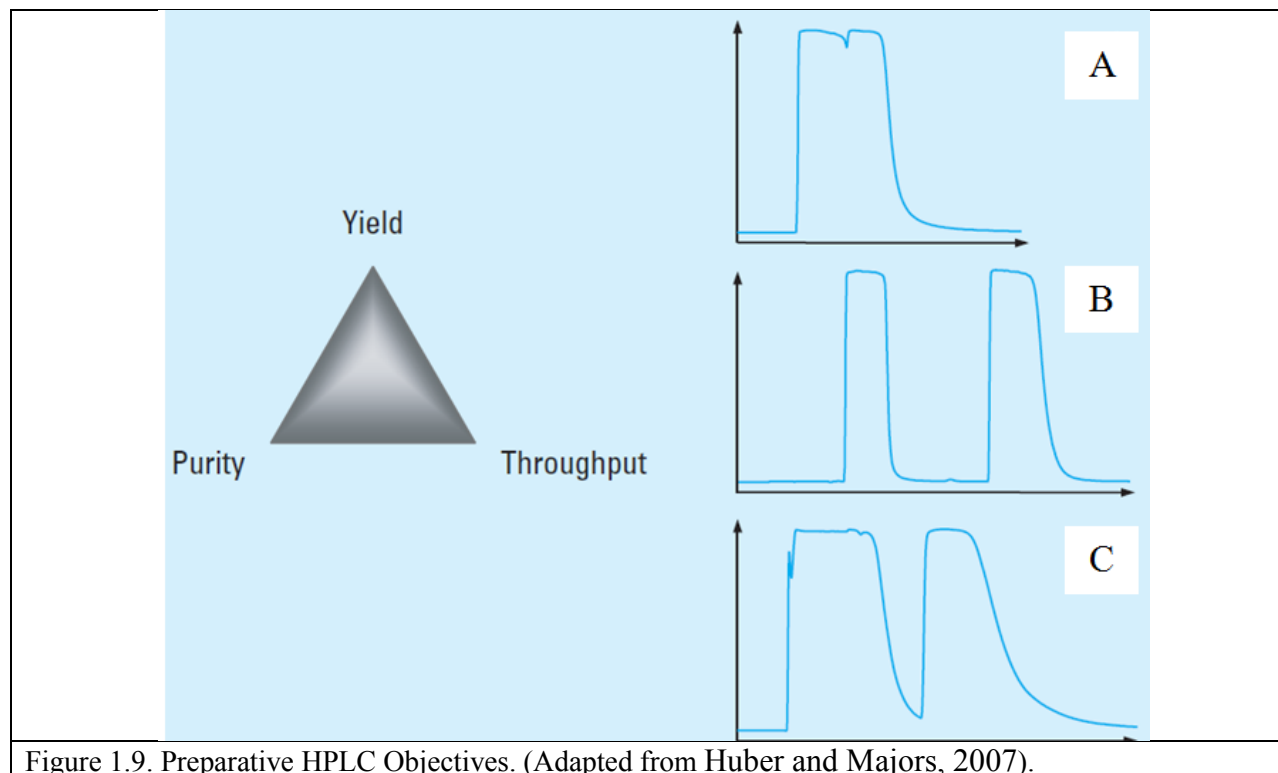
The desired peak is one that has a Gaussian curve-like shape. The peak's conformity to the Gaussian curve shape and symmetry can be described by its standard deviation (σ_v). The retention time (RT) of a sample can be described as related to a non-retained compound (t_0) which refers to the capacity factor (k') of the column for the given sample. The adsorption of an individual compound will become non-linear at a certain amount of injected material. The peak



of the compound will appear asymmetrical exhibiting tailing as the capacity factor decreases which may lead to overlapping peaks as described previously (Figure 1.8). Each compound may have a unique capacity factor (Huber and Majors, 2007).

HPLC objectives

The major aspects of an optimized preparative run are throughput, yield, and purity of product. These three aspects depend on each other, so a run which compromises the three is often the best. The chromatograph of Figure 1.9A represents a preparative HPLC run that has high throughput, but its separation is relatively poor as compared to the chromatograph in Figure 1.9B. In A, the yield of either nearly pure peak will be poor with only a single fraction collected, but in B, the purity and yield of the peaks are both high but with less throughput. However, in Figure 1.9C, the peaks are nearly baseline-separated. This high throughput run has high purity and high yield. For this project, separations like Figure 1.9B with greater yield are the goal. However, the third separation, Figure 1.9C, could also be used, by just collecting fractions from before and after the non-baseline separation (Huber and Majors, 2007). These three principles dictate the column selected for a particular project.



Column Selection

Flexirubins have a molecular weight (MW) of less than 2000, usually about 700 MW, and are more soluble in organic solvents than water. The flexirubins are slightly soluble in hexane, but more so in methanol, acetone, or THF. These observations suggest the use of a reverse-phase column such as C18 (Figure 1.10) (Agilent ZORBAX Column Selection Guide for HPLC, 2007).

The bonded phase, packing pore size, particle size, diameter, and length are the major column variables. A good starting column for reverse-phase method development is a C18 column. The C18 stationary phase has the maximum retention for non-polar to moderately polar analytes. Small molecules of less than 2000 MW usually can easily disperse through a 80-120Å packing pore size. A 5 µm porous particle size is typically used for both large and small

compound separations. Smaller particles (such as 3.5 μm) provided better resolution and efficiency. An analytical column of a 4.6 mm internal diameter (ID) is also the usual starting point for new HPLC separations. The internal diameter and length of the column have a major effect on the separations. The selectivity of the stationary phase determines the throughput of a method while particle size has little influence. However, small particles of the stationary phase are required and internal column diameter also establishes the throughput. The internal diameter largely determines the amount of sample that can be loaded on the particular column. For Zorbax columns of C18 bonded-silica with a 4.6 mm ID, the typical sample load is 0.1 to 1.5 mg with a

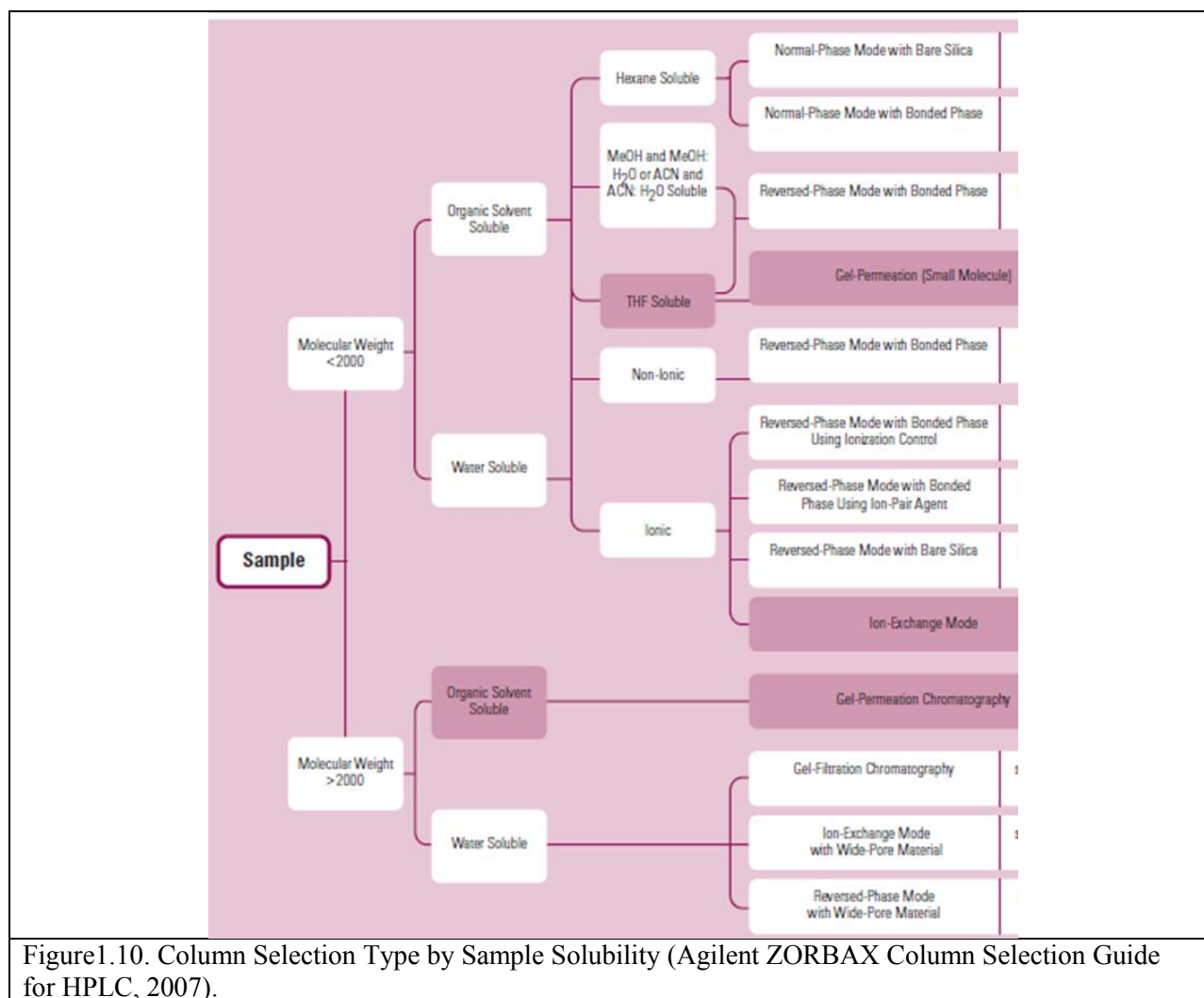


Figure 1.10. Column Selection Type by Sample Solubility (Agilent ZORBAX Column Selection Guide for HPLC, 2007).

flow rate of 0.5 to 3 mL/min (Agilent ZORBAX Column Selection Guide for HPLC, 2007). The separation of individual peaks, or resolution, increases with longer columns. Standard column lengths are 150 mm and 250 mm. HPLC methods of about 30 minutes can be developed using these long lengths with ample separation (Agilent ZORBAX Column Selection Guide for HPLC, 2007).

Options for Large-Scale Purification

Utilizing an analytical system, there are two options for large-scale purification as needed for natural product purification: scale-up of the all parameters of the analytical system to a preparative system, or column-overloading (Huber and Majors, 2007).

$$Scale - up\ factor = \frac{r^2\ prep}{r^2\ analytical} = \frac{\left(\frac{preparative\ ID}{2}\right)^2}{\left(\frac{analytical\ ID}{2}\right)^2}$$

When going from an analytical to preparative HPLC system, the factors of the system is maintained by applying a scale-up factor. The scale-up factor can be determined using the above formula based on the ratio of areas for both the preparative and analytical columns. Using the scale-up factor, the chromatographs should remain the same with symmetrical and sharp peaks (Huber and Majors, 2007; Scientific Instruments and Consumables). The flow rate, tubing diameter, dead volume, sample volume, and method gradients have to be applied to this scale-up factor (Scientific Instruments and Consumables). Given the necessary scale-up factors, the

Table 1.2. Scale-up factor for different Internal Diameter (ID) Columns. Scale-up factor is relative to 4.6 mm ID and determined with previous formula. (Scientific Instruments and Consumables).

Column ID (mm)	Scale-up factor (Relative to 4.6 mm ID)
2.1	0.21
4.6	1.00
10	4.70
21.4	21.60
41.4	81.00

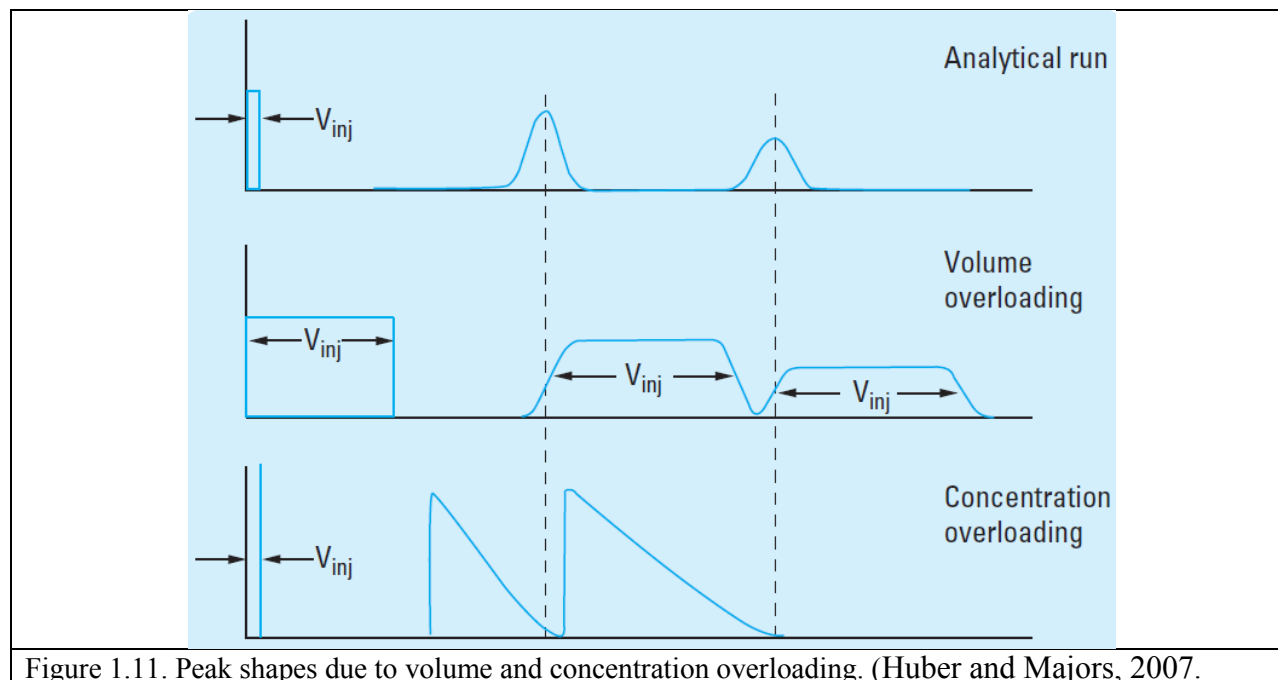


Figure 1.11. Peak shapes due to volume and concentration overloading. (Huber and Majors, 2007).

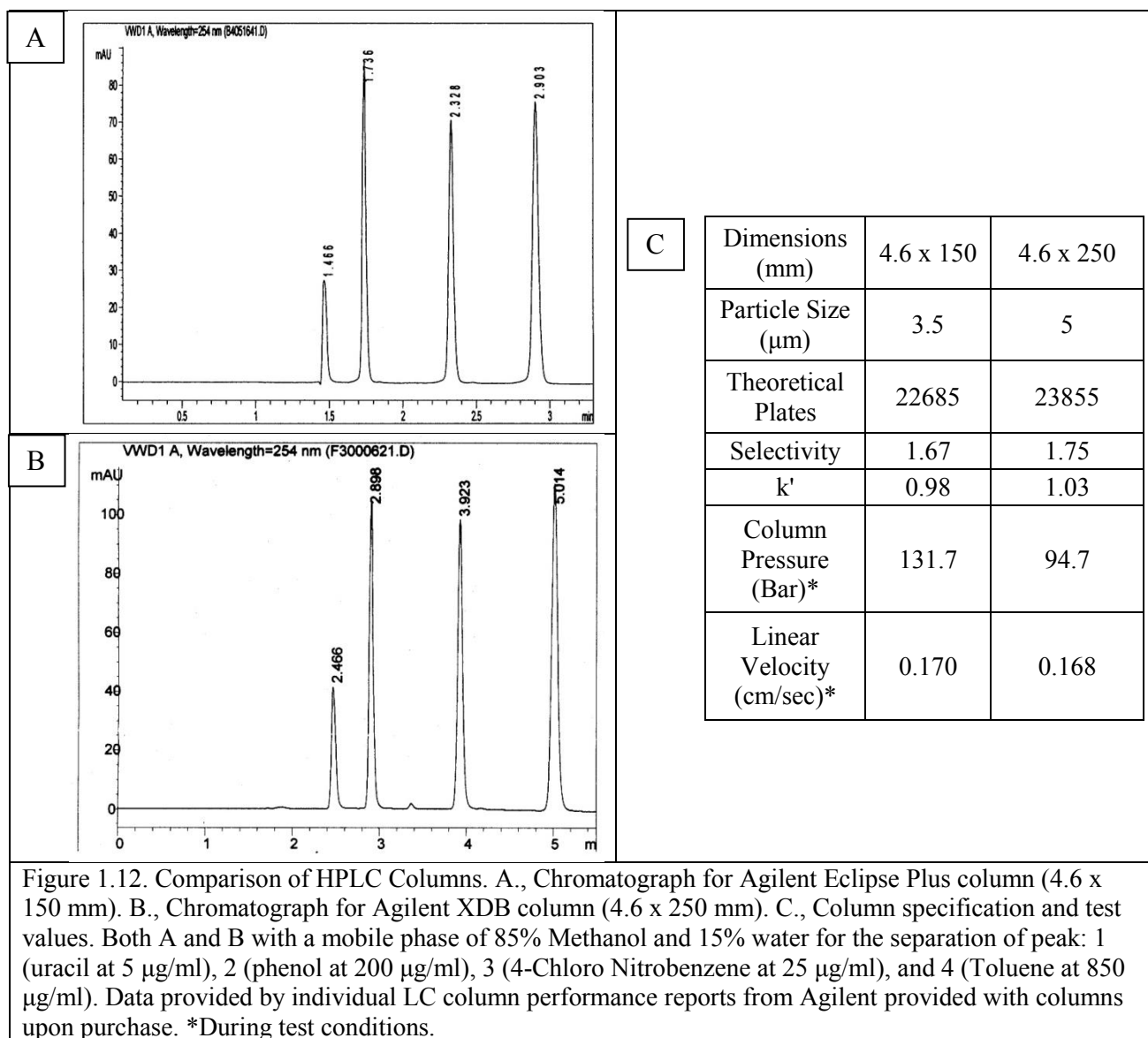
preparative system is very expensive with higher solvent volumes and large columns so that that the column-overloading is the more economical and advantageous of the two options (Table 1.2) (Huber and Majors, 2007).

Column overloading occurs when the amount of the sample loaded on an analytical column with the same conditions (flow rate, tubing diameter, method gradients, etc.) is greater than its loading capacity. There are two options for column overloading, concentration overloading or volume overloading, both of which enable samples to be separated on an analytical column in the milligram range. Concentration overloading should only be used if the sample loaded on to the column has good solubility in the mobile phase of the optimized method. For concentration overloading, the sample volume remains the same while the concentration is increased. The capacity factor (k') decreases causing the peak shape to change from its normal Gaussian curve to more of a triangle (Figure 1.11). Volume overloading is the preferred method for samples that have poor solubility in the mobile phase in which the volume of the sample is increased. The peak heights tend to not increase and the peaks adopt a rectangular shape and

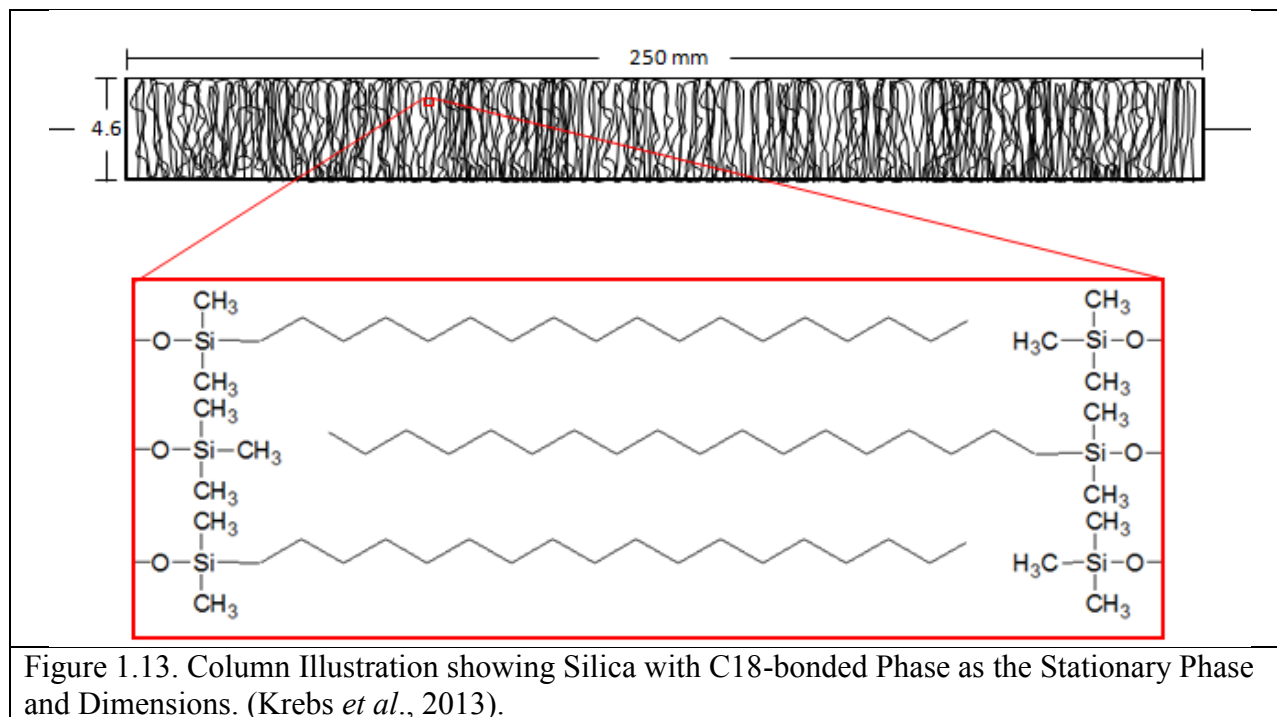
become very broad when loading past an analytical volume (Figure 1.11). Uniquely for some compounds, the capacity factor will increase with increasing overloading causes a strongly fronting peak to appear in the spectra. Concentration overloading usually enables a greater amount of sample to be injected on the analytical system so it is more favored, but both concentration and volume overloading can be used in a combination (Huber and Majors, 2007).

Column Specifications

The two types of reverse-phase, C18 columns used in this project are: an Eclipse Plus



analytical column (4.6 mm ID x 150 mm) and an Eclipse XDB column (4.6 mm ID x 250 mm). Both columns have the same internal diameter (ID) and therefore the same loading capacity as previously described. The larger particles within the 250 mm column cause the running pressure to decrease. A decrease in pressure enables a wider range of overloading-based methods to be tried. In addition, the selectivity, theoretical plates, and k' parameters increase with the 10 cm longer column. All three factors aid in better separation of closely related natural products. By comparing the retention times of the analogous peaks of the two chromatographs, the longer column has a greater retention by about 68% more for each tested component. A greater retention time may be helpful to better separate more closely-related molecules if needed (Figure 1.12). The column used for the optimized preparative runs has a length of 250mm and is filled with C18 –phase bonded to silica (Figure 1.13).



HPLC Methods for Natural Products like Flexirubins

Some natural products were found in the chemical literature that have similar structures to flexirubins. The HPLC based methods used to purify these compounds utilized different solvents, column lengths, and solvent gradients. Most methods used an organic modifier of acetic acid (Table 1.3). The organic modifier added to the acetonitrile or methanol should help keep the solvent at a low pH even with the decrease of the low pH buffer. The low pH ensures that the hydroxyl groups remain and do not ionize while on the column. Looking at similar natural products not only helps with designing HPLC purification methods, but also aids in studying the function of the flexirubins.

The natural occurrence and proposed biological activities of the avenanthramides, Tranilast, and alk(en)ylresorcinols is also of most interest when considering any possible functions of flexirubins. Avenanthramides and tranilast have the most similar structure to any published flexirubins; the only difference in structure being the amide bond instead of an ester bond and the 5-7 more polyenes in flexirubins (Table 1.3). Avenanthramides, collectively, are a class of phenolic antioxidants which are usually found in oats (Mattila *et al.*, 2005). Avenanthramides have been shown to have significant antioxidative activity and heat stability as well as intermediate lipophilicity. Specifically, it is thought that these compounds inhibit nonenzymatic and lipoxygenase-activated fatty acid oxidation (Dimberg *et al.*, 1993). Some avenanthramides have been shown to inhibit the spore germination specifically of the crown rust fungus (Miyawawa *et al.*, 1995). Similarly, alk(en)ylresorcinols concentrate in the outer layers of grains and are thought to have many biological activities (Mattila *et al.*, 2005). Interestingly, it has been suggested that some alk(en)ylresorcinols increase membrane permeability to sucrose, D-glucose, glycerol, polyethylene glycol 1000, and m-erythritol (Kozubek, 1987). Overall, flexirubins may

Table 1.3. Natural Products Similar to Flexirubins and Described HPLC Method to Purify Each. All Methods based a C18 Reverse-phase HPLC system. Data from references as described.

	Chemical Structure	Name	Variation	HPLC Method		Ref	
				Time	% B		
A		Avenanthramide	R ¹ : OH or OCH ₃ R ² : OH	0-50	5-60	(36)	
		Tranilast	R ¹ : OCH ₃ R ² : OCH ₃	50-56	60-90		
				A: 50mM PO ₄ buffer (pH 2.4) B: methanol Flow rate: 0.7 ml/min 150 x 3.9 mm column			
B		Avenanthramide	R ¹ : H, OH or OCH ₃ R ² : H or OH R ³ : H, OH or OCH ₃ n: 1-2	0-5	0-30	5	(33)
				5-20	30-42	5	
				20-25	30-100	5-0	
				25-30	100	0	
				30-33	100-30	0-5	
				33-40	30	5	
				A: water B: acetonitrile C: 10% v/v acetic acid Flow rate: 0.8 ml/min 250 x 4 mm column			
C		Alk(en)ylresorcins	n: 3-9	0-50	5-60	(36)	
				50-56	60-90		
				56-68	90		
				100	100		
D		Resveratol	none	0-15	10-90	(49)	
				15-25	90		
		Naringenin chalcone	none				

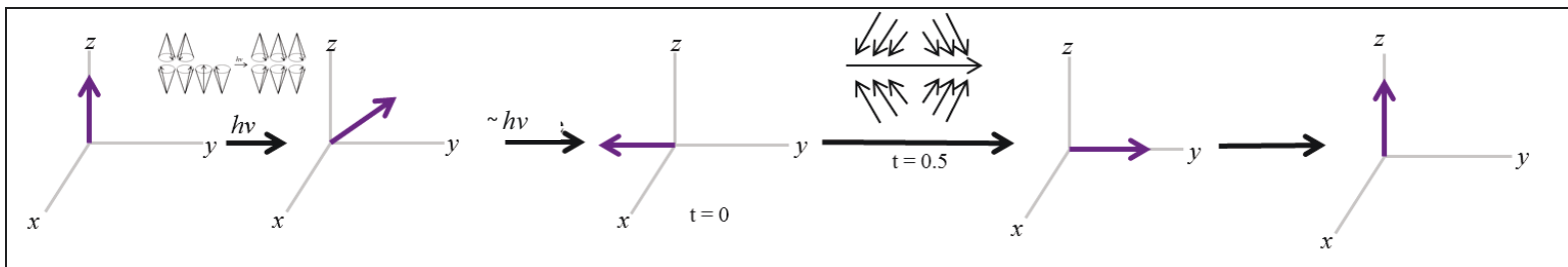


Figure 1.14. Illustration of Classical NMR theory and NMR output. Purple arrows represent the net magnetization vector (NMV) and the smaller black arrows represent protons. See Fig. 2 for details of inset of Classical NMR theory as depicted with cones (Adapted from Kiemle *et al.*, 2005; Dr. McDonald, Spectroscopy Class).

have an effect on the outer membrane and may act as an antioxidant.

Nuclear Magnetic Resonance (NMR)

Figure 1.14 illustrates the mechanisms of Nuclear Magnetic Resonance (NMR). The net magnetization factor represents a pool of protons in an oscillating radiofrequency field and in a homogenous B_0 , in the z axis, is pulled down into to the xy plane after a 90° pulse. The protons now spin about the z plane. After excitation but before relaxation, the nuclei spin around the z-axis. About 5s after the pulse, the proton population starts to dephase. This portion of the mechanism is termed spin-lattice relation in which the dephasing of the nuclei yields a loss of the xy-component. After spin-lattice relaxation, spin-spin relaxation occurs in which the anti-parallel nuclei fall back down to parallel, regenerating the z-component of the Net Magnetization Vector (NMV). During relaxation, the absolute value of the y-component of the NMV decreases with time. The signal as seen in the top of Figure 1.15B is generated; this sine wave is generated per each NMR pulse and relaxation. The middle figure represents the many sine waves (from many NMR trials of pulse and relaxation) of nonequivalent chemical environments which overlay. The bottom of the figure shows ^1H NMR spectra after a Fourier transform of time on the x-axis of particles per million (ppm) (Kiemle *et al.*, 2005).

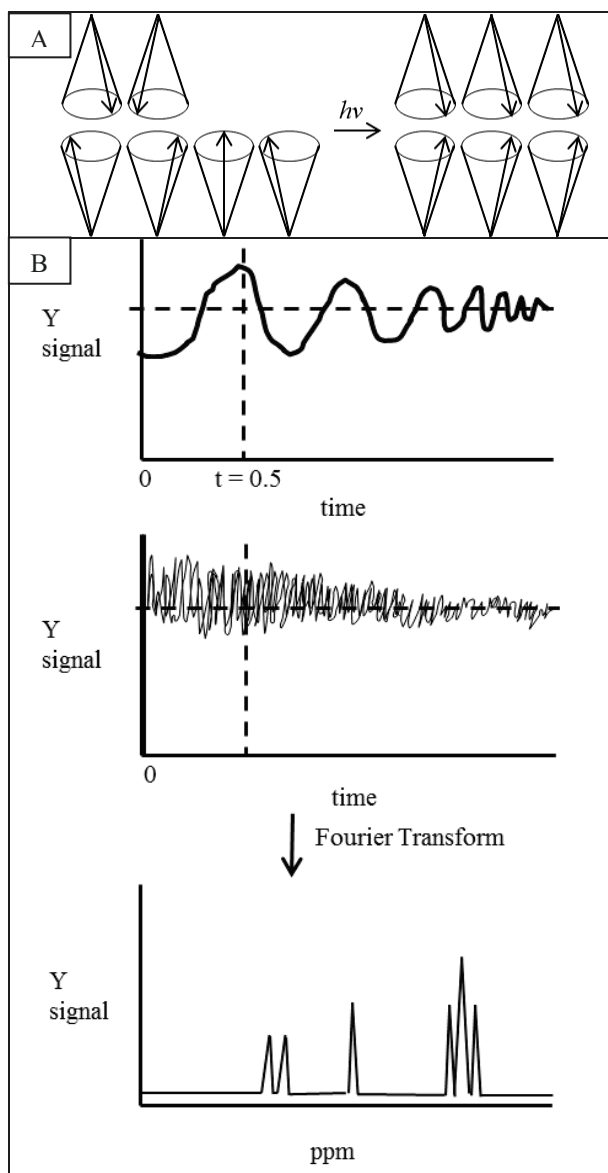


Fig. 1.15. Illustration of Classical NMR theory and NMR output. A., Classical NMR theory (each cone is a hydrogen, the arrow illustrates the magnetic dipole of the hydrogen). B, Output from NMR. Top. represents the sin wave of one proton run. Middle, represent all the sine waves of the runs of proton NMR. Bottom, represents the Fourier Transformed data yielding a spectra that be utilized (Adapted from Kiemle *et al.*, 2005; Dr. McDonald, Spectroscopy Class).

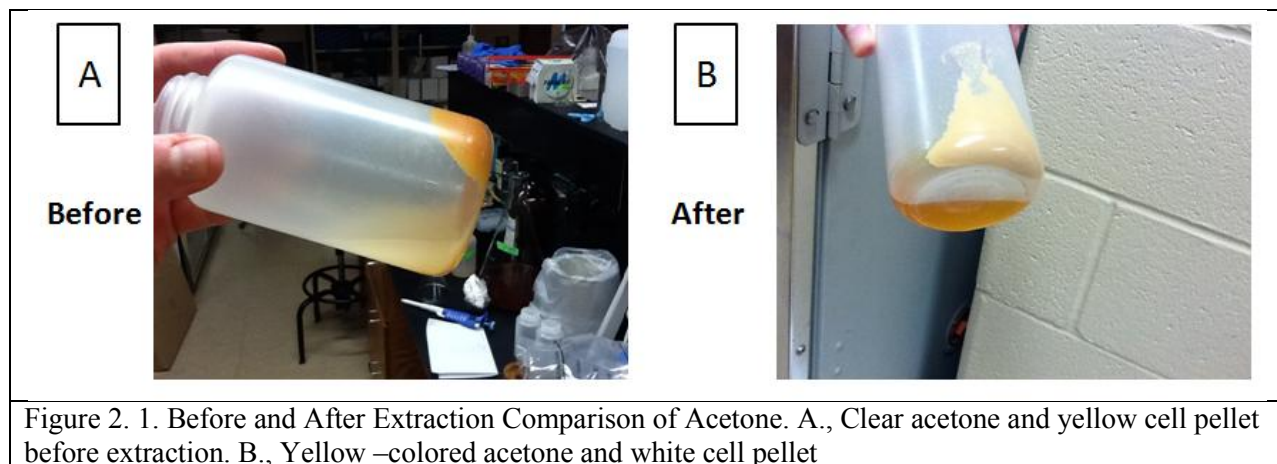
Figure 1.15A, also seen above the pulse arrows in Figure 1.14, represents the classical mechanical NMR theory in which magnetically active nuclei are precessing around the magnetic field vector like tops. Also the external magnetic field, B_0 is pointing up in this figure (not illustrated). The nuclei to the left of the arrow are dephased and in unequal populations and parallel to B_0 . The nuclei to the right of the nuclei are “phased” and the nuclei populations are equalized into parallel and anti-parallel (Kiemle *et al.*, 2005).

Many versions of NMR, one-dimensional proton and carbon NMR and two dimensional proton-proton (COSY) and proton-carbon NMR (HMQC) will be utilized by this study. About 10 mg of material will need to be collected for each purified fraction to obtain NMR spectra (McDonald, personal communication). Other techniques that will be used for structural analysis include: infrared spectroscopy (IR), mass spectroscopy (MS), and UV-vis spectroscopy.

Ch. 2. Optimization of Preparative HPLC Method

General Methods

Flexirubins from *C. oranimense* LMG 24030 were first purified so that chemical analysis leading to a molecular structure could be completed. Briefly, cultures of *C. oranimense* were grown for about 30 hours at 30°C while shaking in TSB. Media was decanted after centrifugation (10,000 rpm x 10 minutes at 4°C using the Sorvall SLA-1500 rotor) to leave behind a cell pellet. About 25 mL of acetone was added to each cell pellet that was originally 250-300 mL of culture (Figure 2.1). The cell pellet and acetone was shaken for at least 10 minutes at 4°C, RT, or 30°C. Each sample was then spun and extract was decanted and filtered through filter paper (Whatman, 1 or 3 qualitative grade). An acetone extract of the raw pigments was prepared for further HPLC purification by solubilizing an HPLC-grade solvent.



Initial Runs

Initially, the crude, yellow pigment extract was resolubilized at about a 1% w/v solution in acetone. The first few HPLC runs were based on the sample injected in acetone (Figure 2.2A). After checking the solubility of the dry flexirubin extract in multiple solvents, it was determined that the dry flexirubin extract was most soluble in glacial acetic acid. It was therefore decided to

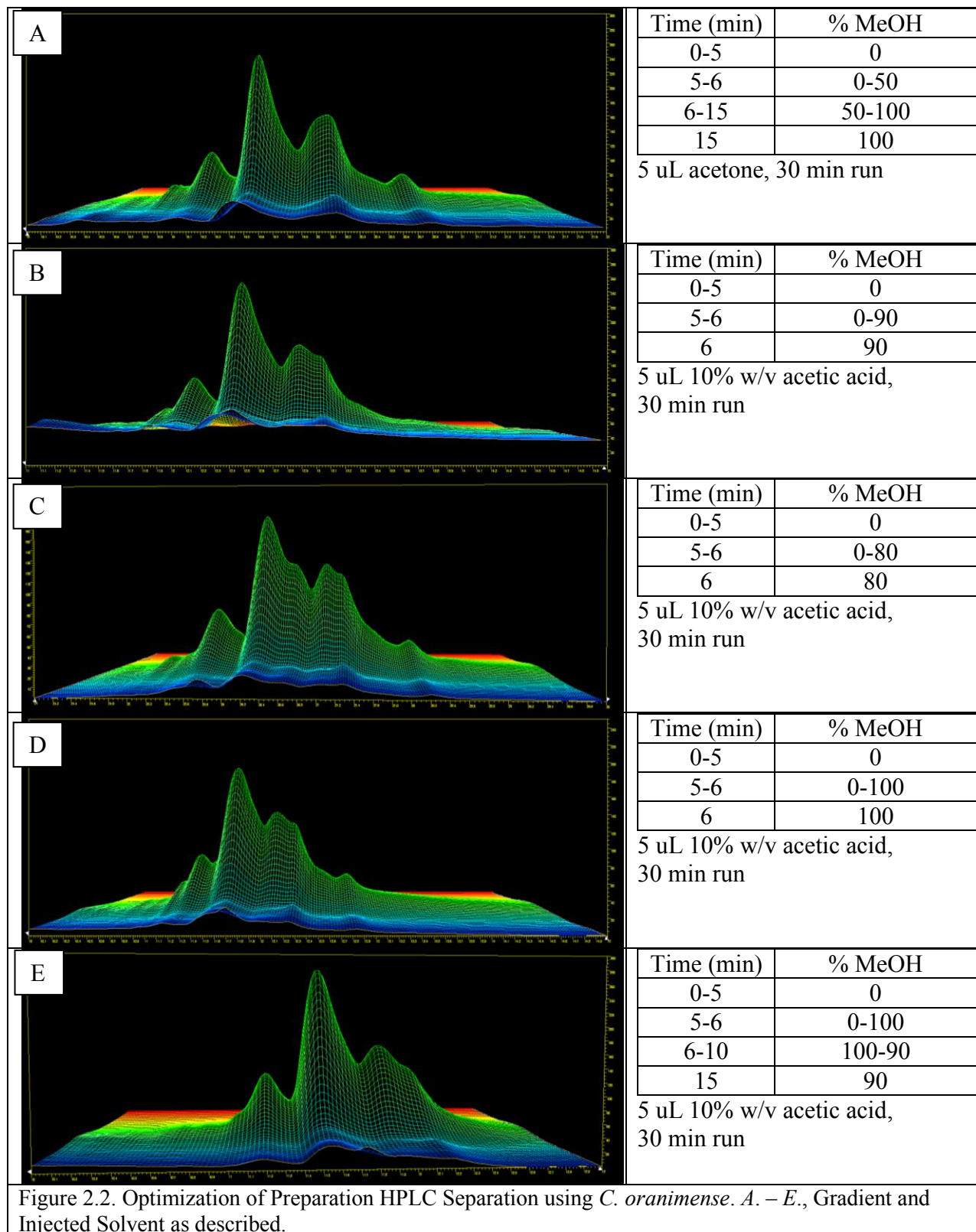


Figure 2.2. Optimization of Preparation HPLC Separation using *C. oranimense*. A. – E., Gradient and Injected Solvent as described.

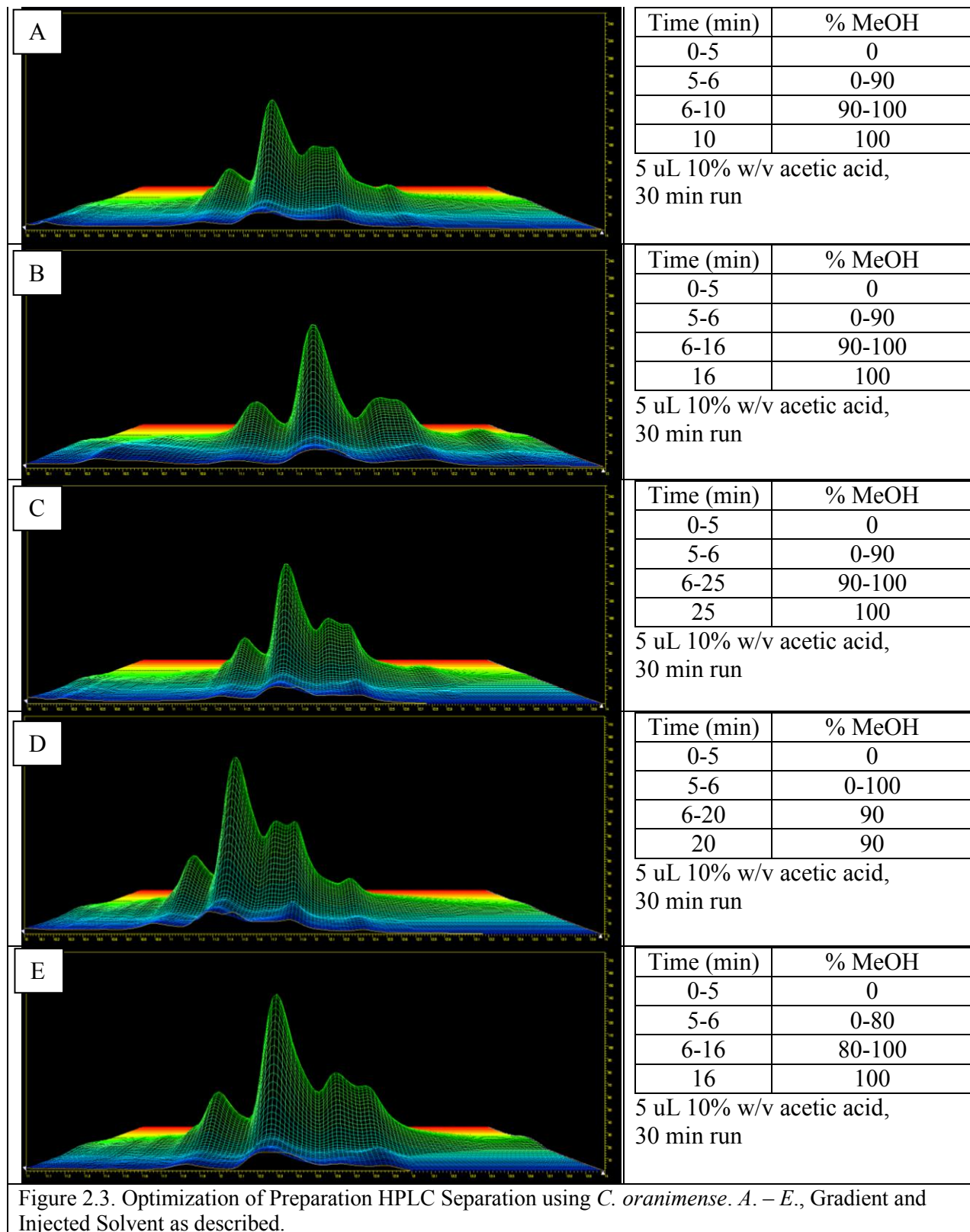
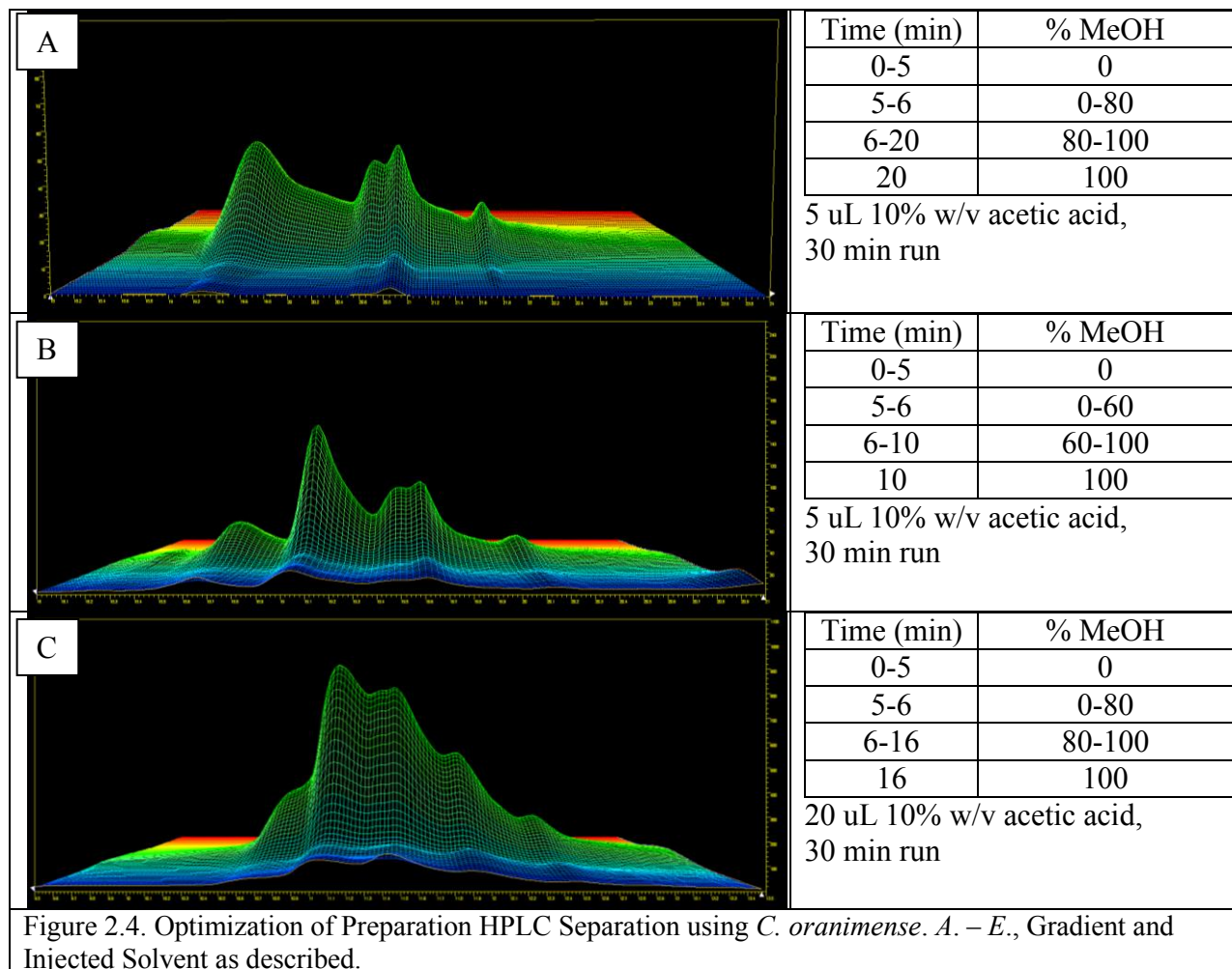
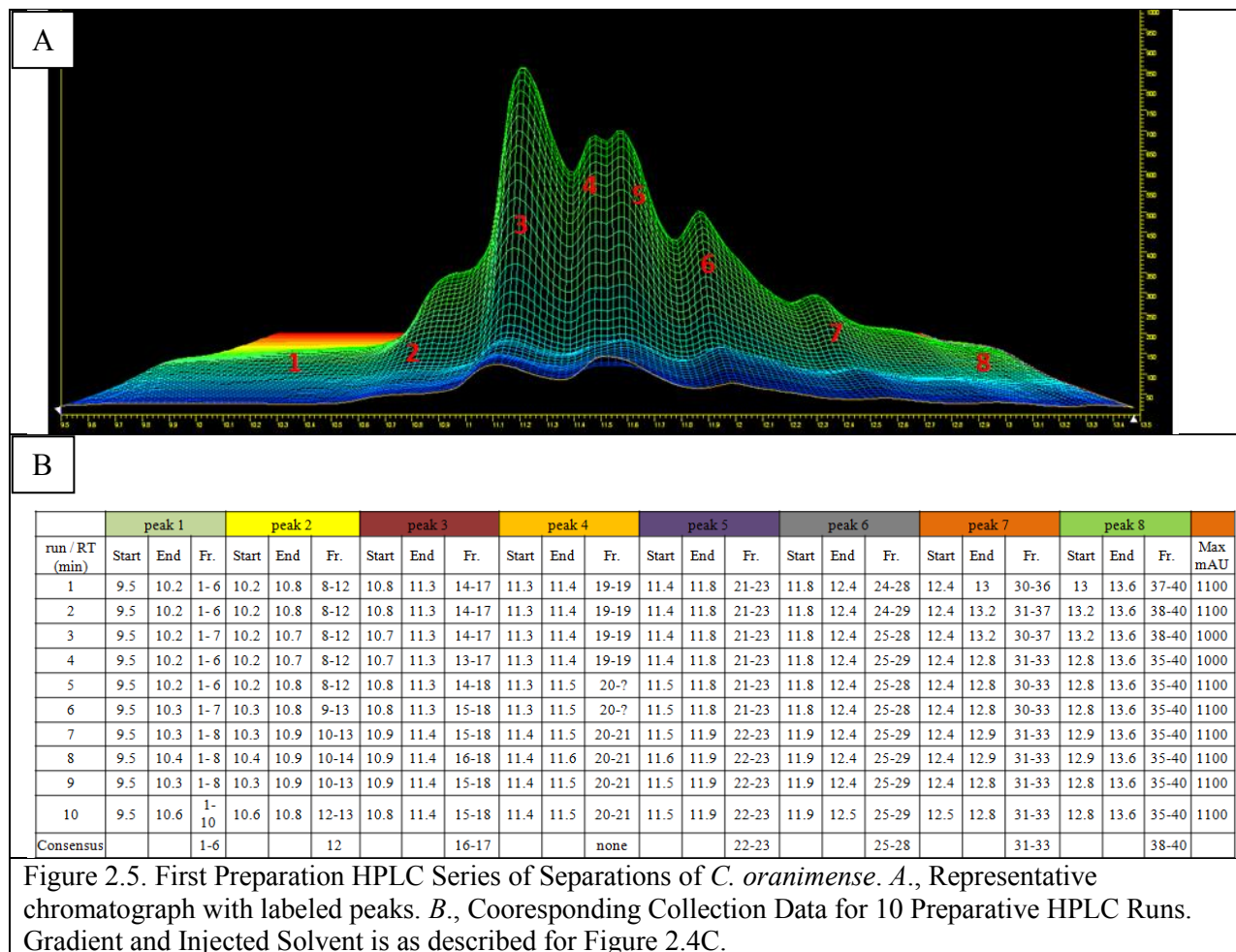


Figure 2.3. Optimization of Preparation HPLC Separation using *C. oranimense*. A. – E., Gradient and Injected Solvent as described.



prepare the extract in glacial acetic acid at a 10% w/v solution to be able to get more material on the column. All other separation methods of the initial runs utilize glacial acetic acid as the sample solvent.

Many gradients were tried to achieve the optimal separation with injection of sample prepared in acetic acid so that fractions could be collected during preparative HPLC runs. Better separation was achieved for slower gradients or those with lower percentages of methanol. Baseline separation was not achieved for even the most optimized run represented by Figure 2.3E, but the separation was thought to be good enough to enable the collection of partially pure fractions. The amount of material put on the column with this method was increased for fractions



with greater yields per run and was the first attempt to perform a series of preparatory HPLC runs (Figure 2.4C).

Preparative fractions were collected by separation of flexirubin molecules via reverse-phase based high-performance liquid chromatography (HPLC) using a H₂O/MeOH gradient (0-5 minutes, 0% MeOH; 5-6 minutes, an increase to 80% MeOH; 6-16 minutes, an increase to 100% MeOH; 16-30 minutes; 100% MeOH) with a 20 μ L sample injection (Figure 2.4A). Fractions were collected every 1 minute once initiated with the flow set at 1 mL/min. The time based fractions were pooled accordingly and allowed to dry in a fume hood (Figure 2.5).

Fraction 3, containing the major peak, was prepared for NMR to check its purity. The RG

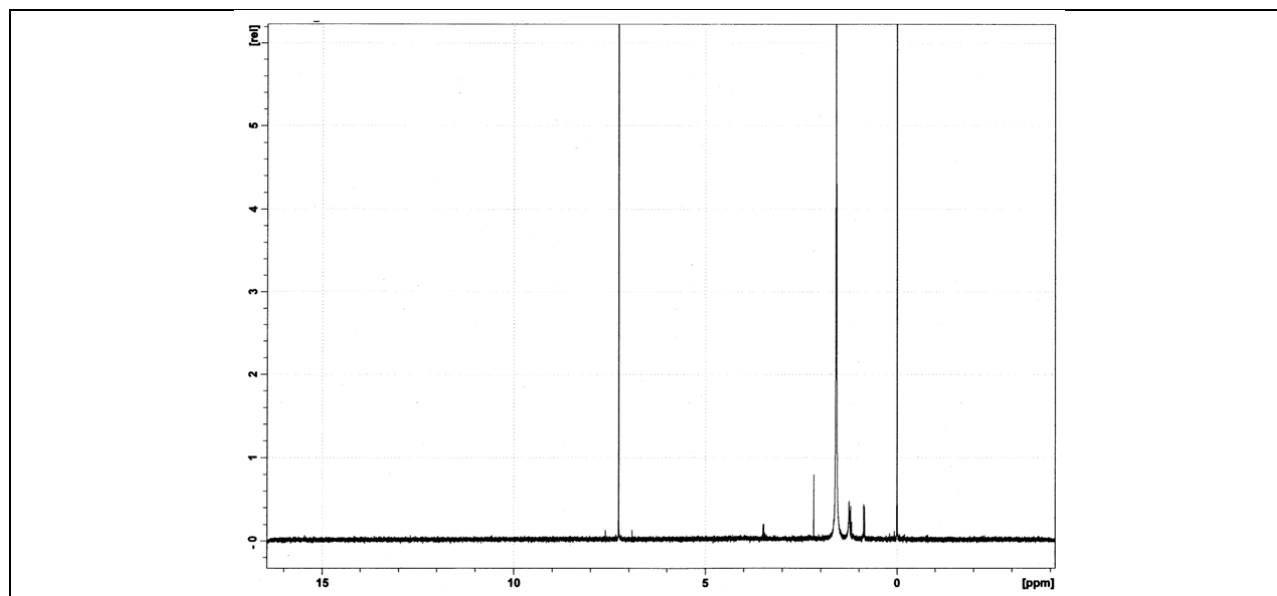


Figure 2.6. ¹H NMR Spectrum for peak 3 fractions. Produced after 64 scans on Bruker Avance 300 MHz NMR.

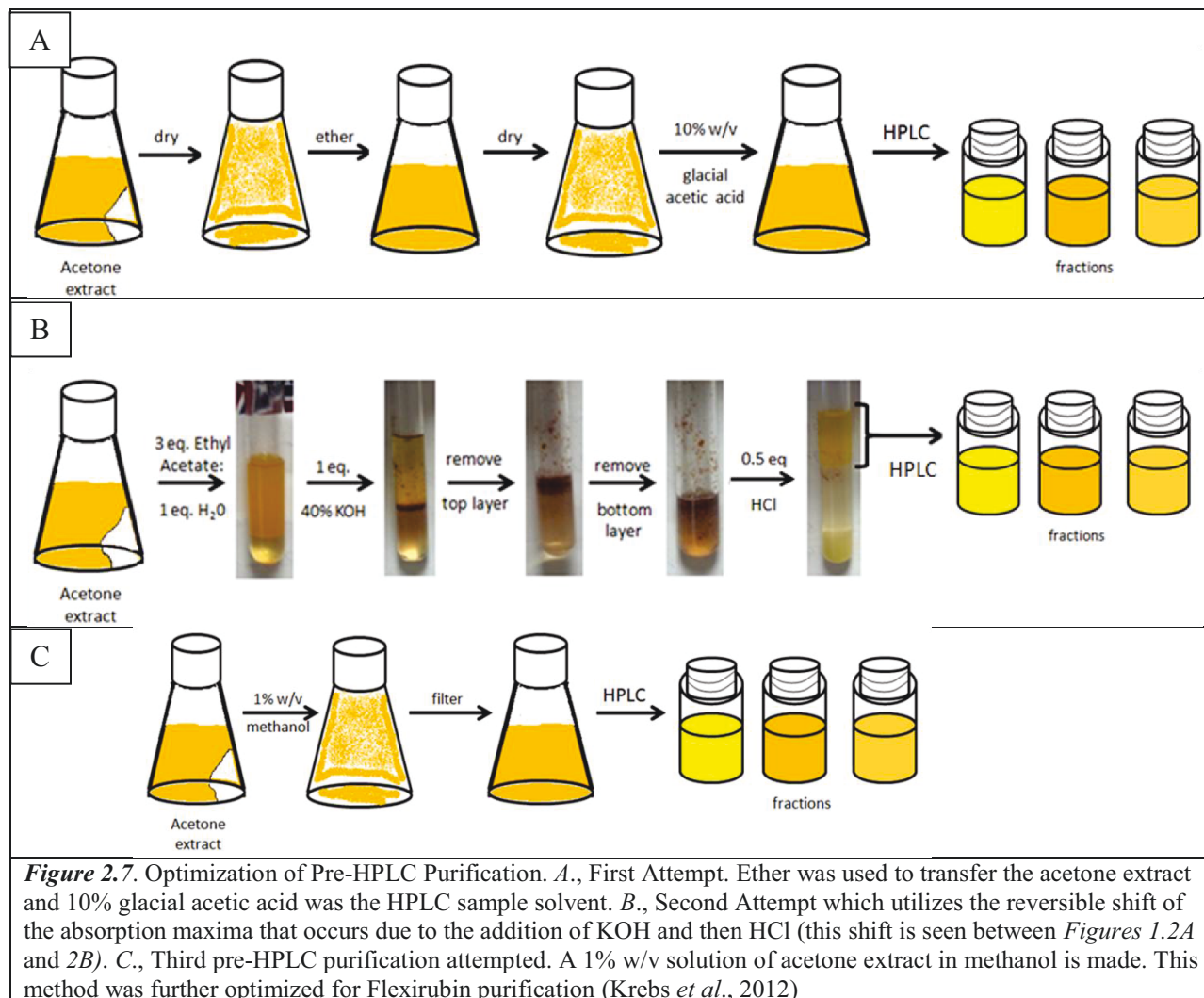
value of the spectrum was nearly 1300 indicating the sample to be at a low concentration. A few peaks that were expected to have higher concentrations were relatively low as well. With lack of material necessary for structural analysis, effort was shifted to optimizing the preparative method again, first with the pre-HPLC purification.

Pre-HPLC Optimization

The solvent systems for the pre-HPLC method and the final HPLC purification have been determined after three different attempts to purify the flexirubins after the acetone extract was collected. Three methods were attempted to have a final extract which once injected would put sufficient material on the column but would still be well separated.

The first method utilized ether to transfer acetone extract to new glassware. After drying the ether, enough glacial acetic acid was added to make the solution at a 10% w/v concentration (Figure 2.7A). The sample was ready for HPLC purification after a 2 hour preparation. Data from an optimized run for this pre-HPLC preparation method showed that about 8 peaks separated over 4.1 minutes. The area of the largest peak, peak 3, was approximately 16892

mAU*sec (Figure 2.8A). The most optimized run had a 20 μ L injection and used the Flex16Frac.M HPLC method (Table 2.1).



The second method was designed to isolate only flexirubins in the pre-HPLC purification by using the color shift seen when base was added to colonies on TSB plates (Figure 2.7B, Figure 1.2). 3:1 equivalents of ethyl acetate:water was added to a weighed amount of acetone extract. The solvents formed a yellow organic layer and yellowish/clear aqueous layer. 1 equivalent of KOH was added to form a red intermediate layer. The organic and aqueous layers were both removed then, 0.5 equivalents of HCl was added to reverse the color. Ether was used to pull the flexirubins and other now yellow organic molecules away from water and any residual

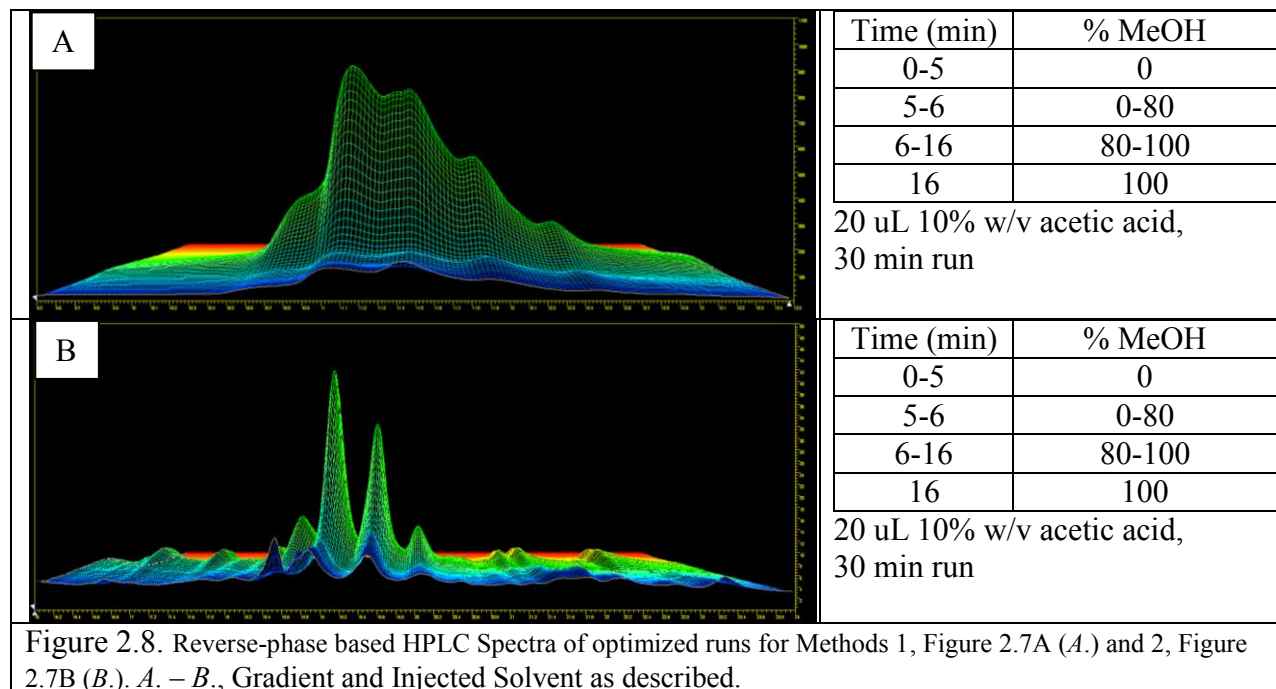


Figure 2.8. Reverse-phase based HPLC Spectra of optimized runs for Methods 1, Figure 2.7A (A.) and 2, Figure 2.7B (B.). A. – B., Gradient and Injected Solvent as described.

HCl of KOH. The ether extract was dried and solubilized in acetone to be injected on the HPLC (Figure 2.7B). This method has about an hour and 20 minute preparation time. A pool of up to 10 flexirubins from *C. oranimense* has been separated over about seven minutes with the optimized HPLC run. The major peak of the set has a λ_{\max} of 452 nm and area of about 18.87 mAU*sec (Figure 2.8B). This purification method utilized the same HPLC conditions as the first purification procedure (Table

Table 2.1. Parameters of the optimization of Flexirubin purification (Krebs *et al.*, 2012).

Method	Reagent System	Preparation Time	area of peak #3	λ_{\max} (nm)**	number of peaks	separation over time (min)	Method
1	1) Ether 2) 10% w/v sample in glacial acetic acid	2 hours	~16892.2* ^t	452	~ 8	9.5 - 13.6	Flex16Frac.M
2	1) 3 eq. ethyl acetate, 1 eq. H ₂ O 2) 1 eq. 40% KOH 3) 0.5 eq. HCl	1 hour 20 mins	~18.87* ^t	452	at least 10	16.4 - 23.8	Flex16Frac.M
3	1) 1% w/v Methanol	15 - 30 mins	~2769.9 * ^s	450	8 to 10	27.0 - 32.8	Flex16Frac50_6.M
			N/A	450	2	36.4 - 37.5	

Data presented based on HPLC absorbance and separation.

* Represents most optimized HPLC separation for respective method. ** λ_{\max} (nm) of #3 peak. *^t at 430 nm.

*^s at 452 nm.

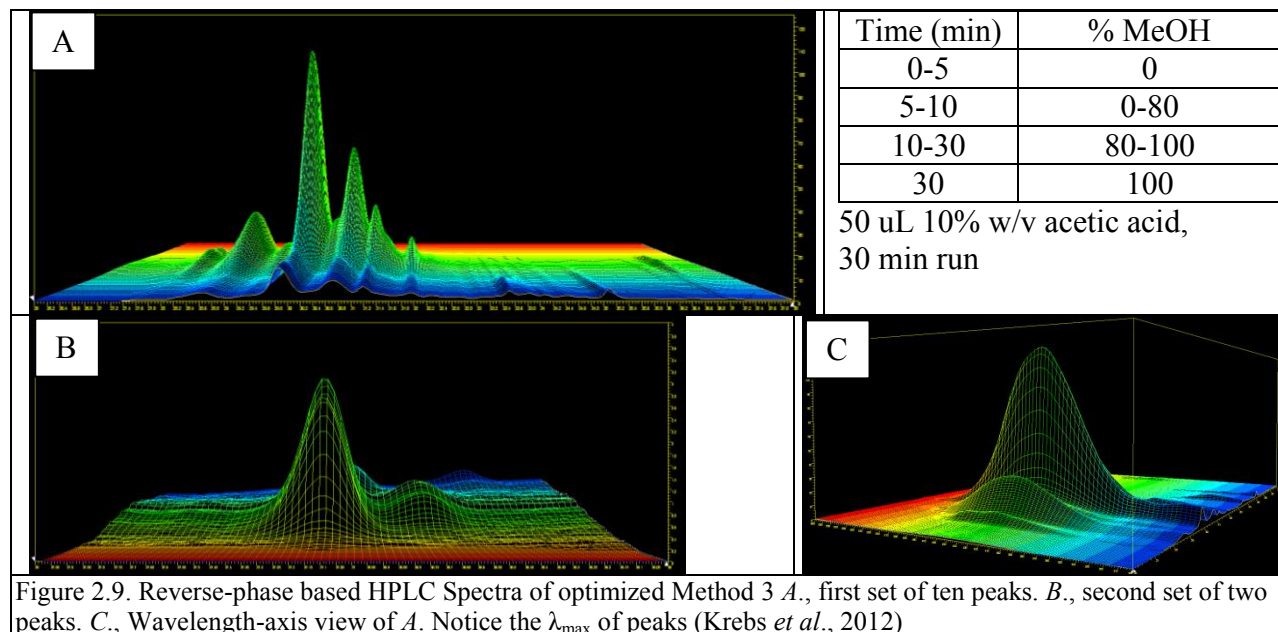
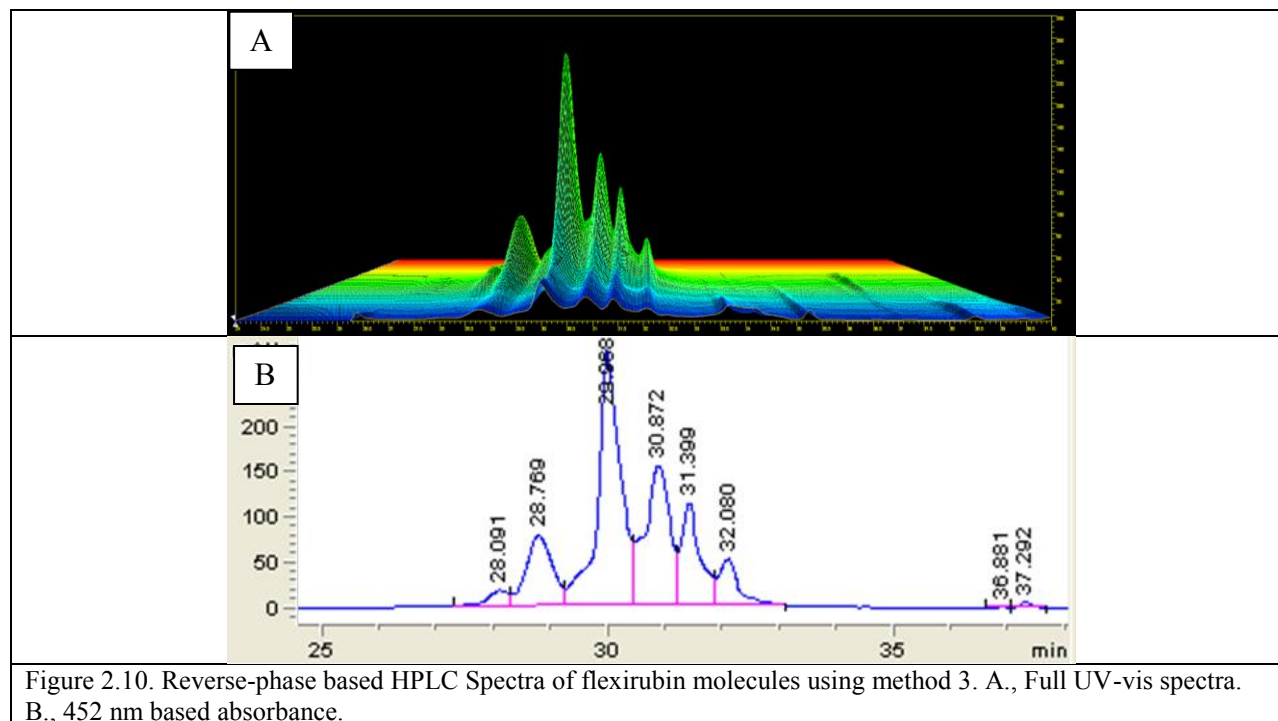


Figure 2.9. Reverse-phase based HPLC Spectra of optimized Method 3 *A.*, first set of ten peaks. *B.*, second set of two peaks. *C.*, Wavelength-axis view of *A.* Notice the λ_{\max} of peaks (Krebs *et al.*, 2012)

2.1). This method yielded peaks that were well separated, however, there was a low amount of material on the column. It would not be worth the materials nor time to collect multiple fractions with such small absorbance values of the eluting molecules. A new method was needed that would put more material on the column with equally good separation of flexirubin molecules.

Method 3 had the best HPLC spectral data and has been further optimized to use for collecting fractions of flexirubins. Solubility testing indicated that the acetone extract was soluble enough in methanol to use as an HPLC sample solvent at a concentration of 1% w/v. Enough methanol is added to a pre-weighed amount of acetone extract to have the sample at a 1% w/v concentration (Figure 2.7C). After the fifteen to thirty minute preparation, the sample is ready for HPLC purification. Two sets of peaks eluted during optimized HPLC runs using the Flex16Frac50_6.M HPLC method and 50 μ L injection volume (Table 2.1). The first set of peaks is analogous to the set of peaks seen with the first two methods (Figures 2.9A and 2.9B). This set of peaks has about 8 to 10 peaks separating over 5.8 minutes. Peak #3 has a λ_{\max} of 450 nm and an area of approximately 2769.9 mAU*sec (Figures 2.9A and 2.9C). The second set of peaks



has two peaks that separate over 1.1 minutes; these latter peaks had not been observed in the HPLC UV-Vis data from runs of the previous two methods (Figure 2.9B). This method has been used to further this project. Two sets of 16 and 15 runs have been completed with 40 fractions collected from 27.7 to 31.8 minutes (Krebs *et al.*, 2012). A representative run shows that 6 peaks are separated well over almost 5 minutes followed by two peaks separating at 36.8 and 37.3 minutes (Figure 2.11A). 7 fractions were collected, as shown by the 6 green and 1 orange boxes representing fractions due to the peak-based option of fraction collecting being used. In another run, 8 fractions were collected (Figure 2.11B). Fractions were pooled every few hours as collected. Solvent was then removed from each fraction that was in small 19/22 round bottom flasks using rotovap evaporation.

The masses of each of the 8 fractions indicate that enough material was collected for peaks 3, 6, and 7 for chemical analysis. The purity of peak 3 was then determined with the HPLC purification run. Unfortunately, no flexirubin peak was seen in the UV-vis data. The major 6

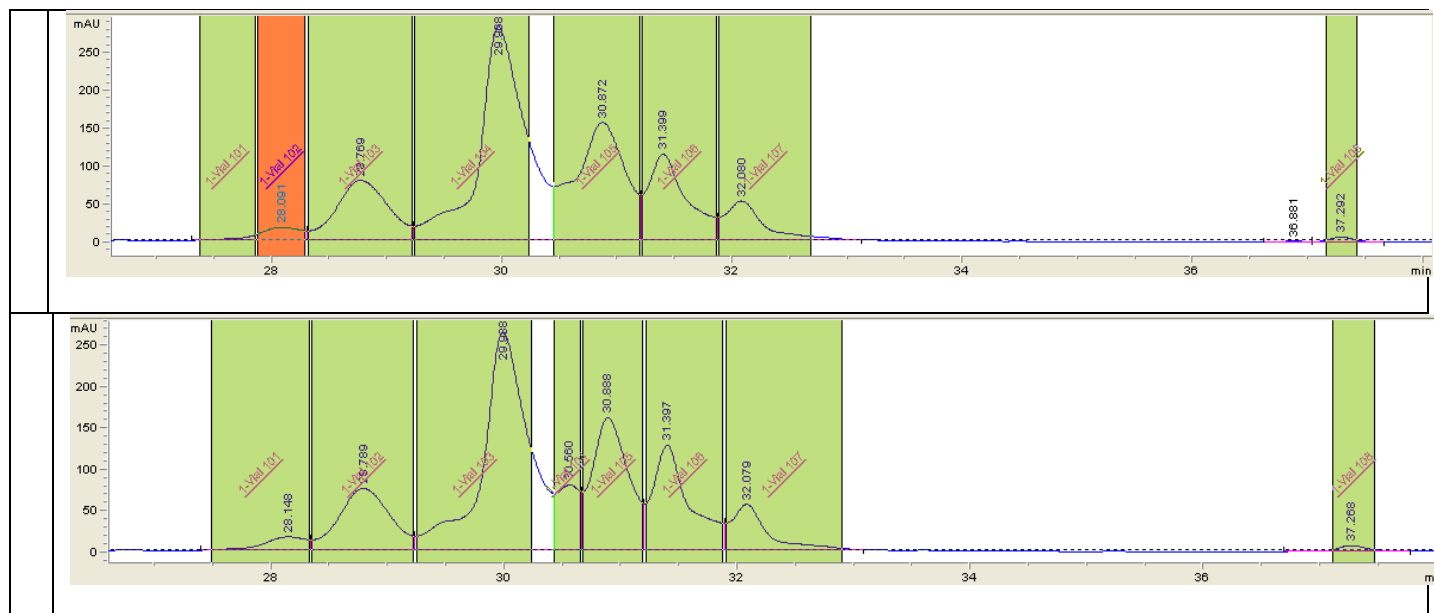
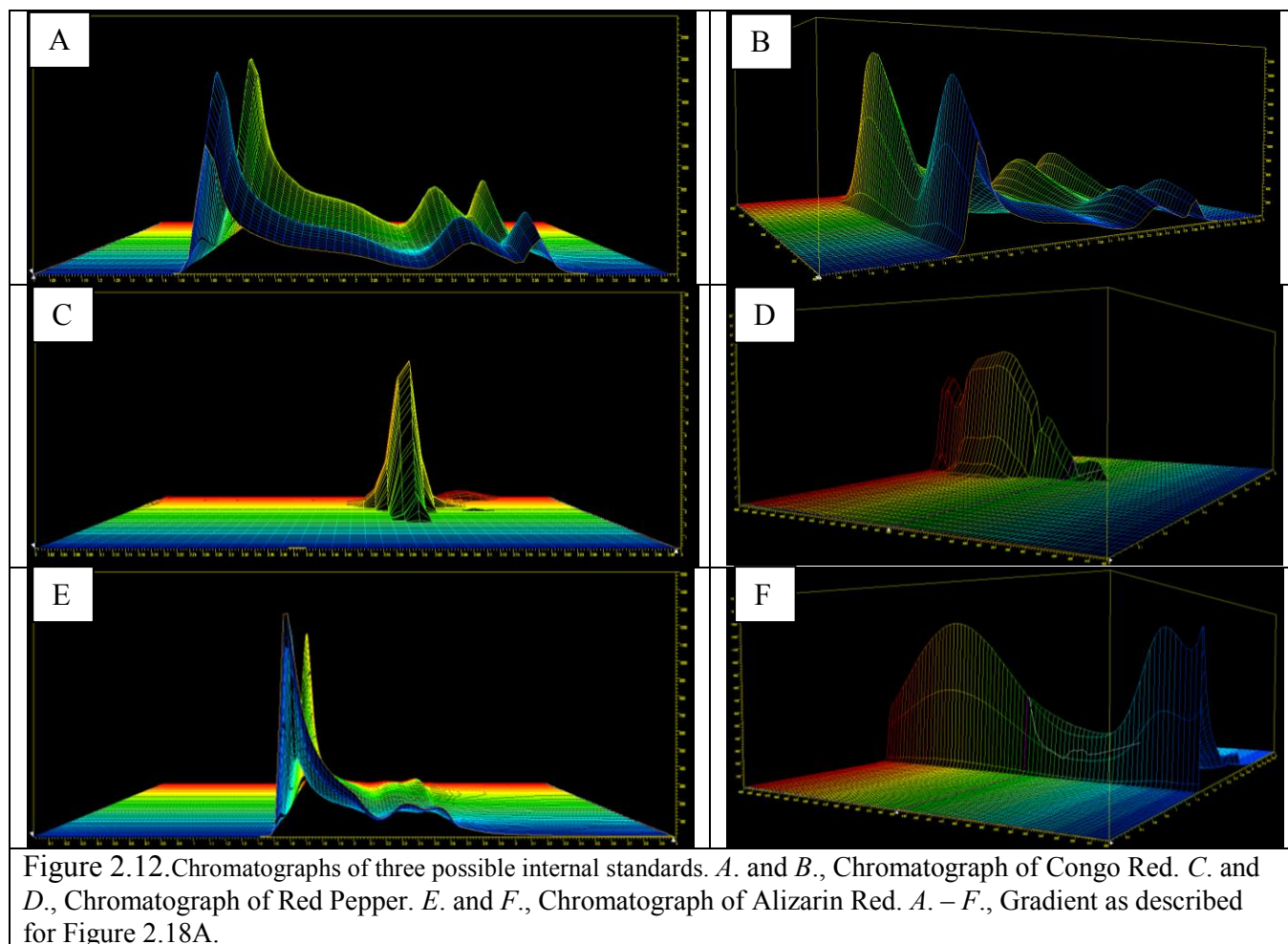


Figure 2.11. Fractions overlaid on 452nm spectra of reverse-phase based HPLC runs. *A.*, Preparative run with 7 fractions. *B.*, Preparative run with 8 fractions.

flexirubin peaks show up from 43 – 57 minutes with the purification runs with the increase of methanol up to 100% from 10 to 60 minutes, but no peaks showed up in the latter range in the 452 nm spectrum. It had then become apparent that the preparative method needed further optimization. However, before performing optimization, time was invested in finding an internal standard which could be of much help for further work.

Fraction	Wet mass (mg)
1	< 10
2	< 10
3	at least 30
4	< 10
5	< 10
6	> 10
7	> 10
8	< 10

Internal Standard Search



During multiple optimizations, it became apparent that an internal standard that had an absorbance near 450 nm but with a different retention time than any flexirubin samples could be very helpful. Three possible internal standards were found in lab based on their color: congo red, red pepper, and alizarin red (Figure 2.12). Of the three, alizarin had the highest absorbance in the 400 – 500 nm range (Figure 2.13E, F). In addition, the red pepper had to be prepared by crushing and then performing a hot extraction into a solvent such as methanol. Many variables with the preparation of red pepper in solution made it an undesirable internal standard. The use of Alizarin red as an internal standard helped to demonstrate problems with a particular method

rather than the flexirubin extract. For example, for a few months a problem was occurring with injections of small volumes. Upon discovering that the needle only lowers to about 7 mm from the bottom of a glass vial by default, alizarin red was utilized to show that small glass vials were necessary for small volume injections. With the small volume problem fixed, time was spent once again trying to further stretch out the multiple flexirubin peaks with various gradients and injection volumes.

Injection Volume and Extended Gradient

Once again, it was baseline separation was attempted with longer gradients and different amounts of material injected onto the column. The more extended gradients with increasing methanol had better separation of peaks. Comparing the separation of peaks can be quite difficult as better divided peaks tend to be more stretched out with less height (Figure 2.12). Fractions were collected to determine whether different molecules were overlapping each other using the longest gradient separation (Figure 2.12E, Figure 2.13A). The fifth fraction of the most optimized run was then separated and another series of fractions were collected. The fifth fraction yielded three peaks which were collected as three fractions (Figures 2.13B, C). The first of the three fractions was then injected on the HPLC. It appears to be mostly one molecule (Figure 2.13E, F, and G). This type of preparative purification may be possible if more materials could be put onto the column initially to increase the efficiency of this method. The sample solvent was once again investigated with the hope that flexirubin extract would be soluble in either DMSO or acetonitrile at a higher concentration. A more concentrated sample would therefore enable more extract to be loaded onto the column per a HPLC run.

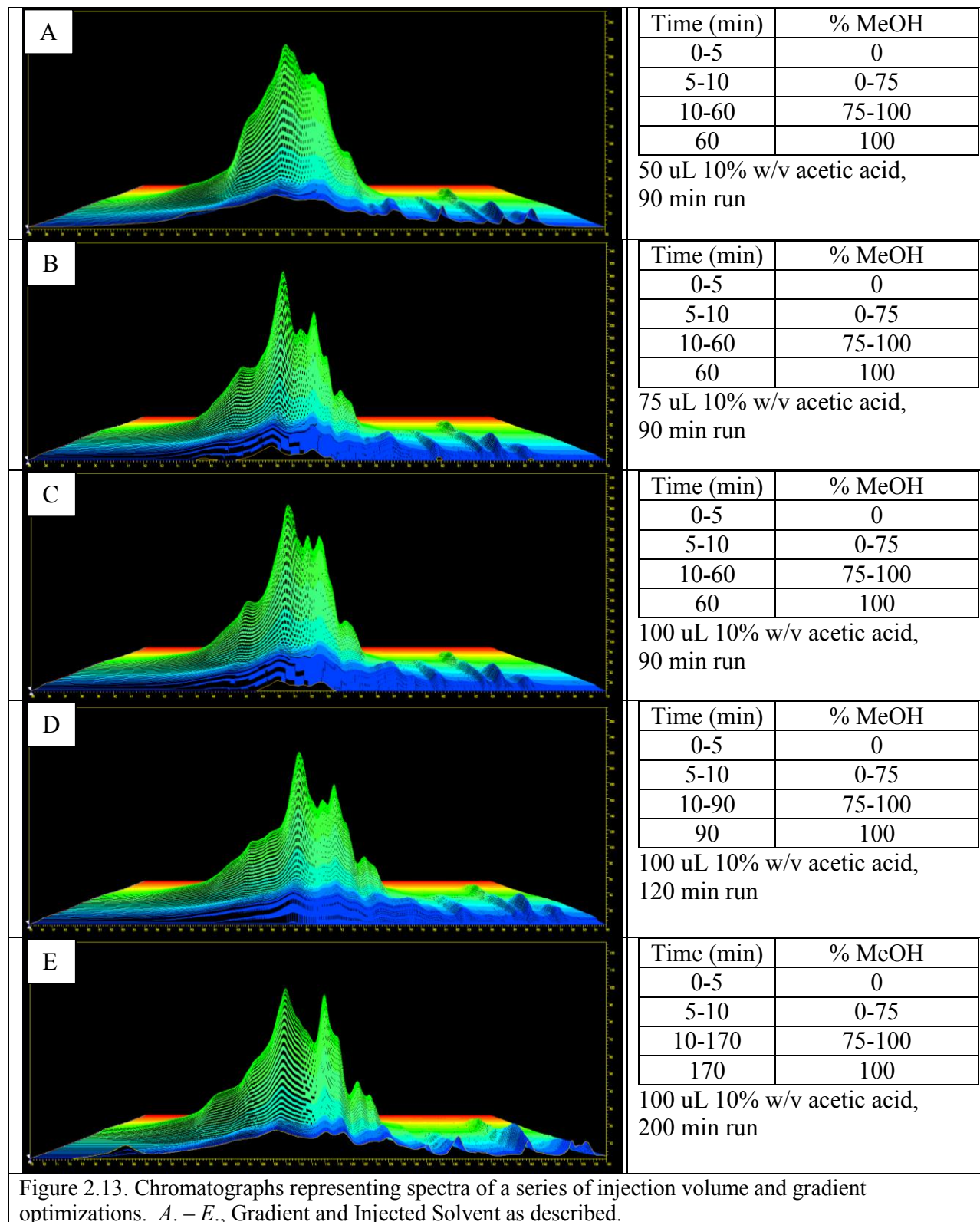


Figure 2.13. Chromatographs representing spectra of a series of injection volume and gradient optimizations. *A. – E.*, Gradient and Injected Solvent as described.

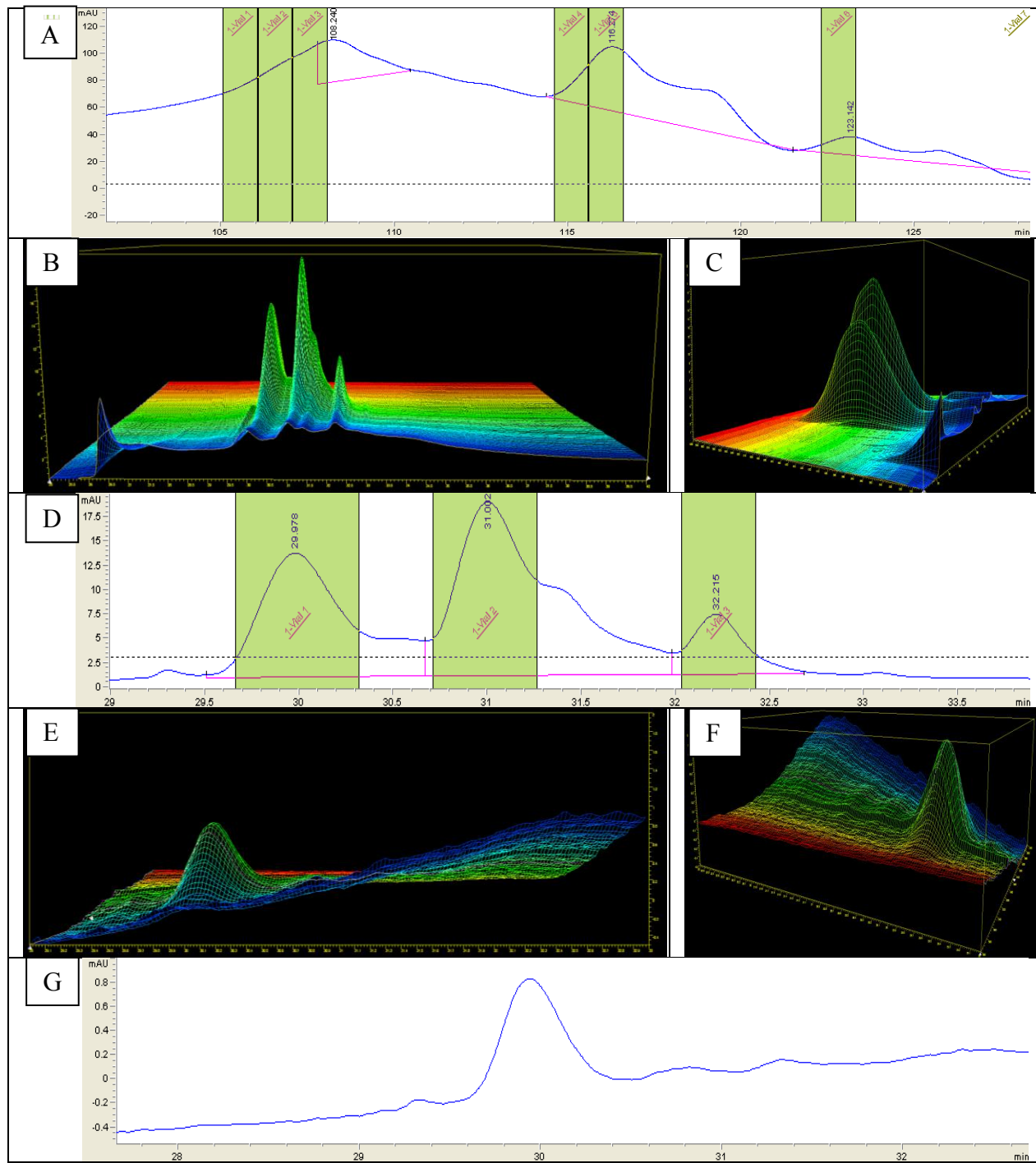


Figure 2.14. Chromatograms representing spectra of a series of collected fractions. *A.*, Collected Fractions for Chromatograms Presented as Figure 2.12E. *B.* and *C.*, Chromatograms of fraction 5 of Figure 2.13A. *D.*, Collected Fractions for Chromatograms Presented as Figure 2.13A and B. *E.* and *F.*, Chromatograms of fraction 1 of Figure 2.13B and C. *G.*, Spectra at 452nm wavelength as shown in Figure 2.13E and F. *A.* – *G.*, Gradient and Injected Solvent as described for Figure 2.18A.

More Sample Solvent Optimization

The use of DMSO and acetonitrile to dissolve the flexirubin extracts was investigated to possibly make more stable and more concentrated samples. Flexirubin extract was soluble at a 20% w/v concentration in DMSO, but was not even soluble in acetonitrile at a 15% w/v solution. Therefore, flexirubin extract was prepared in DMSO as described previously in lieu of methanol at a 20% w/v concentration. The samples were well separated even with 20 μ L injections (~2mg of extract) (Figure 2.15A-D). However, the extract was not stable in DMSO even at about a 15% solution. Sample stability is a key issue when designing automated runs. Samples that fall out of solution may enable precipitates to form and be injected on to the HPLC. A pressure spike caused the third run to fail for this very reason. Therefore, the preparation of extract in DMSO was not investigated further. Instead, the method of preparing the samples in glacial acetic acid at a 10% w/v concentration was continued. Next, the variable of the column temperature was studied briefly.

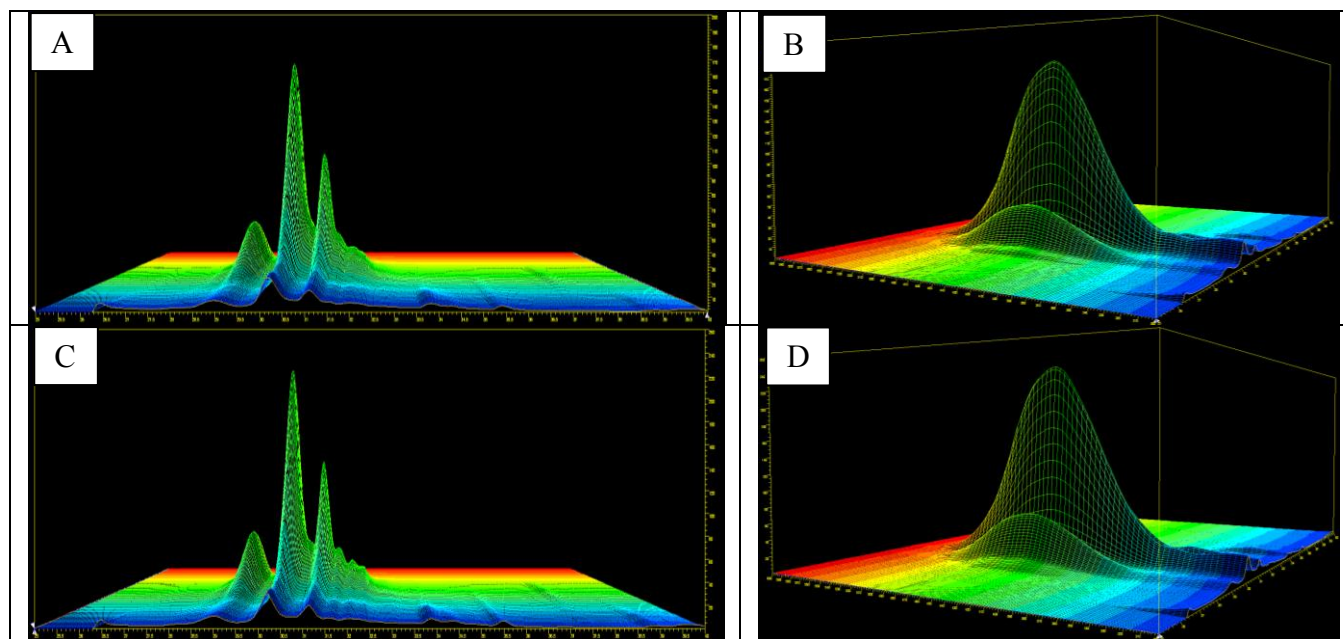
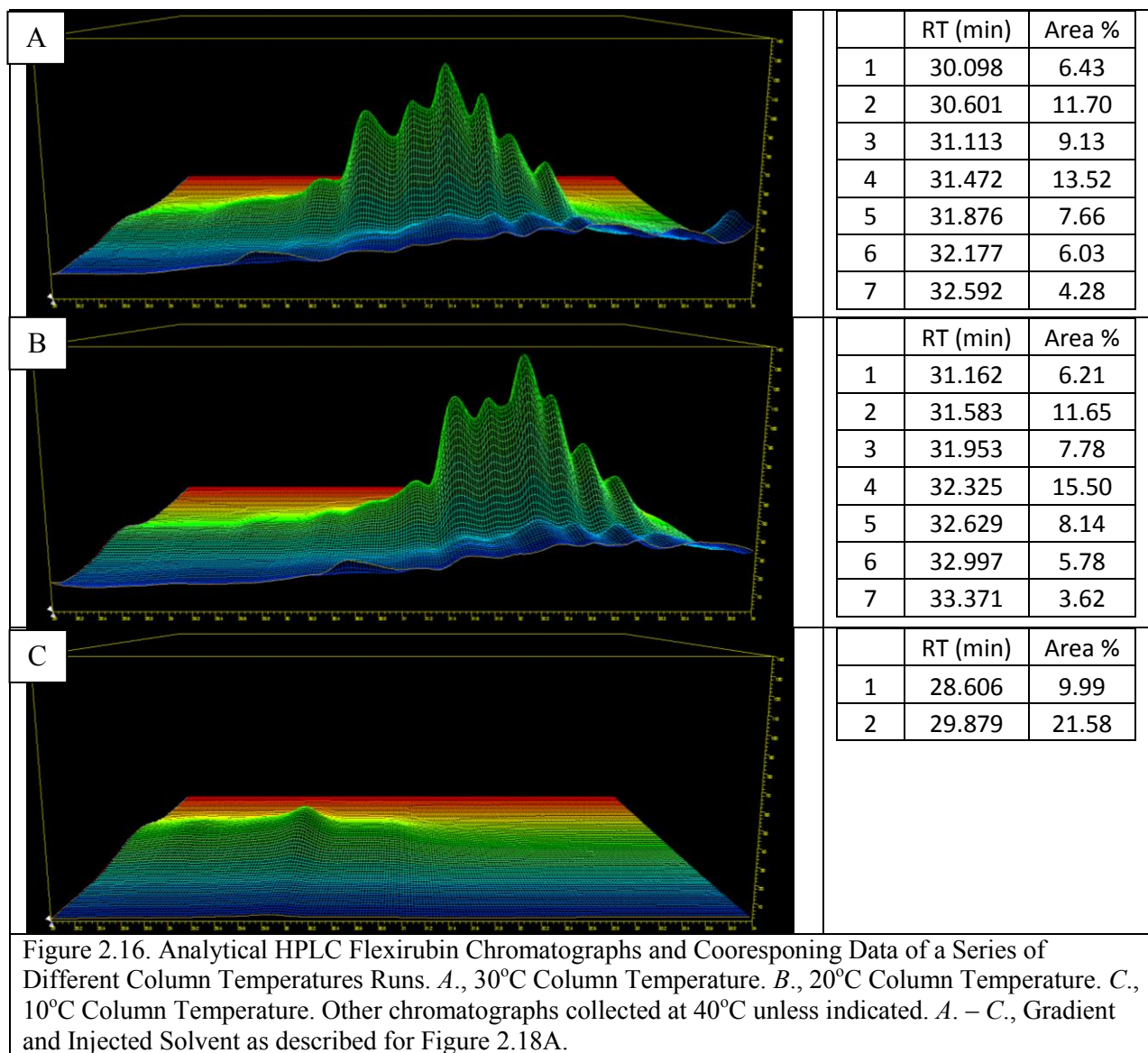


Figure 2.15. Chromatograms of Samples Prepared in DMSO. *A.* and *B.*, First Run. *C.* and *D.*, Second Run. *A.* – *D.*, Gradient and Injected Solvent as described for Figure 2.18A.

Column Temperature

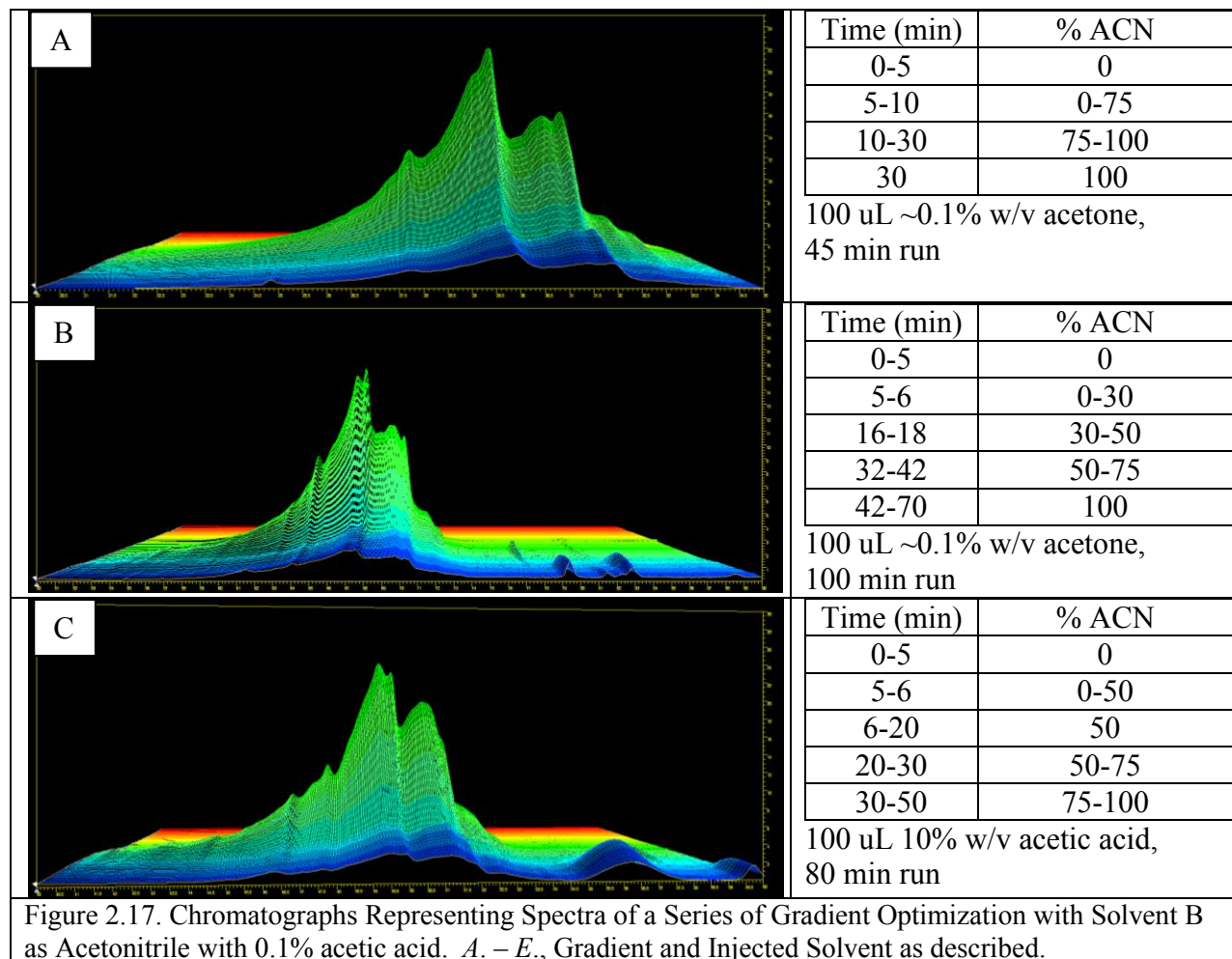


The HPLC column is able to be set at temperatures from 0-80°C. A few runs were completed to determine how the column temperature may affect a particular separation. Usually and as shown before, all other runs were completed at 40°C. Three runs were completed at 30, 20, and 10°C utilizing the same sample. Comparing the 30°C and 20°C runs, the 30°C has less retention by about 0.8 minutes on average per a run (Figures 2.16A, B). However, both spectra were very similar; the area % of each peak were relatively the same. The 10°C column failed due

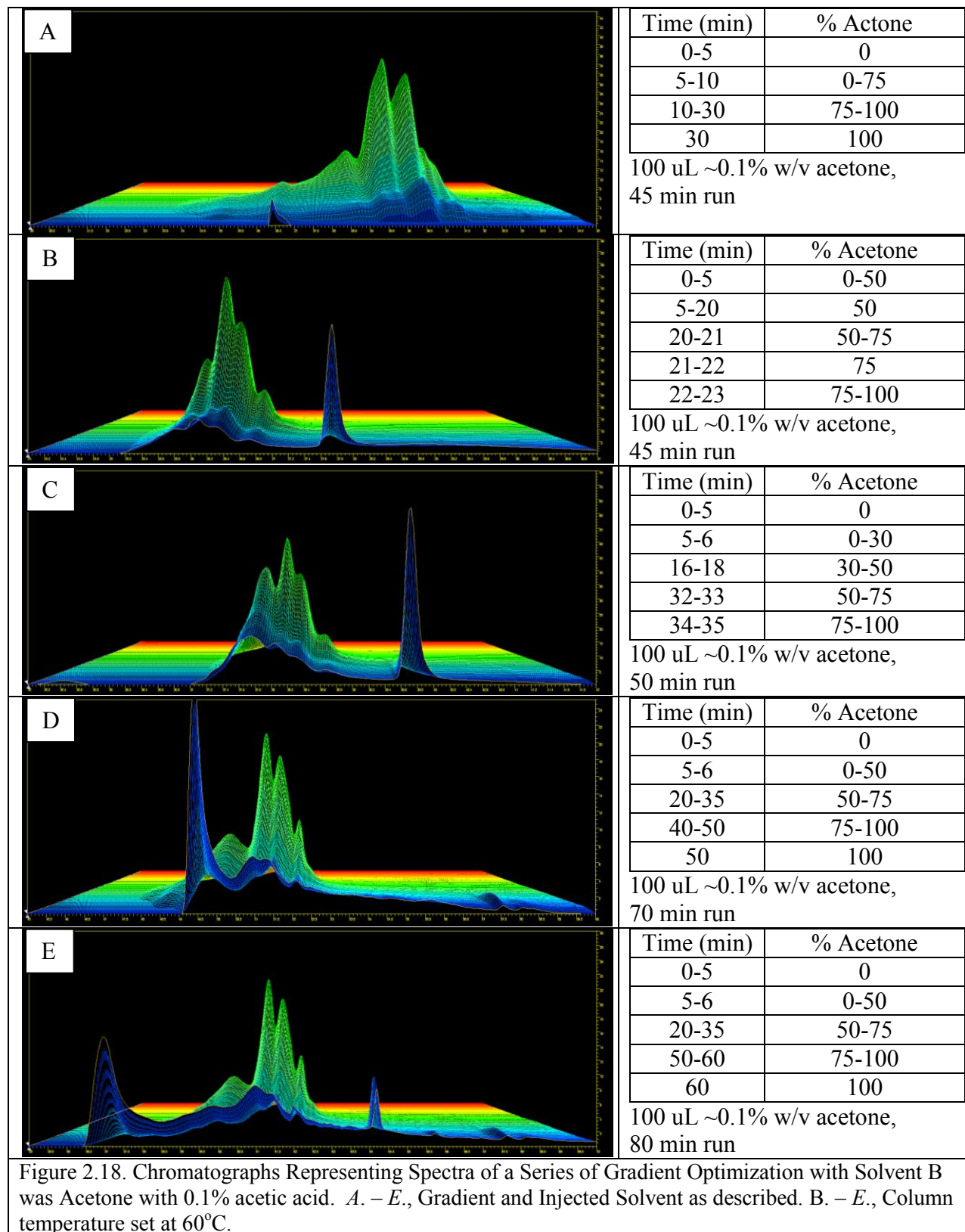
to a pressure spike (Figure 2.16C). At the low temperature, molecules were not able to flow through the column fast enough causing pressure to increase. This particular experiment demonstrated that the column temperature could not be decreased past 20°C at least. The temperature column was then maintained at 40°C for future runs as a decrease in temperature did not have better separation of flexirubin peaks. After looking at the variables of column temperature and gradients, the variable of running solvent was investigated.

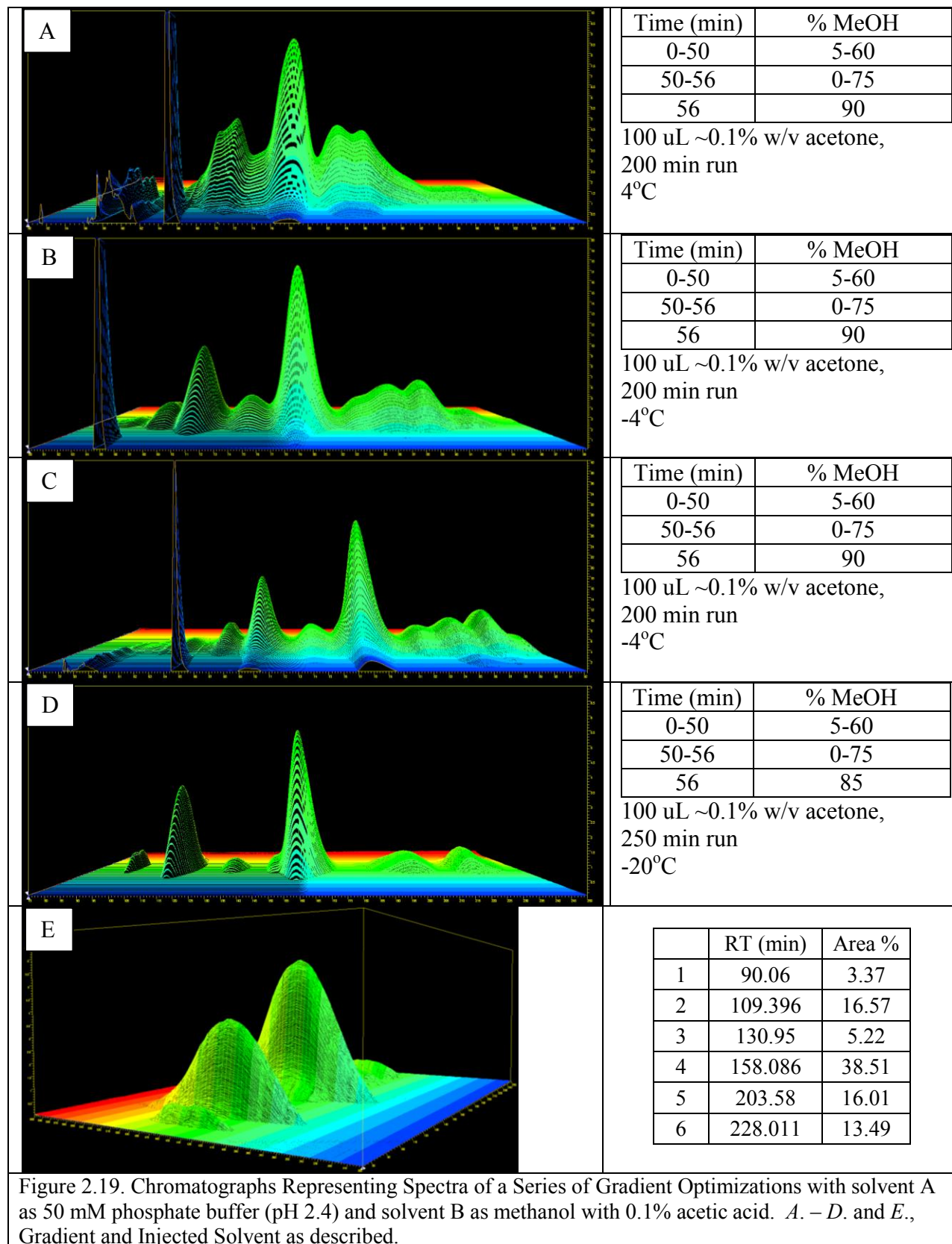
Solvents

The solvents used for a particular HPLC run have a major effect on the separation of the injected molecules. As the separation is dictated by the polarity of the two solvents used in each method, this optimization step held a possible promise to be interesting. The current solvent used for all previous runs was A, water and B, methanol. The next solvent system studied was A, water and B, acetonitrile both with 0.1% acetic acid. The separation was not any better with the solvent change to acetonitrile and water, but arguably appeared to be worse. As compared to the previous solvent, the peaks seemed to be trailing and overly stretched out. Better separation was seen with slower and longer gradients as suggested before. Of the various gradients, the 14 minutes at 50% methanol may have aided in the better separation seen in Figure 2.17C compared to Figure 2.17A and B in addition to the other longer gradients. With the separation no closer to baseline, the solvent change to acetonitrile and water was not desirable. After these few spectra were collected based on acetonitrile and water, another new solvent system, acetone and water, was studied. The new solvent system of acetone and water with 0.1% acetic acid had better separation than the use of acetonitrile and water. This can be easily seen by comparing the first run of each solvent system (comparing Figures 2.17A and 2.18A). The chromatographs based on acetone and water had two major peaks. The first major peak was separated down to a third by a



preceding peak, whereas the whole complex of the analogous acetonitrile and water run had less distinct peaks. The series of optimizations had nearly similar separation and neither had achieved baseline separation that was desired (Figure 2.18B-E). With the lack of baseline or nearly baseline separation, another solvent system needed to be designed. The next solvent system tried was A, 50mM phosphate buffer (pH 2.4) and B, methanol with 0.1% acetic acid.

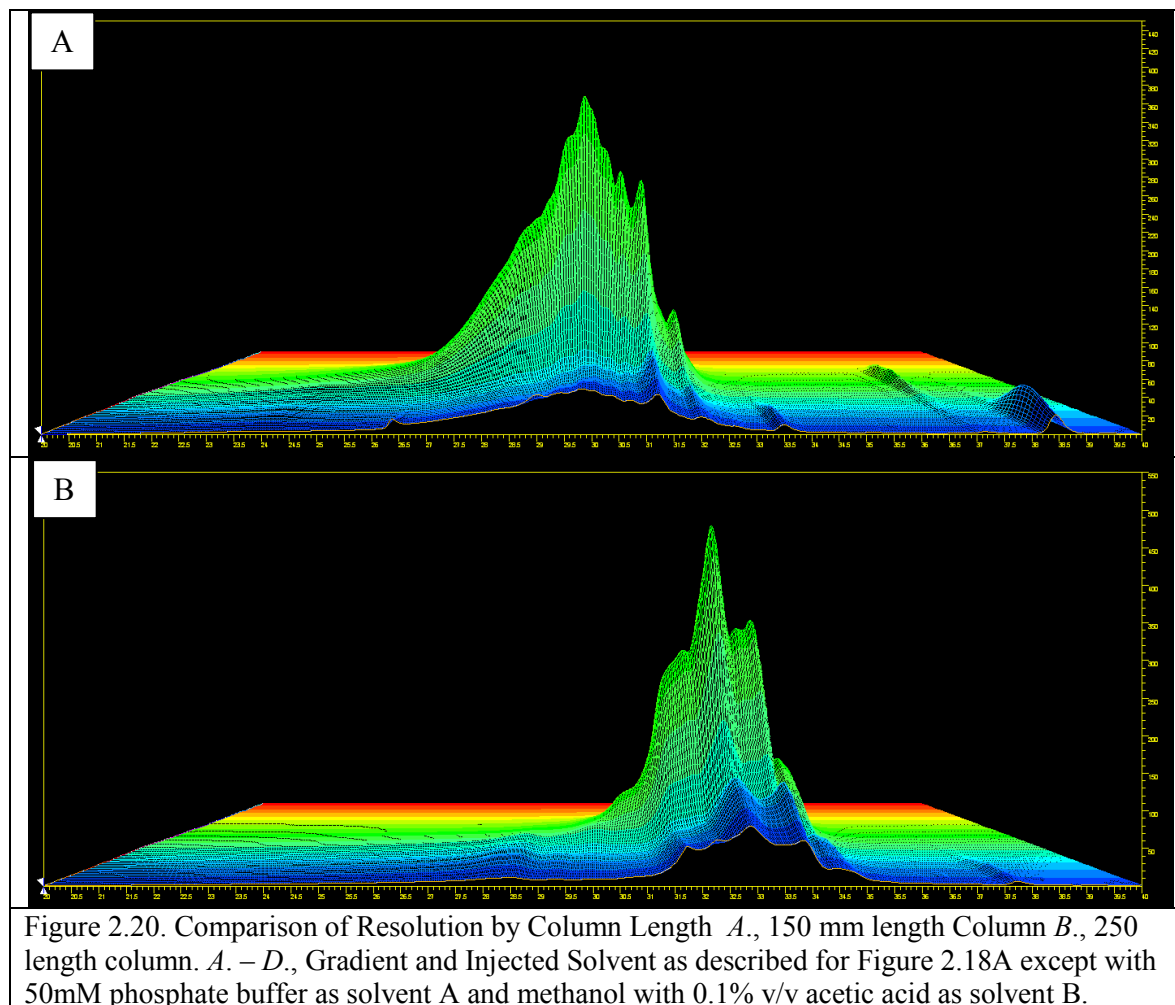




The solvent system of low pH phosphate buffer and methanol with an organic modifier of acetic acid finally showed better separation. The amount of separation, about 30%, between the major peak from adjacent peaks of the first run demonstrates this better separation (Figure 2.19A). The first three runs of the optimization series showed that near baseline separation was achieved for the sample that was allowed to come to room temperature after remaining at -80°C (Figure 2.19A, B, and C). The data presented for these three runs may be misleading as the temperature of the injected sample should have little effect on its separation. Finally, after 9 months of optimizations, baseline separation was achieved, albeit for small injection samples (Figure 2.19D and E). The optimized small scale run (100 uL of a ~0.1% w/v concentration) shows 6 well separated peaks. While the baseline separation was encouraging, 1200 runs of the small scale runs would have to be run to collect about 10-12 mg of material of the major peak. 1200 runs would not be possible due to time constraints and the excess use of materials. Therefore, the same baseline separation needed to be achieved with larger amounts of material on the column. The best way move towards this goal was to extend the length of the column.

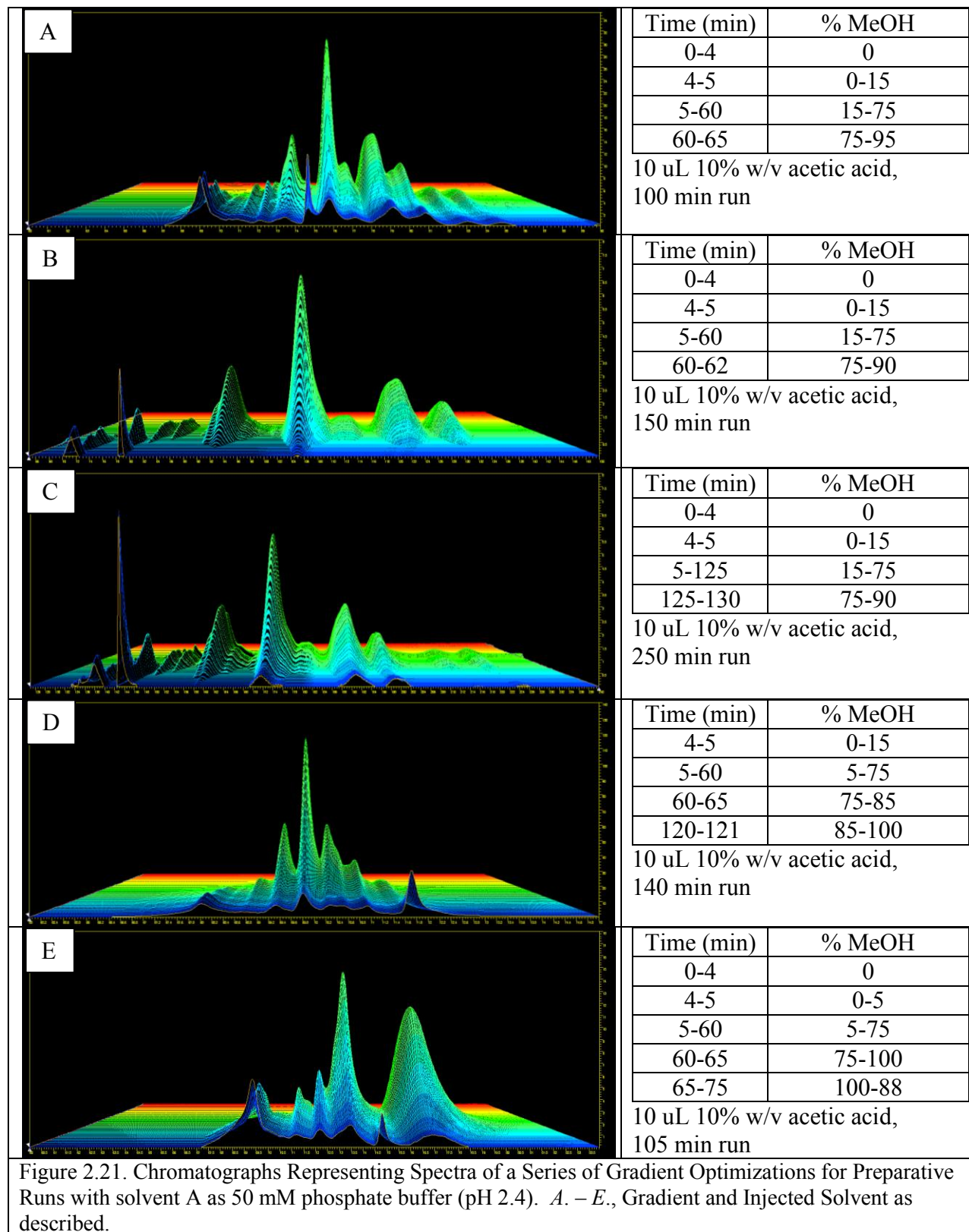
Column Length

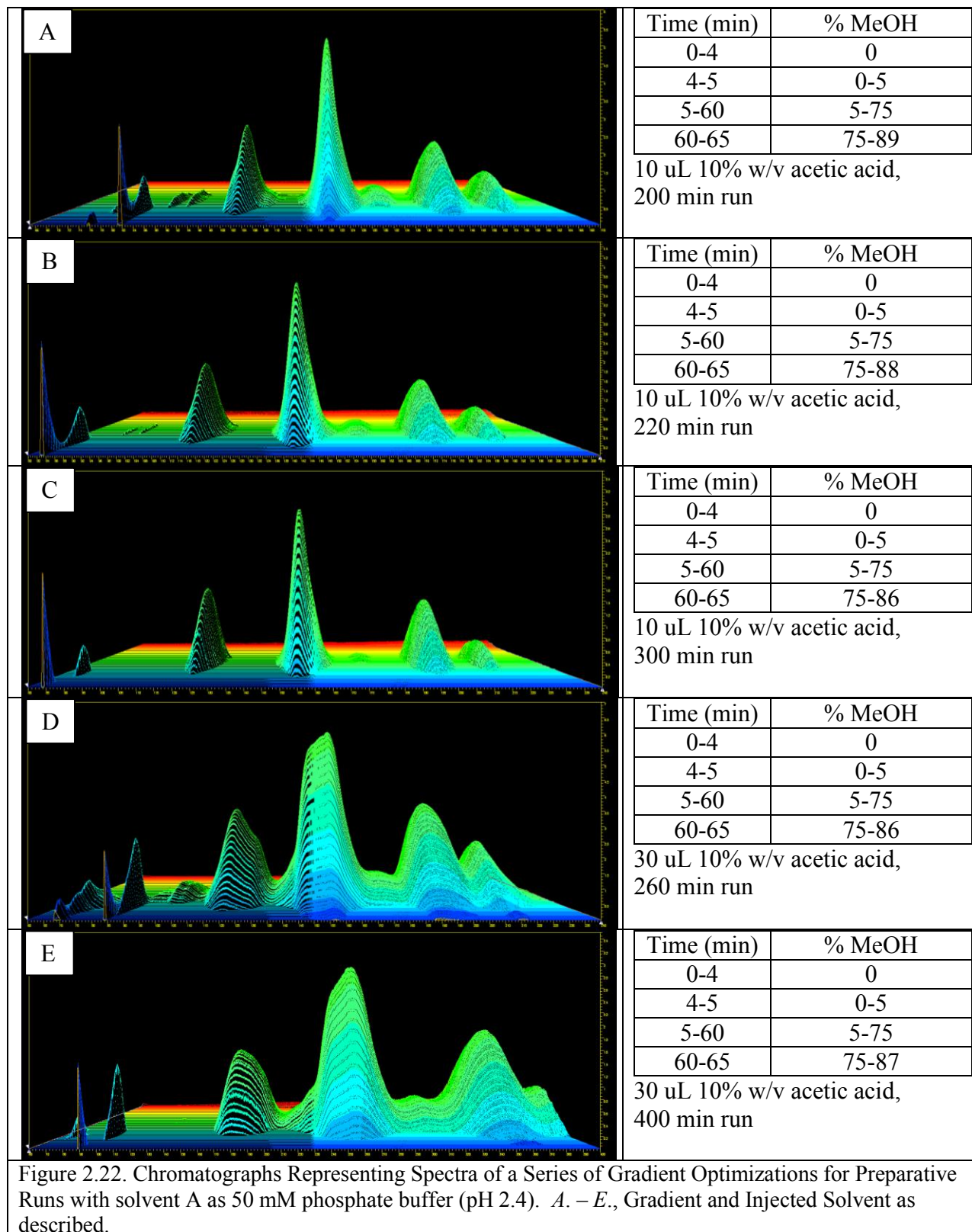
Column Length was the last variable studies for this HPLC method optimization. As shown in Figure 1.10, more than a 60% better resolution is possible with the 250 mm column as compared to the 150 mm column. An experiment was performed to see if better resolution could be observed with the change out to the longer column. Comparing the lowest absorbance between adjacent peaks, the major peak has 15% better separation with the longer column. However, the separation of other minor peaks is difficult to compare. The next planned step was to increase the amount of material injected on the column with a similar method as used to achieve the baseline separation observed previously the small scale (Figures 2.19D and E).



Upgrade to Preparative Runs

Specifically, the goal was initially to achieve baseline separation for at least 1 mg of extract and then to increase that amount if possible. The optimization of the large scale separations was much more straightforward with the knowledge of about 5-6 major peaks present in the *C. oranimense* extract (Figure 2.19D and E). The key to this series of optimizations was finding the eluting percentage of methanol that enabled baseline separation but still kept the run at a minimum time. The shorter the time, the more efficient the optimized run would be. In addition, the shorter the run, the higher the separated peaks would be; and the easier it would be to collect them in fractions. Initially, a percentage at 95%





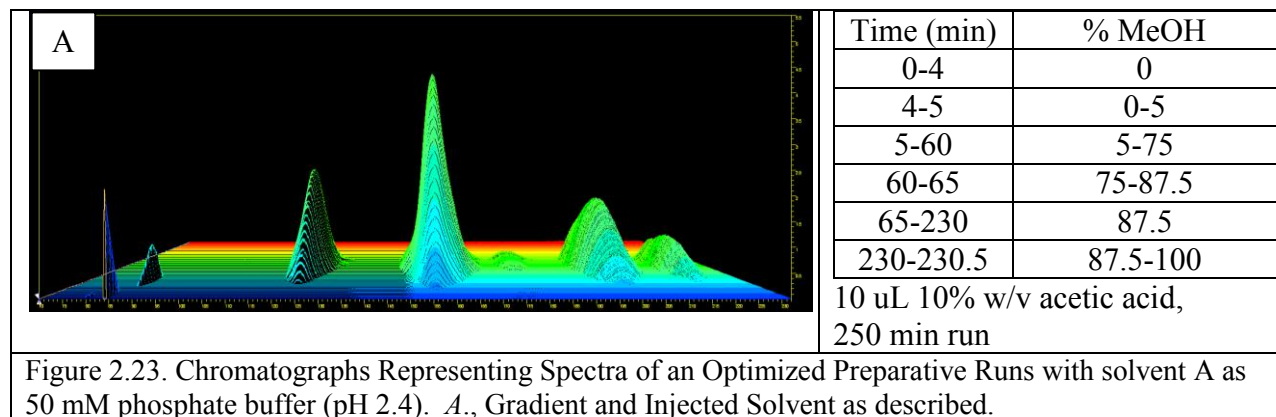


Figure 2.23. Chromatograms Representing Spectra of an Optimized Preparative Runs with solvent A as 50 mM phosphate buffer (pH 2.4). *A.*, Gradient and Injected Solvent as described.

methanol was tried, but the separation was lacking (Figure 2.21A). 90% , 89%, and 88% methanol were close, but did not yield baseline separations (Figure 2.21B and C, Figure 2.22A and B). The 86% methanol run did have a baseline separation (Figure 2.22C). When the material injected onto the column was increased from 1 mg to 3 mg, baseline separation was not attained at either 86% or 87% methanol (Figure 2.22D and E). Baseline separation of 1 mg of extract was achieved at a eluting percentage of 87.5% methanol (Figure 2.23A). Two runs were attempted in which the eluting percentage was decreased to increase the retention time of the later eluting molecules, but neither were successful (Figure 2.21D and E). With the optimized dichotomy of 1 mg of extract and an eluting 87.5% of methanol figured out, finally multiple preparative runs could be completed and fractions collected.

General Discussion

After performing this optimization, it became apparent that a flow path for future optimization of preparative HPLC methods would be very helpful. First, an efficient method of extraction of the compound from its microbial source must be determined. Usually and as was the case for this study, the extraction can be found in literature sources. Second, an efficient sample preparation must be determined as well. The sample needs to be prepared in a solvent of

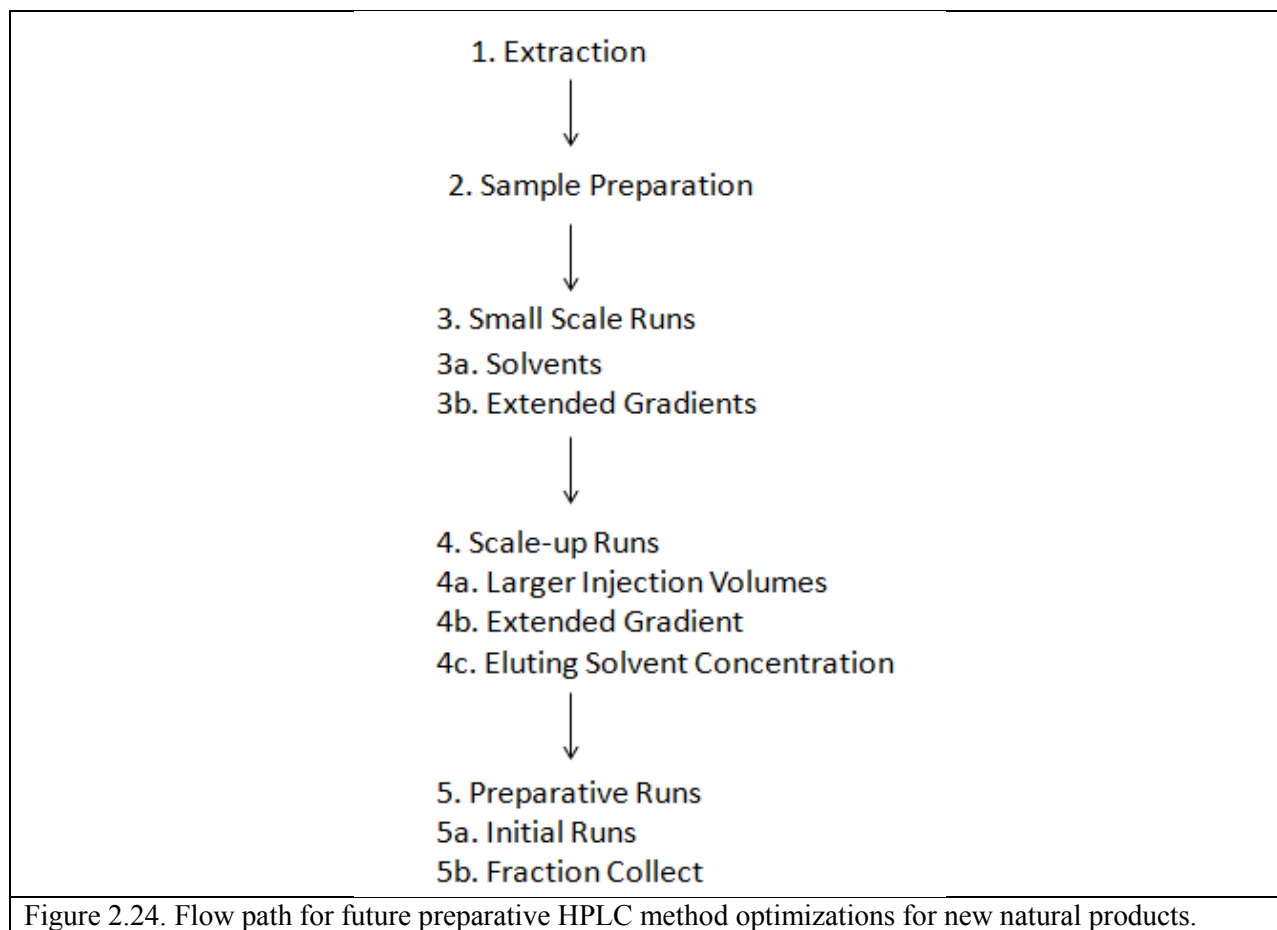


Figure 2.24. Flow path for future preparative HPLC method optimizations for new natural products.

which it can be highly concentrated in and stable at room temperature (for HPLC injection) and at 4°C (storage in refrigerator). The first HPLC runs attempted need to be done at a small scale. Specifically, only 0.1 to 0.5 mg of prepared extract should be injected onto the HPLC for initial runs. Small scale runs ensure that minimal changes in peak separation will be observed when variables are changed. The first variables to be changed should be solvent and the solvent gradient. The first solvent tried should be water (A) and methanol (B) or 50 mM phosphate buffer (A) and methanol (B) if ionizable groups are expected on the compound under study. The first solvent gradient with these two solvents should be as described in Figure 2.18A. A few runs with gradients longer by 15-30 minutes per the last increase of methanol should be attempted with this first solvent. The series of longer solvent gradient should then be attempted with other

solvents such as water (A) and acetonitrile (B) or 50 mM phosphate buffer (A) and acetonitrile (B); and water (A) and acetone (B) or 50 mM phosphate buffer (A) and acetone(B). The solvent and solvent gradient with the best separation should then be used to achieve baseline separation by further extending the solvent gradient if necessary. Once a reliable solvent and solvent gradient has been optimized a small scale, larger volume should be utilized so that up to 1 mg of extract is injected on the column. As the volume of material increases, the gradient will need to be extended or the eluting concentration of the organic solvent may need to be modified. As before, once the scale-up runs again have baseline separation, preparative runs should then be optimized in which up to 10 mg of extract are loaded onto column. However, a scale up to 3 mg from 1 mg is much easier than to the full 10 mg; the gradient and eluting organic solvent concentration will only need slightly modified. For any 4.6 mm ID columns, any amount of material past 1.5 mg starts to enter the realm of column overloading. Column overloading is only efficient and therefore necessary if time and solvent is saved by using this option. Once an optimized run has been designed in which less than ten runs will need to be run to collect 10 mg for NMR, fractions should start to be collected. At the scale of preparative runs, the amount of solvent used and the amount of time per run needs to be as minimal as possible with the most amount of baseline separated material.

- Do not run the column at temperatures below 20°C nor above 40°C.
- Samples must be stable at room temperature and kept away from direct light.
- All purified fractions should be pooled accordingly, dried, and put under an inert atmosphere as quick as possible.
- Always double check the configuration of the fraction collector vials before starting a run in which fraction collected was selected.
- Any samples less than 7 mm high in the HPLC vials must be loaded into the glass inserts for injections.

Figure 2.24 Cautions when using the Agilent 1200 Series HPLC.

While either optimizing a HPLC run or running optimized HPLC runs, the user needs to adhere to the listed cautions in Figure 2.25. Following these warning ensures the longevity of the utilized column and HPLC and the quickness of the optimization itself.

Ch. 3. Purification and Structural Determination of *C. oranimense* peaks

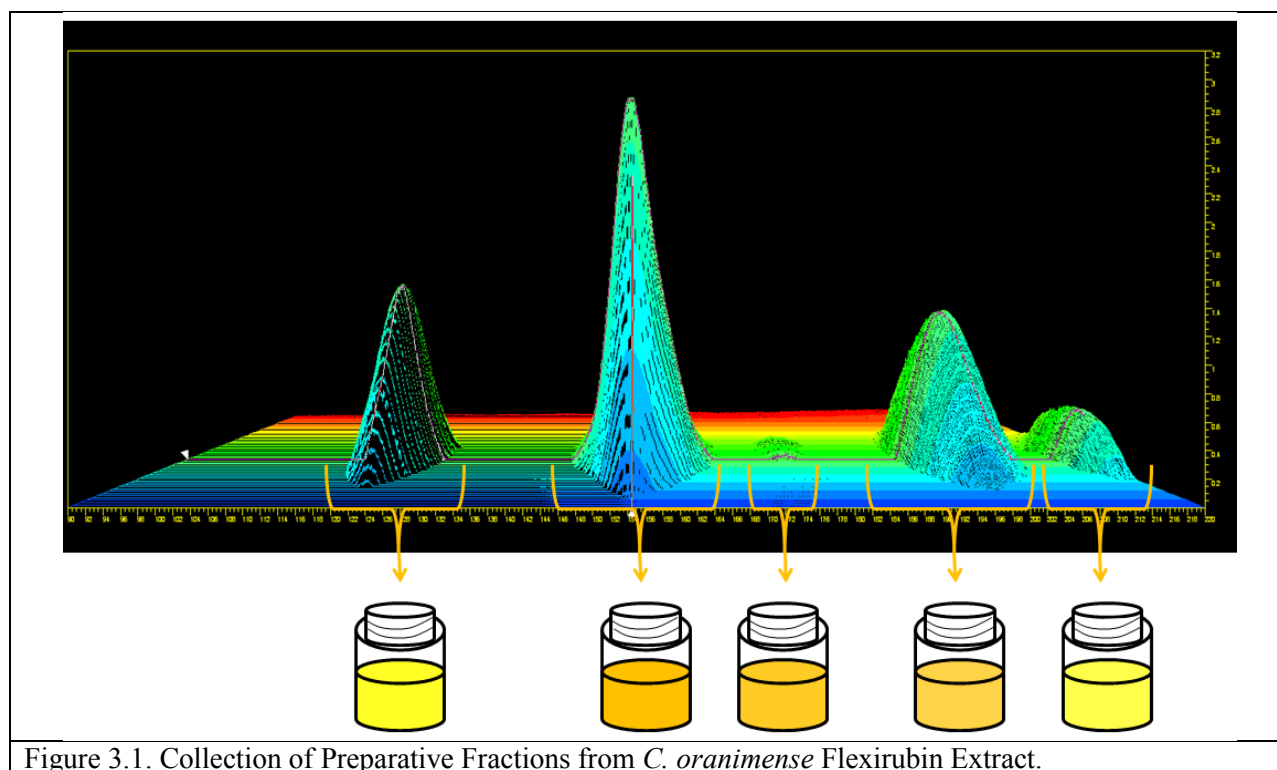


Figure 3.1. Collection of Preparative Fractions from *C. oranimense* Flexirubin Extract.

With the optimization of the preparative HPLC runs for *C. oranimense* completed, the method could finally be utilized to collect the peaks for structural analysis (Figure 3.1).

Preparative fractions were collected by separation of flexirubin molecules via reverse-phase HPLC using a 50mM phosphate buffer (A) and methanol with 0.1% acetic acid gradient (B) solvent gradient (0-4 minutes, 0% MeOH; 4-5 minutes, an increase to 5% MeOH; 5-60 minutes, an increase to 60% MeOH; 60-65 minutes; 87.5% MeOH, constant 87.5% MeOH for 65-230 minutes, 230-230.5 minutes, an increase to 100% methanol which remains constant for remainder of the 250 minute run) with a 10 μ L sample injection (prepared at a 10% w/v solution in glacial acetic acid). Fractions were collected per the “time-based” option or according to the total time elapsed since the start of the analysis (3 fractions collected from 114-129 minutes, 4 fractions collected from 145.5-165.5 minutes, 2 fractions collected from 172-179 minutes,

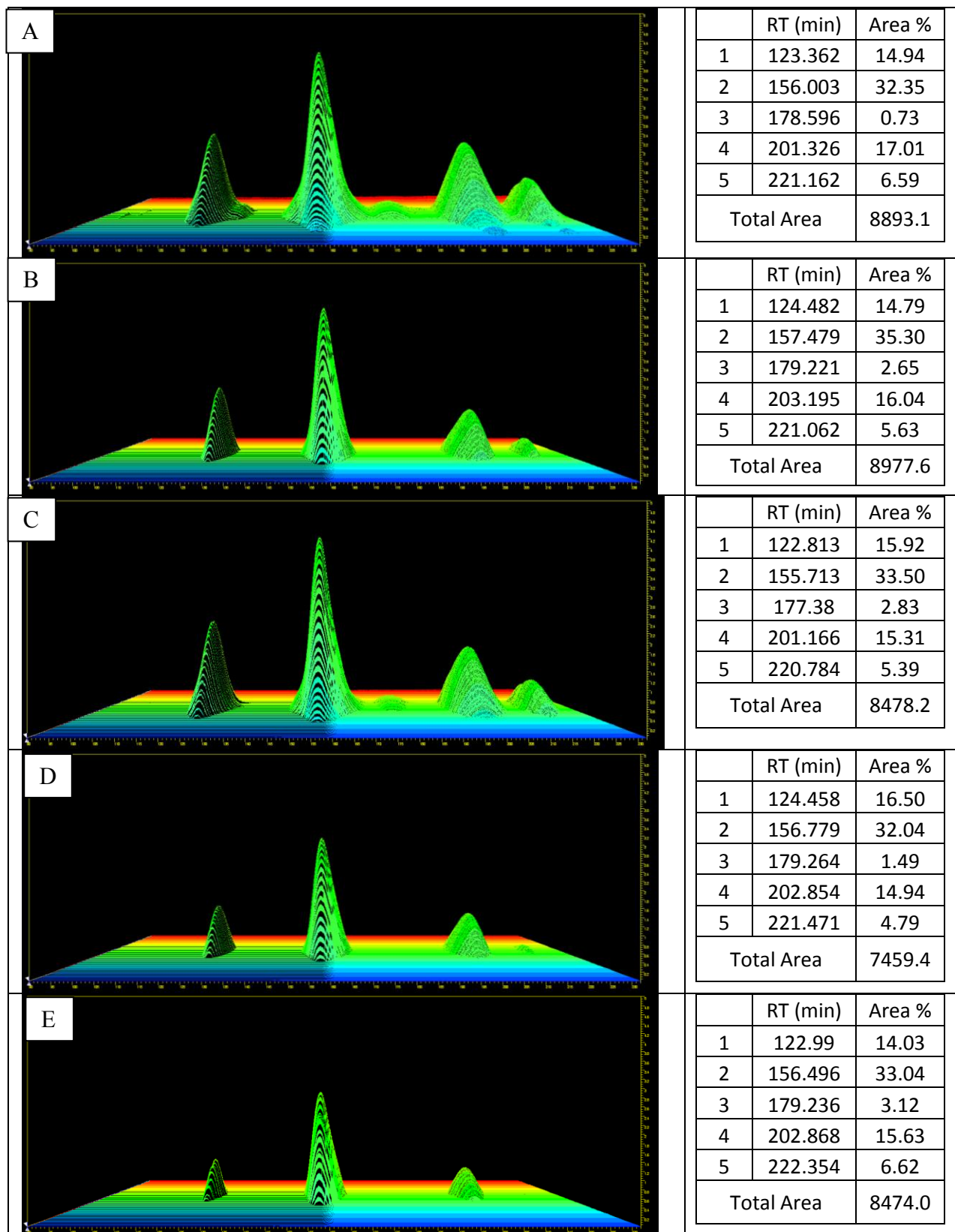


Figure 3.2. Preparative HPLC *C. oranimense* Flexirubin Chromatographs and Corresponding Data. A. - E., based on method described in Figure 2.23A. Total Area given in as mAU*sec.

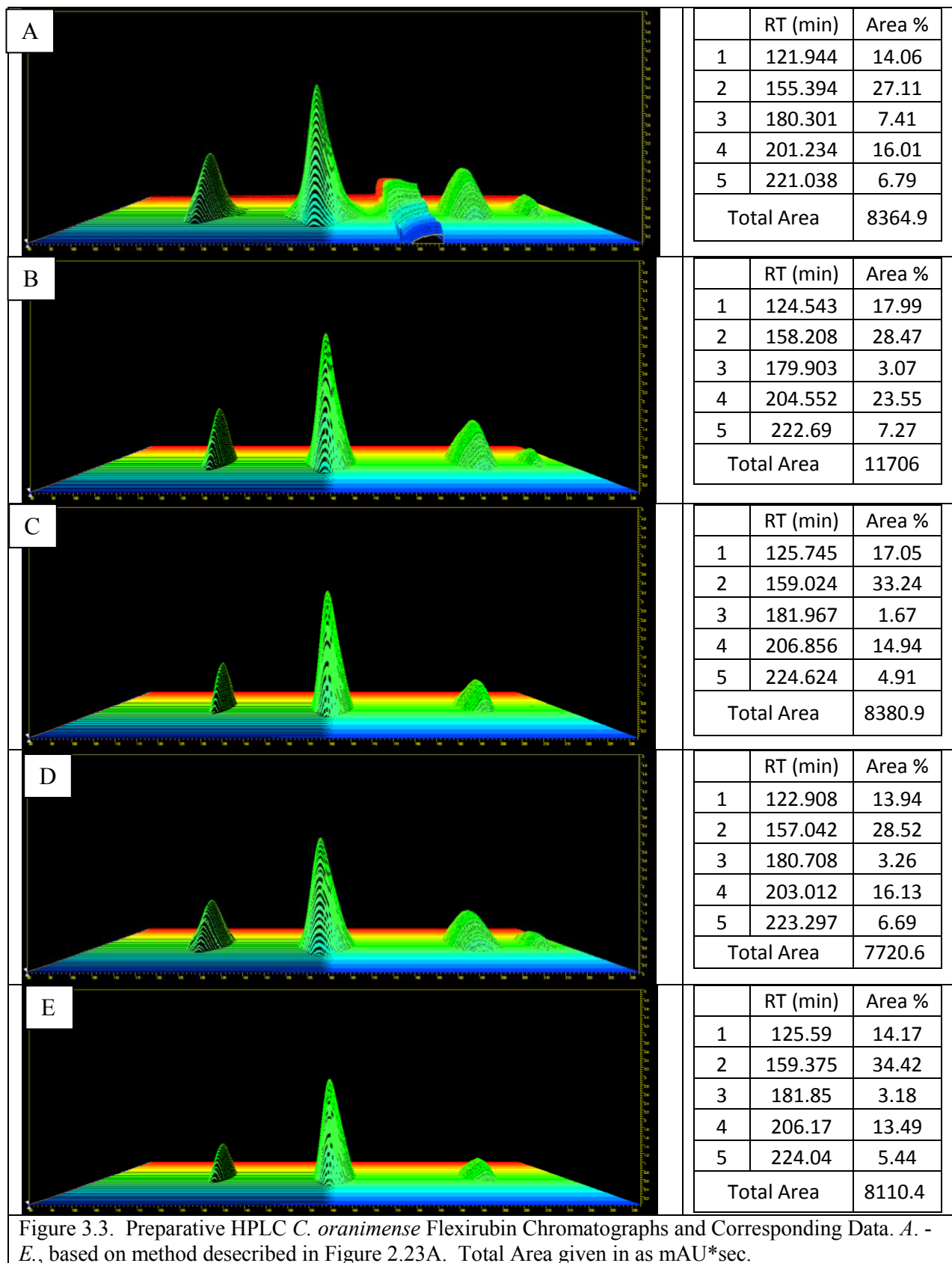
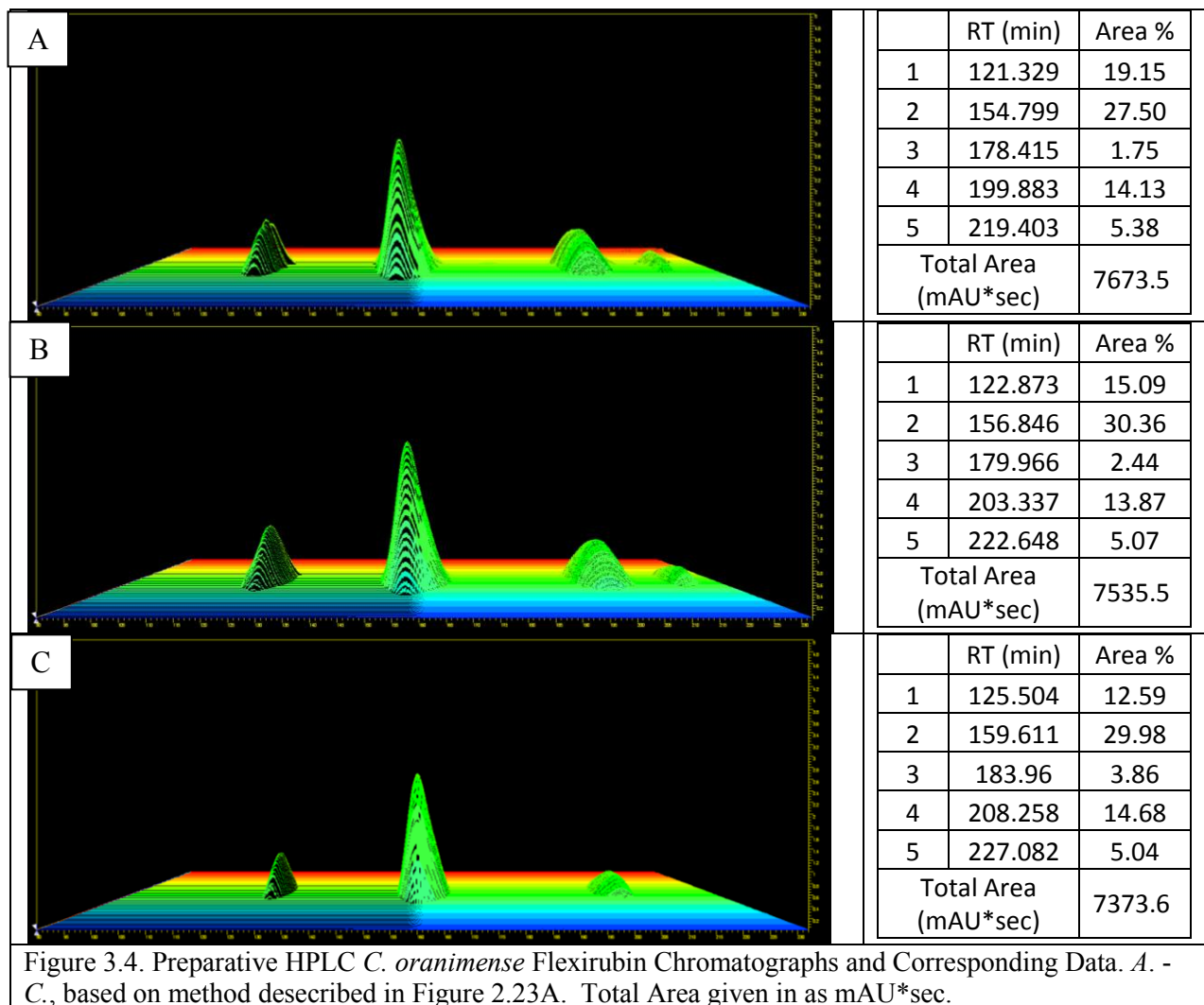


Figure 3.3. Preparative HPLC *C. oranimense* Flexirubin Chromatographs and Corresponding Data. A. - E., based on method described in Figure 2.23A. Total Area given in as mAU*sec.



4 fractions collected from 190-210 minutes, and 2 fractions collected from 215-225 minutes).

The peak specific fractions were pooled accordingly and solvent removed by drying and subsequent vacuum pumping of each fraction before analyzing on the NMR.

Currently, 13 preparative runs have been completed. An estimated 3.25 mg and 2 mg of the major peaks (the second and fourth in preparative chromatographs) should be purified, respectively. The runs are reliable with few exceptions. Most have total areas of about 8000 mAU*sec and a consistent percentage peak area. Interestingly, the retention time does seem to be slightly variable to about 2 minutes per individual chromatographs. The dissimilarity of the RT

and any peak percentage areas may be due to errors of the manual integration. Overall, the optimized preparative run is reliable, but more runs need to be completed before the structural analysis can be underway.

The pooled second fraction, containing the major peak, was prepared for NMR after drying in the hood over a week. A white layer had formed in the bottom of the beaker of the pooled fraction. The extract that was soluble in CDCl₃ was put on the NMR (Figure 3.5). The RG value was about 1290 indicating a low concentration of the molecule. The major peaks at 7.3 and 1.58 ppm are solvent, so only two peaks at 2.19 and 1.27 represent Flexirubin components, specifically the alkyl chains. After working up the NMR, it was realized that the white layer is precipitated phosphate from the 12.5% of the 50mM phosphate buffer that would be eluting along with the collected flexirubin fractions. An additional step in the purification was designed for the pooled fraction. The pooled fractions will be dissolved in a small volume of chloroform and larger volume of water. The phosphate precipitates will then be dissolved into the water

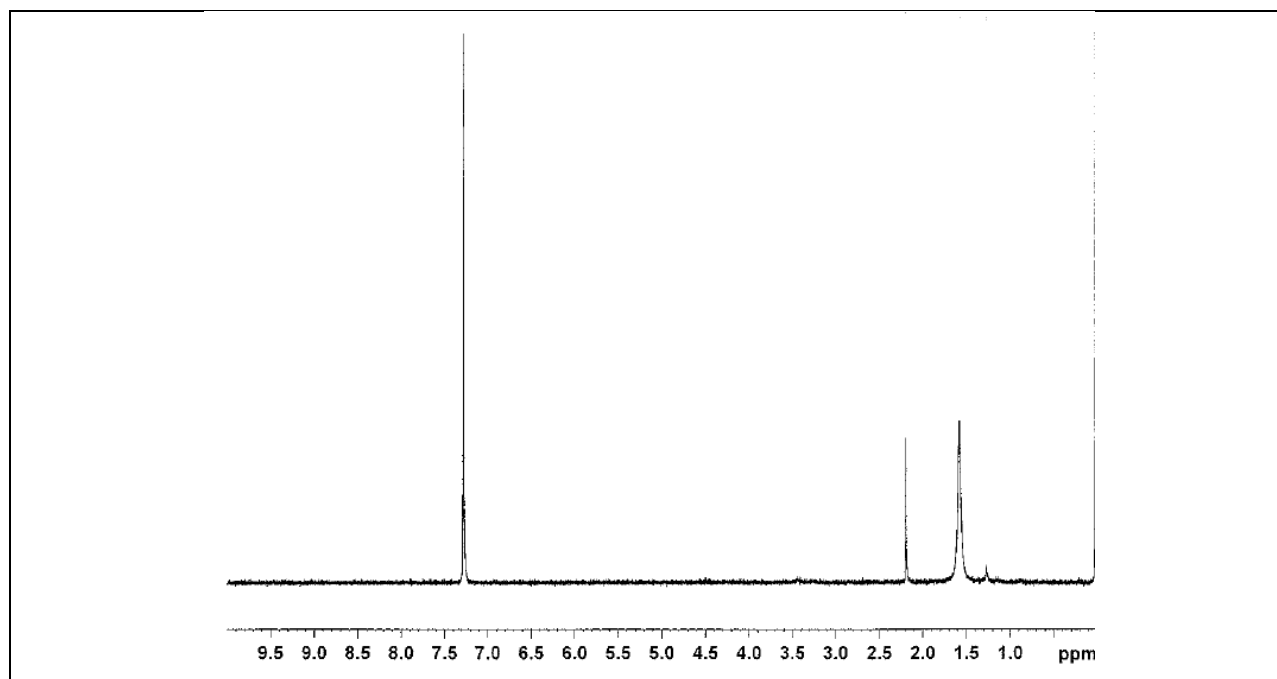
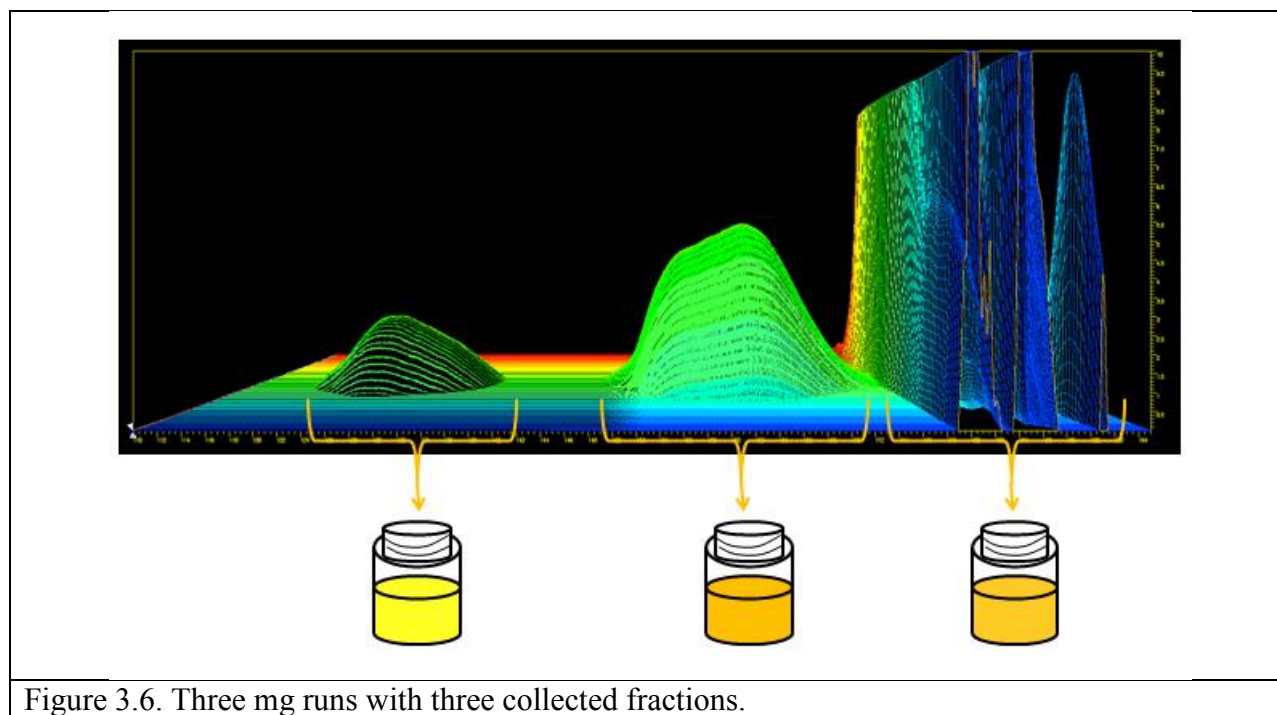


Figure 3.5. ¹H NMR Spectrum for peak 3 fractions. Produced after 64 scans on Bruker Avance 300 MHz NMR.

layer while the flexirubins will dissolve into the chloroform layer. This will be repeated three times. The chloroform layers will then be pooled and dried down to repeat the NMR once more material is purified.

A new method with column-overloading had been designed to enable faster collection of fractions. 3 mg runs were optimized so that about ten runs would be needed to have a sufficient amount of material for NMR of the major *C. oranimense* peak (Figure 3.6). As described earlier, the maximum loading capacity for the utilized column is 1.5 mg. Therefore, the injection of 3 mg utilizes the scale-up factor of column overloading. As the flexirubin have relatively poor solubility in methanol of only up to about 1%, volume overloading was utilized. This could be noticed especially with the second peak as it seems to be becomes more rectangular at its maximum height. In addition, at 175.5 minutes, at the end of the second peak eluting off the column, the methanol concentration increases to 100% so that the remaining non-separated *C. oranimense* peaks are collected in 3 fractions for later separation. With this



modification, the runs are about 3.25 hours long instead of 4.25 hours. Ten runs were completed with this method; therefore, the first pooled fraction should have 4.5 mg of a purified flexirubin and the second pooled fraction should have about 7.5 mg of purified flexirubin. The phosphate buffer was removed from the pooled fractions as described above. Briefly, a 10% volume of HPLC grade water was added to the pooled fraction. This addition of water was necessary so that the phosphate could be seen as cloudiness. About 5% volume of chloroform was added to the mixture, mixed in a separatory funnel, and collected. This was completed three times. The chloroform layers were pooled as collected and then dried via a rotovap and further with 2 hours on the vacuum pump. NMR spectra were not able to be obtained due to current problems with the NMR.

Future Work

The future work to complete the study of *C. oranimense* flexirubin structures is to analyze the purified structure and collect more material if necessary to perform this analysis. The NMR spectra, mass spectrum and IR spectra data will then be used to determine the structure of at least the two first peaks of *C. oranimense*. The collected non-separated peaks should then be separated to purify and collect the second major peak that eluted with this set of peaks. The structural analysis should then be completed as well. Then, KOH should be added to a small portion of each remaining fraction to investigate the bathochromic shift via UV-Vis, IR, MS, and NMR spectra.

Ch. 4. Variation of Flexirubin Pigments

A key to this project was to determine if flexirubins have a chemotaxonomic value as suggested before (Reichenbach *et al.*, 1974). This chapter describes an experiment in which flexirubin extracts were prepared from 25 different species and at least partially separated simply for detection with an analytical scale HPLC method.

The extracts were prepared similarly as described earlier. Briefly, 24 species (*C. shigense*, *C. soli*, *C. greenlandense*, *C. "gleum"* NRRL B-14798, *C. diehli* BLS 98, *C. joostei*, *C. vrystaatense*, *C. luteum*, *C. novum* JM1, *C. novum* FH2, *C. aquaticum*, *C. piperi*, *C. soldanellicola*, *C. angstadi* KM, *C. jejeuense*, *Epilithonimonas tenax* DSM, *E. diehli* FM1DSM, *E. lactis*, *F. frigidimaris* JRR, *F. frigidimaris* EED, *F. frigidimaris* KMA, *F. novum* KJJ, *F. granuli*, and *F. novum* R30-53) were grown up either overnight or until high cell density at 25°C in TSBA. Cultures were centrifuged and the media was decanted. Up to 10 mL of acetone was added to each cell pellet depending on the proportional size of each. After at least 10 min of vigorous shaking, the pellet and acetone mixture was centrifuged. The acetone was carefully decanted and filtered. 1 mL (0.5 mL if necessary) of each extract was transferred to a pre-weighed HPLC vial. After the aliquots and full samples were dry, the vials were weighed and enough methanol was added to make 0.25% w/v solutions for HPLC injection. To note, the *C. oranimense* extract prepared for the optimization work was used for this experiment. As will be discussed next, a HPLC sequence was run for nearly 60 hours total. Methanol rather than glacial acetic acid was preferred as the solvent to ensure the long-term stability of each sample.

The gradient system used to purify the *C. oranimense* fractions had to be optimized for these 25 HPLC separations at a small scale. The goal of this optimization was to design shorter runs than the nearly 4.2 hr preparative runs used for *C. oranimense* fraction collecting. The gradient

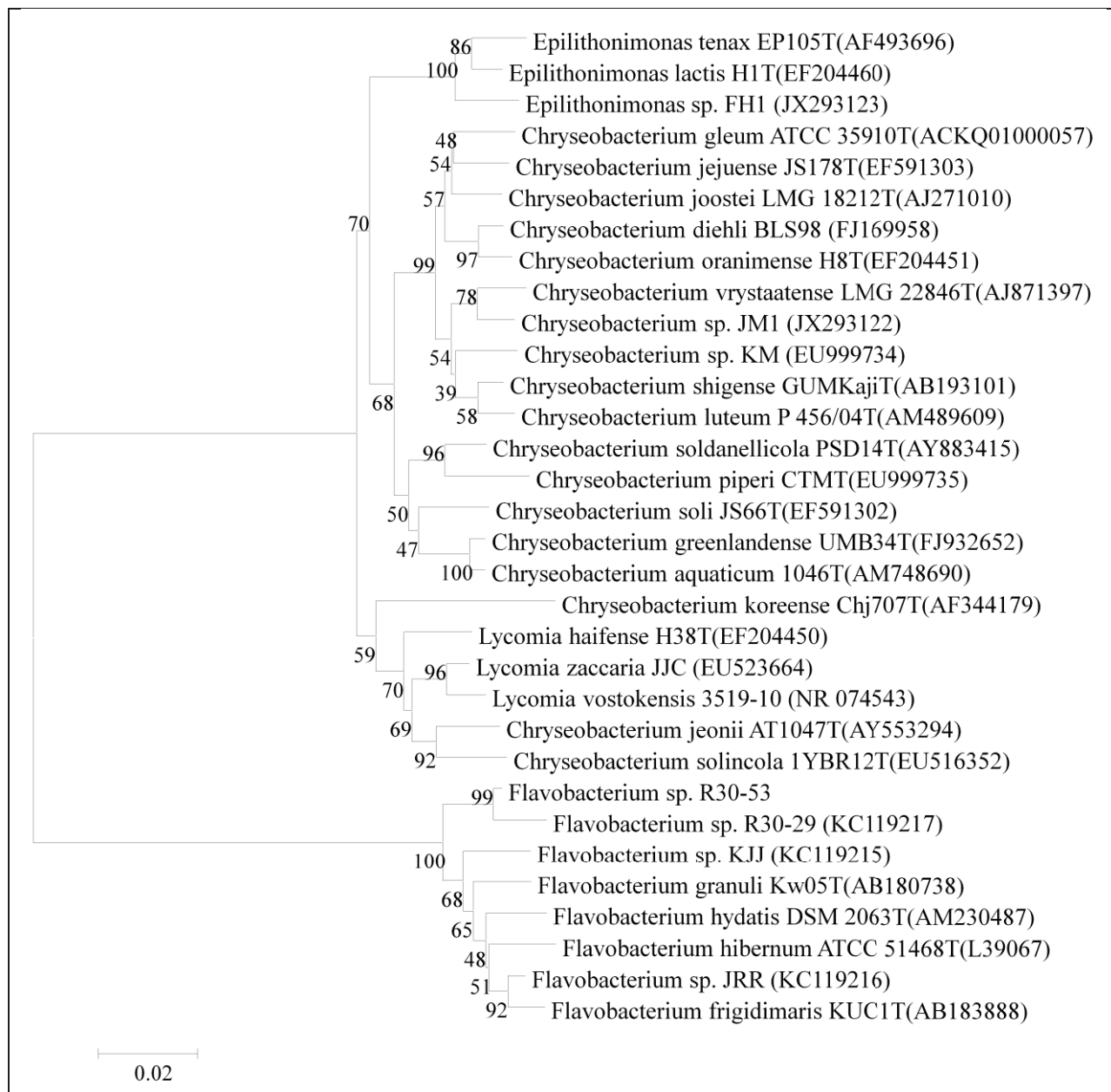


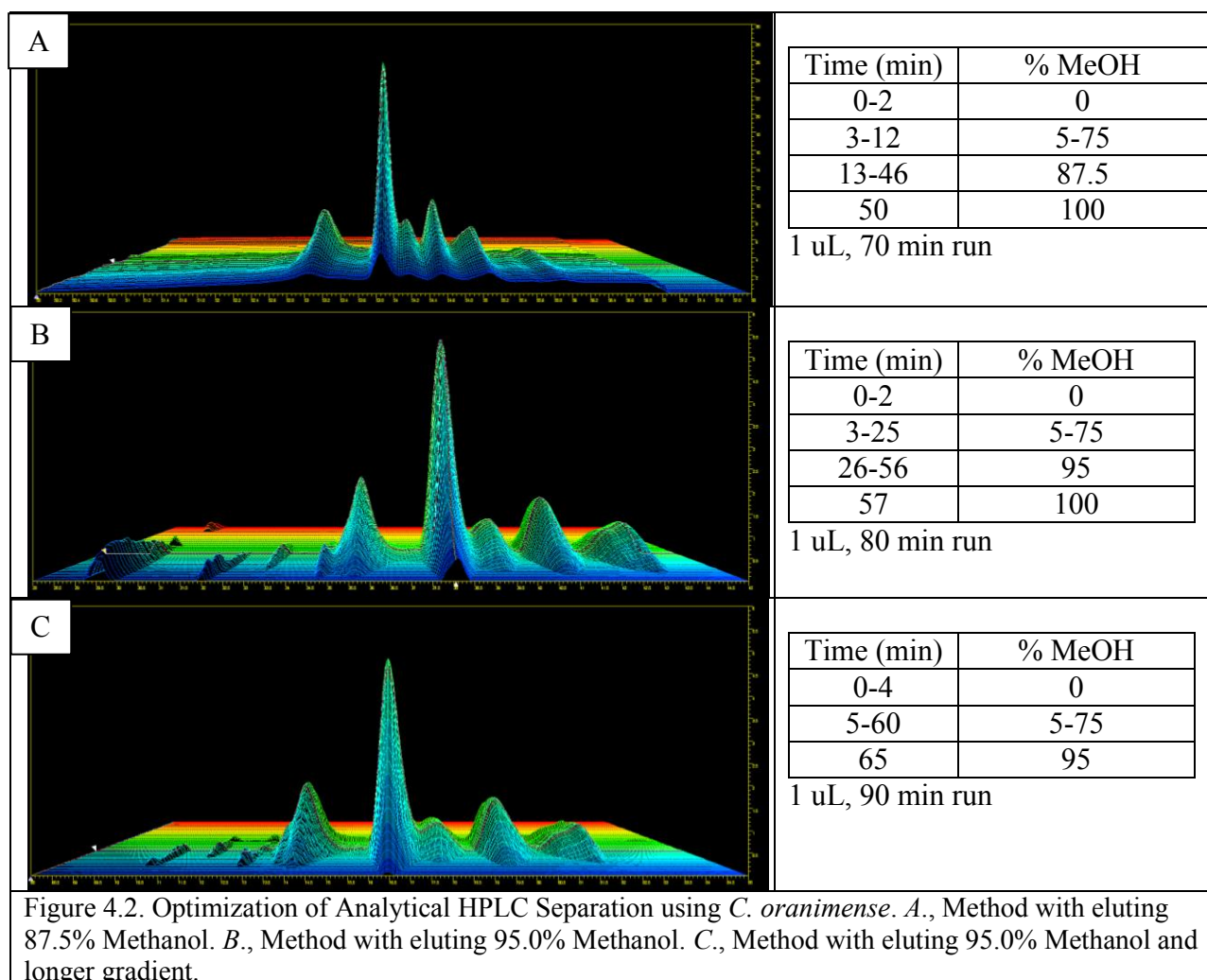
Figure 4.1. Neighbor-joining 16s rRNA tree of species of which flexirubin variation was investigated and other related species. Made using MEGA5 (Tamura *et al.*, 2011).

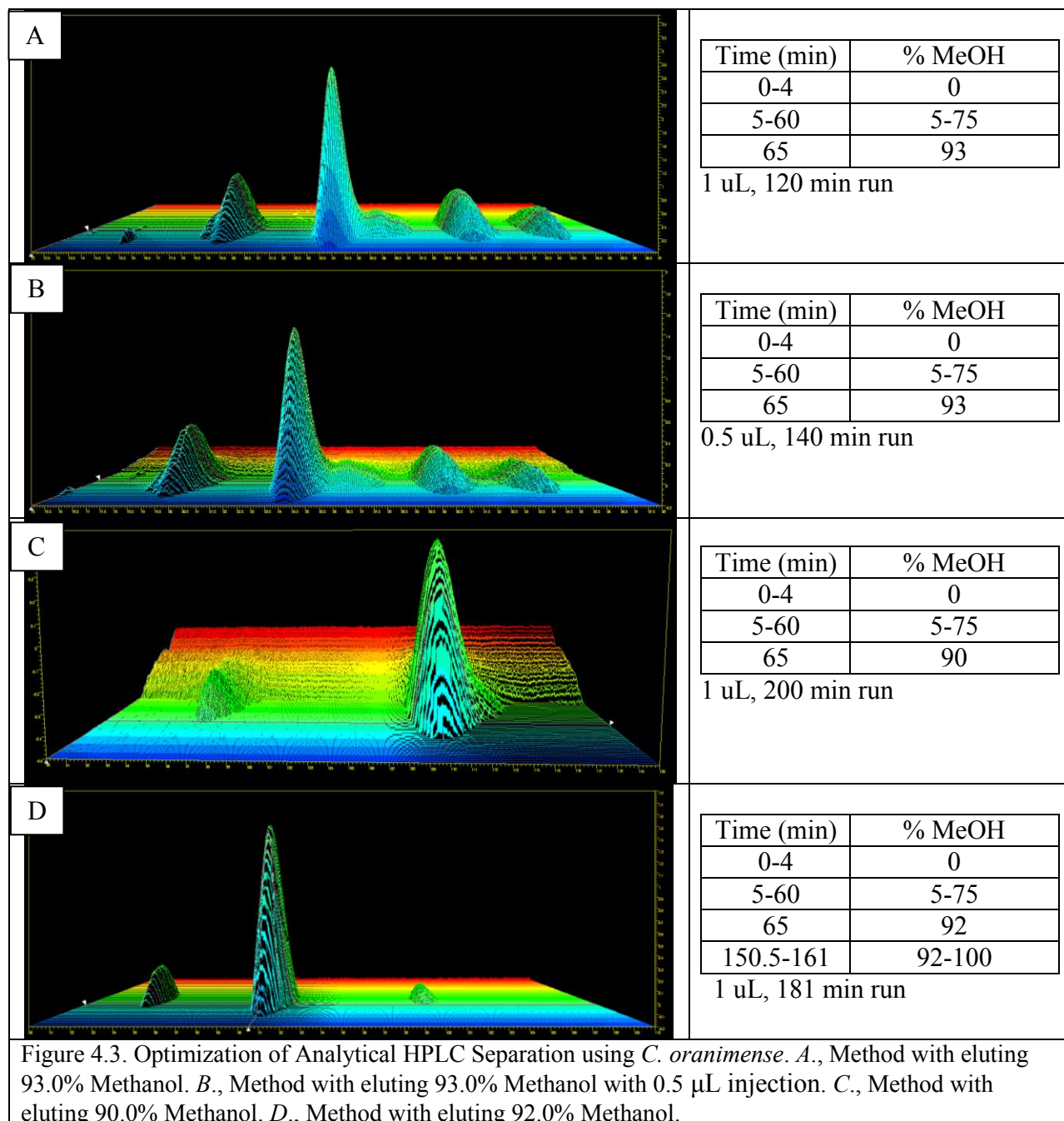
system, volume of the sample injected, and total analysis time was modified through multiple runs to perform this optimization.

The taxonomy of the 25 species for which the flexirubin variation was investigated is represented by a neighbor-joining tree based on the 16s rRNA gene sequence of each species (Figure 4.1). As shown, the *Flavobacterium* branch clusters separately from the originating

branch for the *Lycomia*, *Chryseobacterium*, and *Epilithonimonas* genera. These three genera cluster separately as well as the *Chryseobacterium* genus having two distinct clusters.

HPLC separations were initially designed to be very similar to the *C. oranimense* preparative runs, but quicker and with less material on the column. The *C. oranimense* solution used for these runs was flexirubin extract in 10% w/v glacial acetic acid. Each of the spectra of Chapter 4 has a 1 μ L injection so that only 0.1 mg of extract was being loaded on the column at one time. In Figure 4.2A, the separation was not down to the baseline. The overlapping of the separation between most of the peaks was detectable in Figure 4.2B even with a longer gradient. The gradient major *C. oranimense* and shoulder peak was nearly up to 7 mAU. There was still no



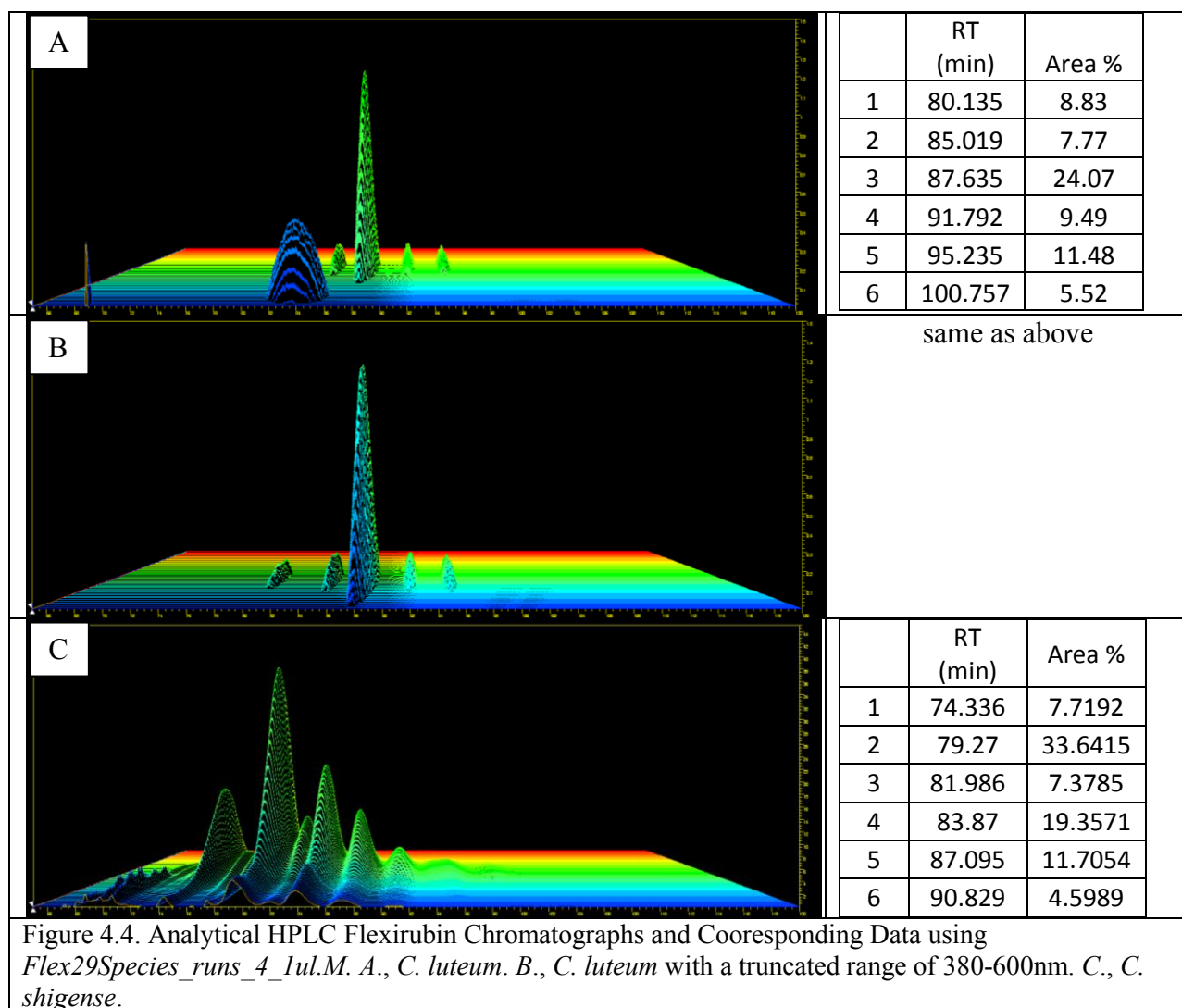


baseline separation when the solvent gradient was extended as far as in the *C. oranimense* preparative runs for the spectra represented by Figure 4.2C. The baseline separation was nearly achieved, but to increase the separation, the eluting percentage of methanol was decreased to 93% for Figure 4.3A. The 93% MeOH gradient nearly achieved baseline separation. As seen in

Table 4.1. Method Flex29Species_runs_4_1ul used for the 24 species analytical HPLC separations with a total analysis time of 140 min.

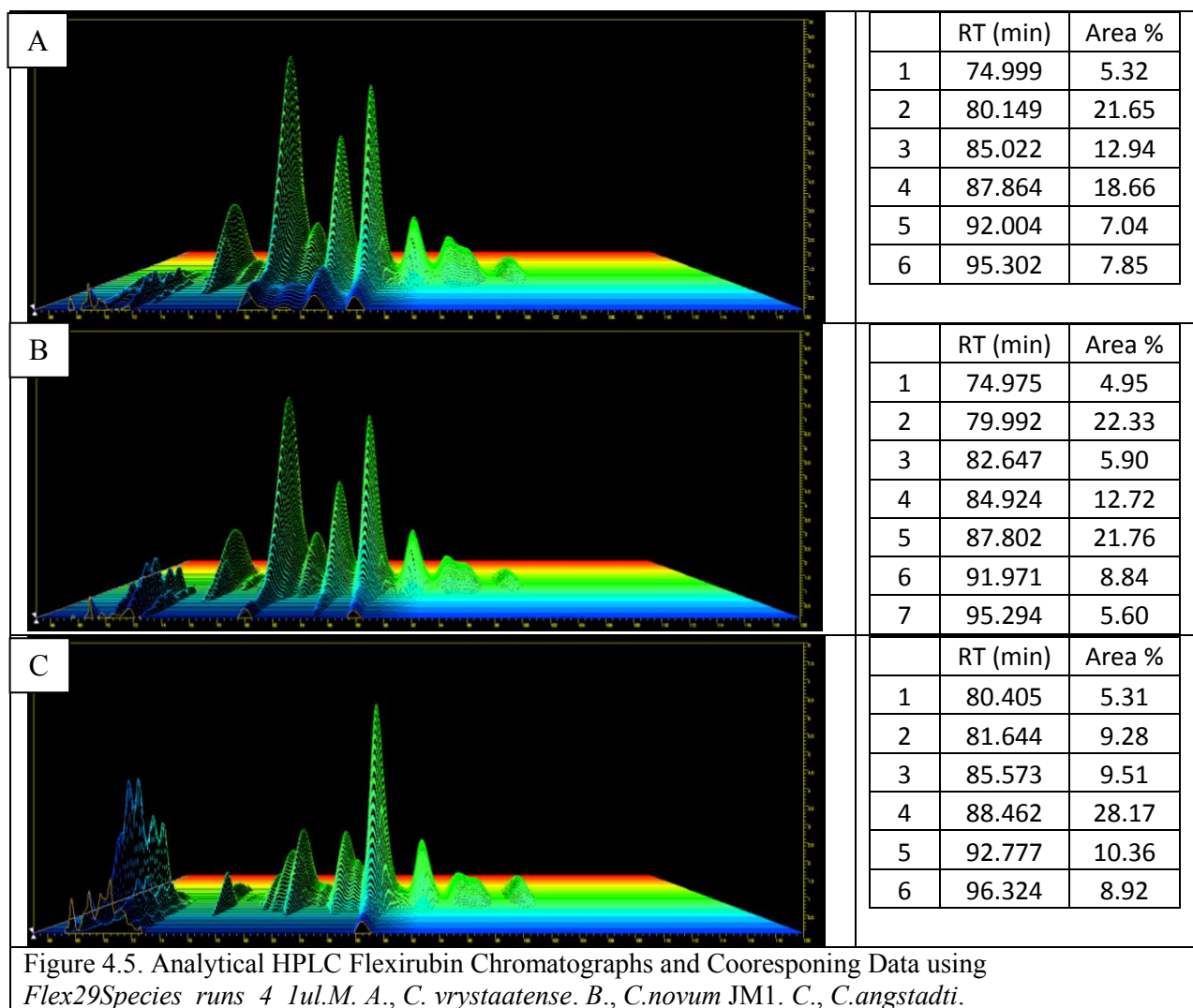
Time (min)	% MeOH
0-4	0
5-60	5-75
65	93
120.0-120.1	92-100

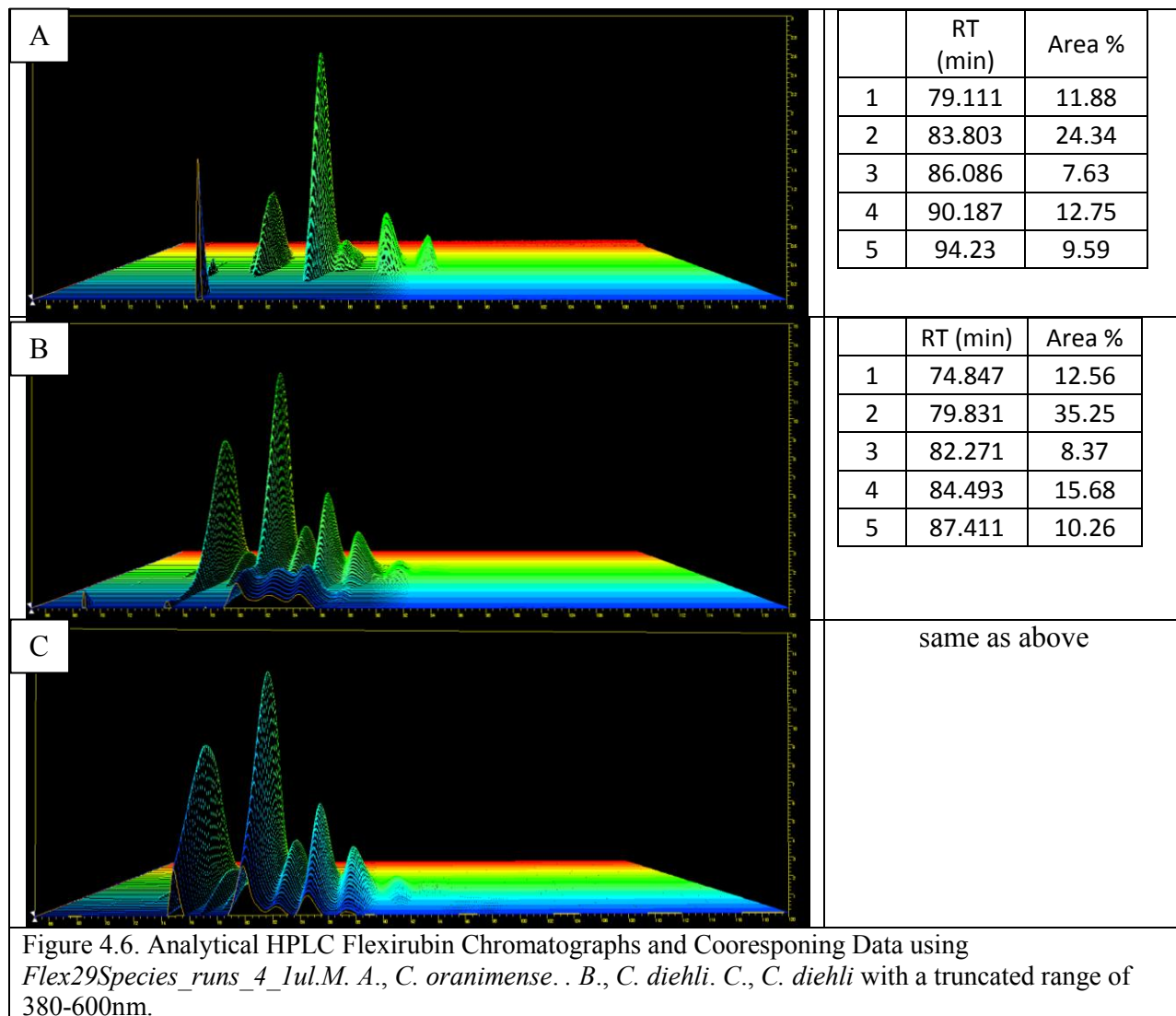
Figure 4.3B, injecting 0.05 mg of flexirubin material on the column, half the amount on the previous run, did not achieve baseline separation either. However, the signal to noise ratio decreases substantially with only 0.05 mg of material on the column. To avoid a signal to noise issue, a 1.0 uL (0.1 mg) injection was desired for the optimized run. Baseline-separation was



achieved with 90% and 92% MeOH as the eluting concentration, but the total time of the runs would use too much methanol and more time than desired, especially when planning to complete 25 runs. Therefore, the 93% MeOH as the eluting percentage was used (Figure 4.3).

The chromatograph of *C. luteum* and *C. shigense* were not overly similar despite their genetic similarity (Figures 4.1 and 4.4). The peaks of *C. vrystaatense* and *C. novum JM1* are nearly identical and similar to *C. shigense*. The major peak of *C. angstadtii* is analogous to the second most major peak of *C. vrystaatense* and *C. novum JM1* (Figure 4.5). *C. shigense*, *C. vrystaatense*, and *C. novum JM1* had similar peaks near 74, 80, and 87 min retention times with



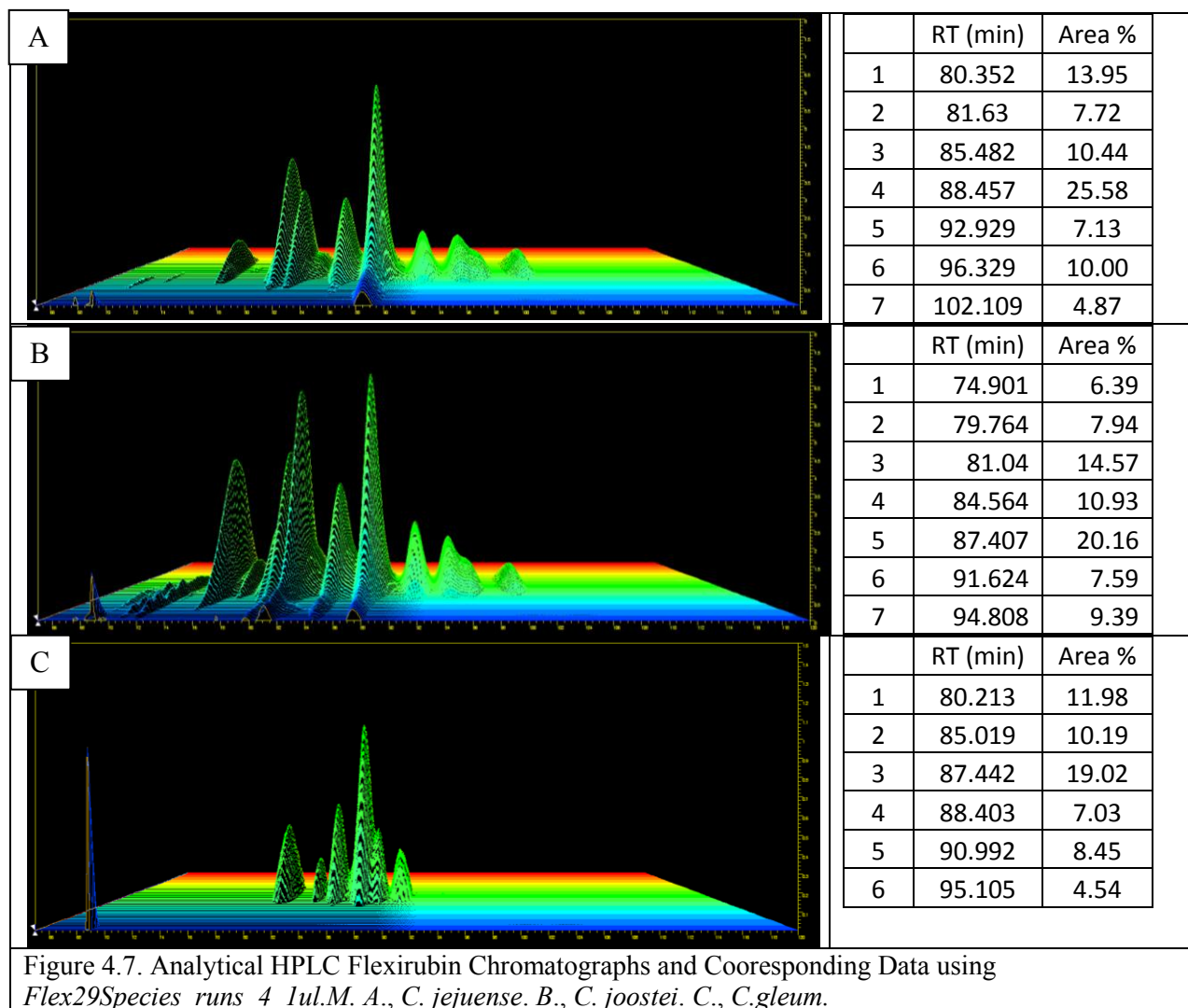


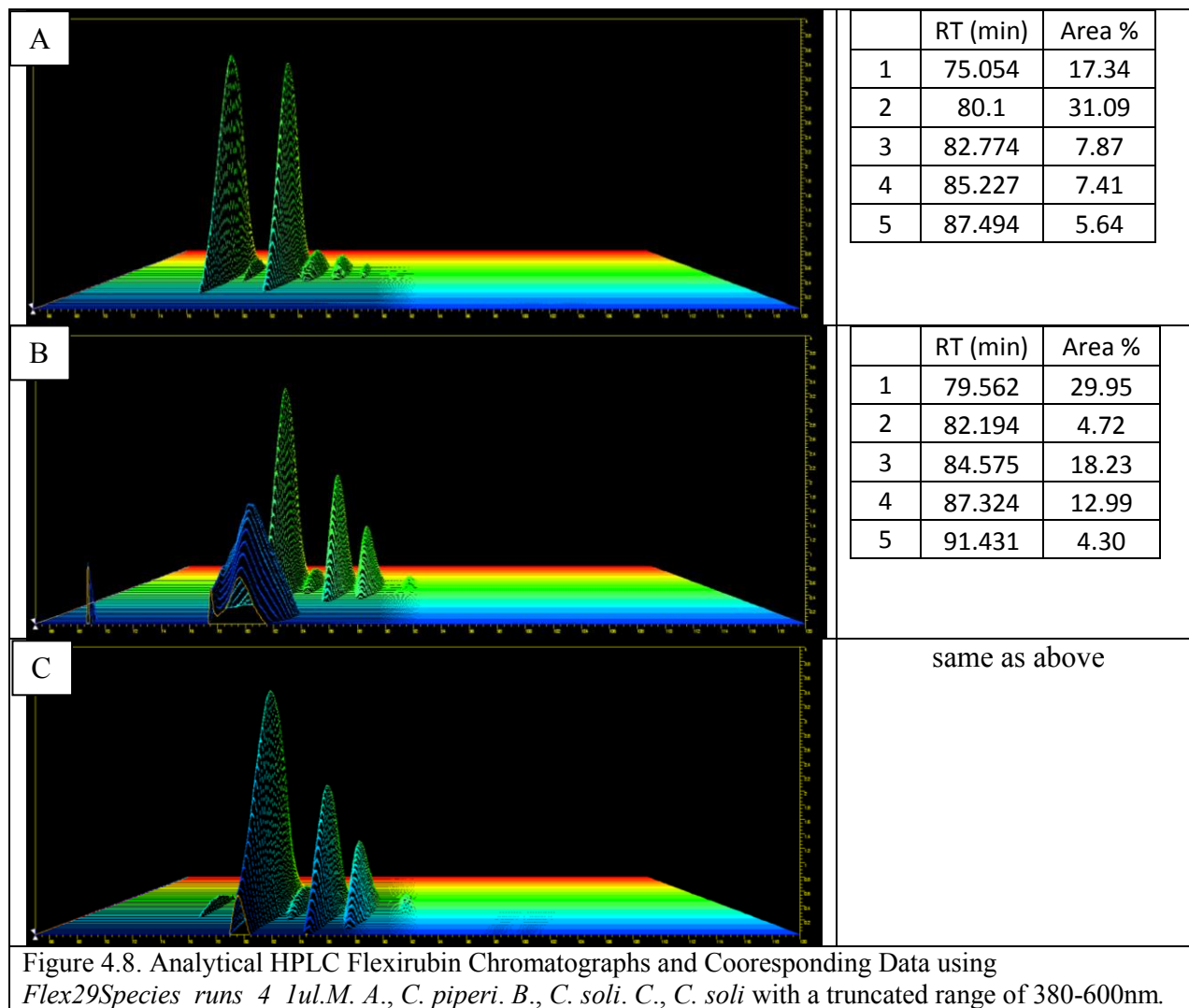
different percentages of area of each. *C. shigense* and *C. angstadtii* had peaks with 82 min retention times. *C. shigense*, *C. vrystaatense*, *C. angstadtii* and *C. novum* JM1 had similar minor peaks after about 92 minute retention time with similar percentages of peak areas and peaks with retention times around 70 minutes and max abosrbances at 328, 344, 392, or 400 nm wavelengths. Other than *C. luteum*, these chromatographs are very similar.

Much like with the comparison between *C. luteum* and *C. shigense*, *C. oranimense* and *C. diehli* are most similar via 16S rRNA similarity, but have widely different Flexirubin chromatographs (Figure 4.6). *C. oranimense* and *C. luteum* share peaks with approximate

retention time of 79 and 83 minutes. *C. diehl* BLS98 has a similar chromatograph to *C. shigense*. The pattern of the absorbance of major peaks at around 450 nm with significant absorbance in the region of 300-380nm is unique to *C. diehli*. However, *C. vrystaatense*, *C shigense*, and *C. luteum* also have chromatographs with different absorbance patterns in this region.

The chromatographs of *C. jejuense* and *C. joostei* were very similar while that of *C. novum* NRRL B-14798 was quite different (Figure 4.7). *C. jejuense* and *C. joostei* both had major peaks with retention times around 80 and 81 minutes (Figures 4.7A and B). The last three minor peaks of *C. jejuense* and *C. joostei* appear similar by retention time and absorbance

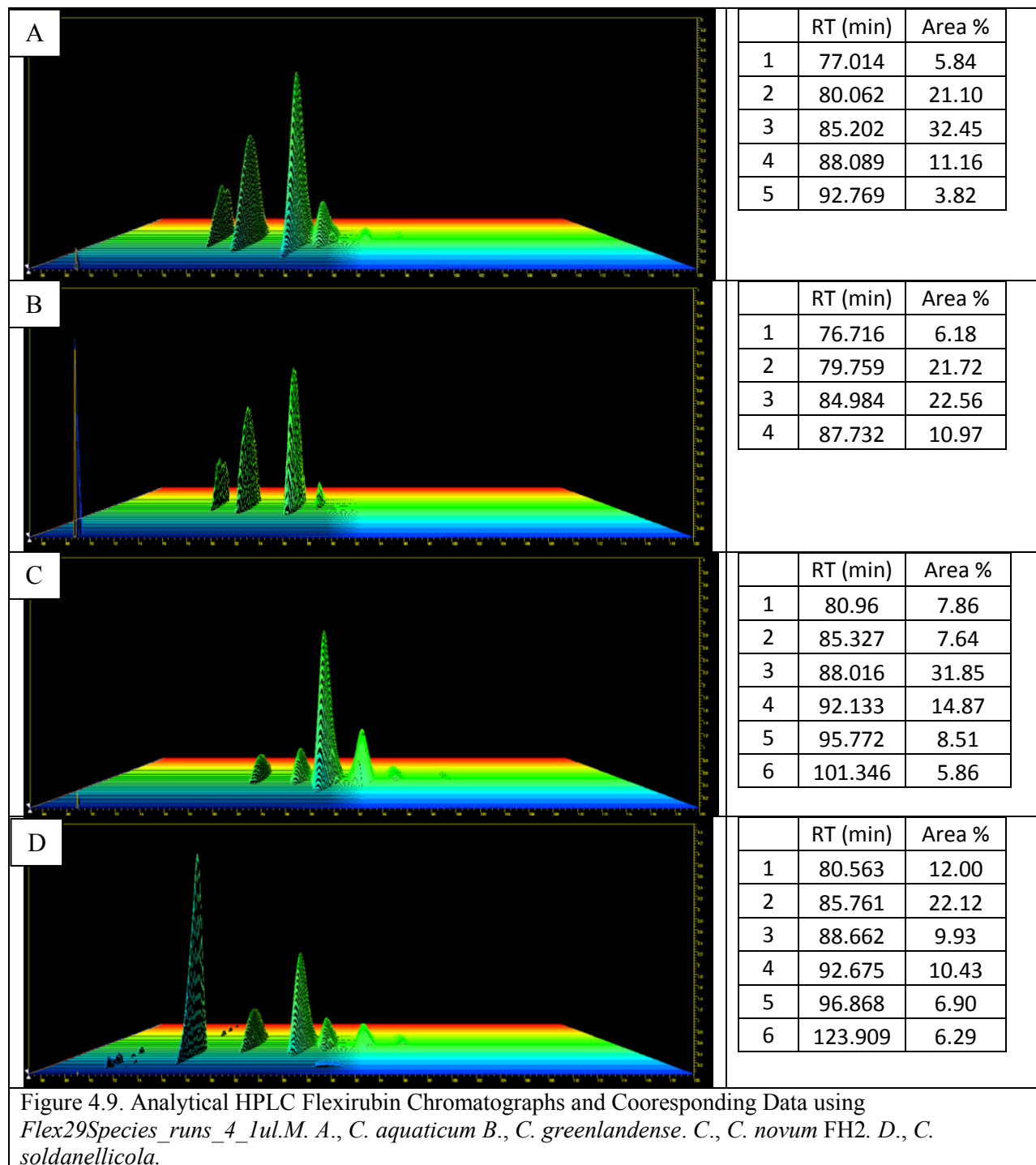




pattern, which is also similar to the chromatographs of *C. shigense*, *C. vrystaatense*, *C. angstadtii* and *C. novum* JM1. The separation of *C. novum* NRRL B-14798 suggests four analogous peaks with retention times of 85, 87, 91, or 95 min of *C. joostei*. The major peak for these three species was within the retention time range of about a minute suggesting similar chemical structures. The major peak eluting off the column after 74 minutes in the *C. joostei* chromatograph resembles the first peak of *C. deihli*.

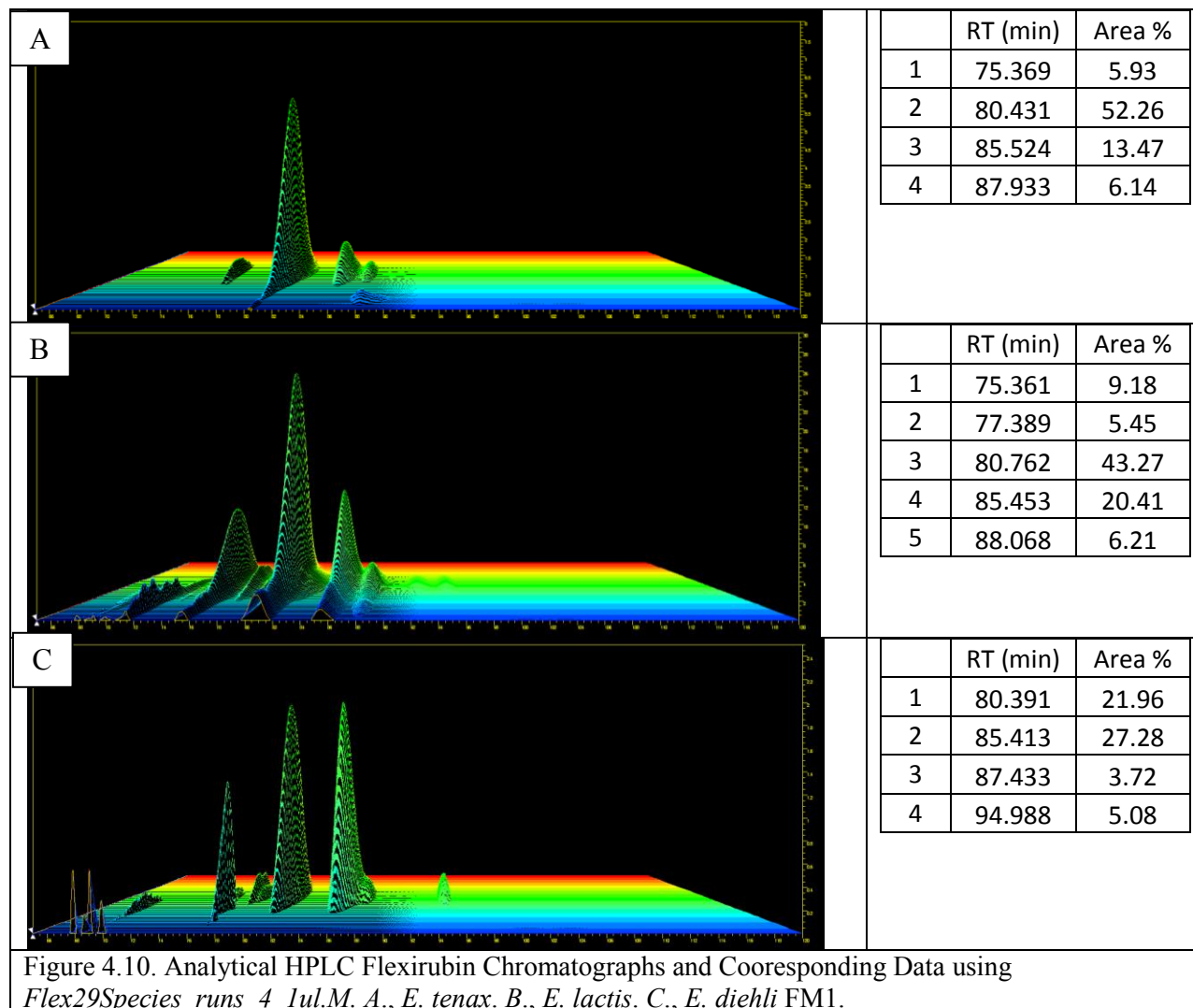
The separation of flexirubin peaks from *C. soli* is moderately similar to other species and *C. piperi* (Figure 4.8). *C. soli* has a peak within a similar 300-380nm region, much like *C.*

luteum. The higher absorbances in the 300-380 nm region indicates more UV absorption for the peaks with this feature from *C. soli*. Both have analogous peaks with retention times of about 80, 83, 85, and 85 minutes. *C. piperi* is unique from all other *Chryseobacterium* species in that it has

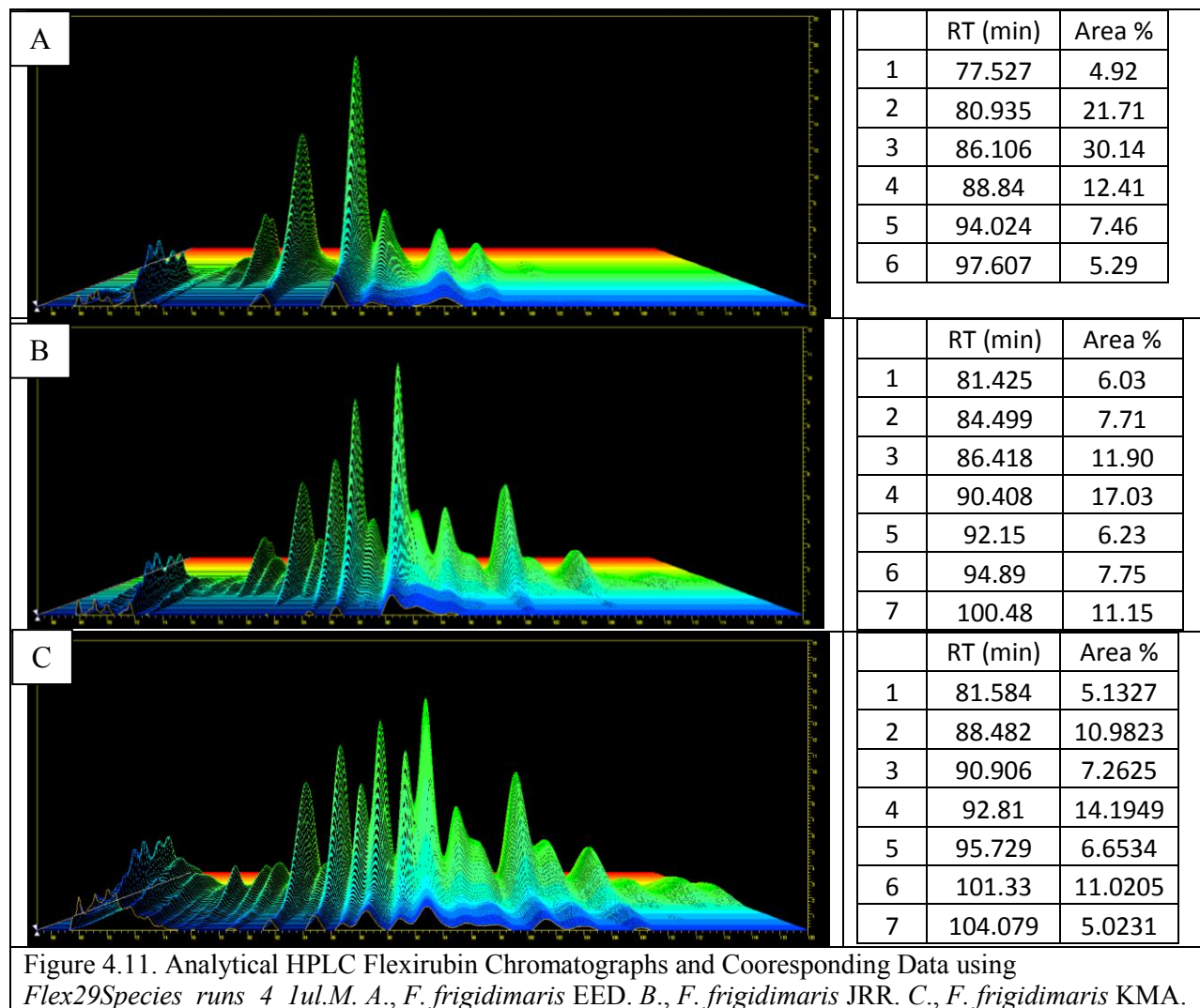


two major peaks with retention times at 75 and 80 minutes; both peaks have a large percent of the total mAU*sec area of the run. The peak of low retention time in *C. piperi* may be the same peak of about the same time observed for *C. joostei*.

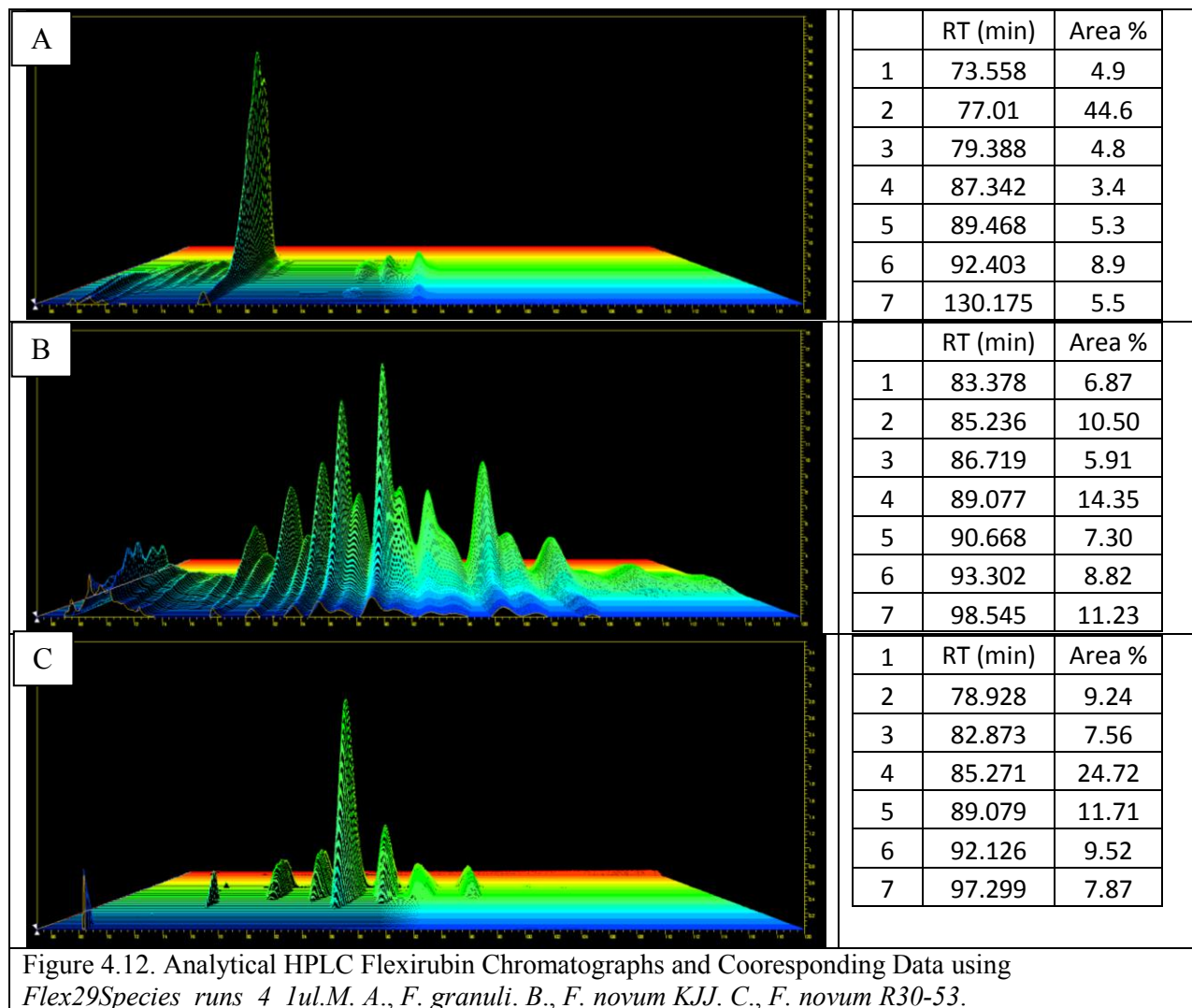
The chromatographs for *C. aquaticum* and *C. greenlandense* are nearly identical (Figures 4.9A and B). The chromatograph of *C. novum* FH2 has analogous peaks to *C. aquaticum* and *C. greenlandense* with approximate retention times at 80 and 85 minutes (Figure 4.9C). Likewise, *C. soldanellicola* has similar peaks with retention times of about 80 and 85 minutes. A peak a retention time of about 92 minutes is also found in *C. aquaticum*, *C. novum* FH2, and *C. soldanellicola* (Figure 4.9). The spectra representing the pigmentation of the *Epilithonimonas* have similar peaks as found in the *Chryseobacterium* but with unique absorbance patterns.



Both *E. tenax* and *E. lactis* have major peaks with retention times of about 75, 80, 85, and 88 minutes and similar absorbance patterns with different magnitudes of each absorbance. *E. diehli* FM1 has similar peaks with retention times of about 80, 85, and 87 minutes, but also a unique peak at about 95 minutes (Figure 4.10). In addition, *E. lactis* has a peak with a maximum absorbance (Abs_{max}) of 344nm at 71.43 minutes and *E. diehli* has peak with a Abs_{max} of 400nm at 75.88 minutes.



The flexirubin chromatographs representing the *F. frigidimaris* strain demonstrate some intra-species variation in flexirubin production (Figure 4.11). Just in the number of peaks, *F. frigidimaris* JRR and KMA are more similar than strain EED with fewer peaks. *F. frigidimaris* JRR and KMA have analogous peaks at 81.5, 90, 92, and 95 min retention times. Both *F. frigidimaris* EED and JRR have major peaks with retentions times around 86 minutes (Figure 4.11). The three *F. frigidimaris* strains have multiple peaks with maximum absorbances of either 344, 396, 400, 412, or 438 nm. Overall, these *F. frigidimaris* strains have many different flexirubin peaks.



Three other chromatographs of *Flavobacterium* were collected. *F. granuli* has a major peak with a retention time of about 77 minutes. This peak may not be a flexirubin as its Abs_{max} is at 364 nm (Figure 4.12A). The chromatograph of *F. novum* KJJ is similar to both *F. frigidmaris* JRR and KMA (Figure 4.12B). *F. novum* R30-53 has peaks with similar retention times as *F. novum* KJJ and *F. granuli*, but with a different absorbance pattern (Figure 4.12C).

The wavelength of the maximum absorbance of each peak also alludes to the variation of possible flexirubin structures of these many species of the *Flavobacteriaceae*. Most of the peaks present in these flexirubin chromatographs have a maximum absorbance near 450 nm. Most

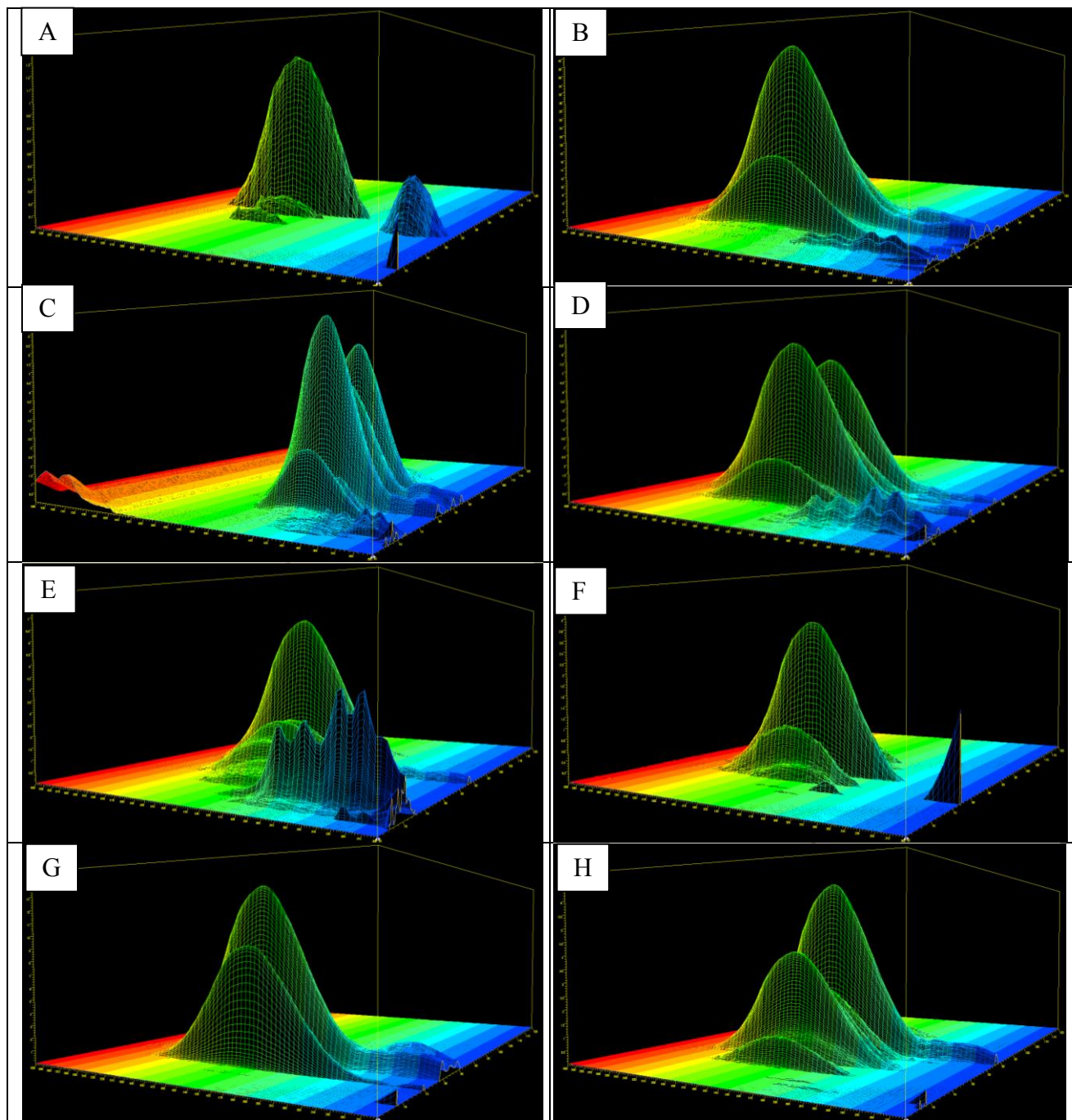


Figure 4.13. Wavelength-views of Analytical HPLC Flexirubin Chromatographs using *Flex29Species_runs_4_1ul.M. A.*, *C. luteum*. B., *C. shigense*. C., *C. vrystaatense*. D., *C. novum JM1*. E., *C. angstadtii*. F., *C. oranimense*. G., *C. diehli BLS98*. H., *C. jejuense*.

species have UV absorbing peaks flanking a major peaks. *C. angstadtii* has a very prominent peak with four maxima which is found in other species but with less distinction (Figure 4.13E). One of the two major peaks of *C. jejuense* has a maximum absorbance at 440nm (Figure 4.13H).

A peak with a maximum absorbance at 440nm is also found in *C. piperi* (Figure 4.14C). The chromatographs of *C. greenlandense*, *C. novum* NRRL B-14798, *C. piperi* and *C. novum* FH2 had no peaks absorbing in the UV range nor any peaks with absorbances deviating much from

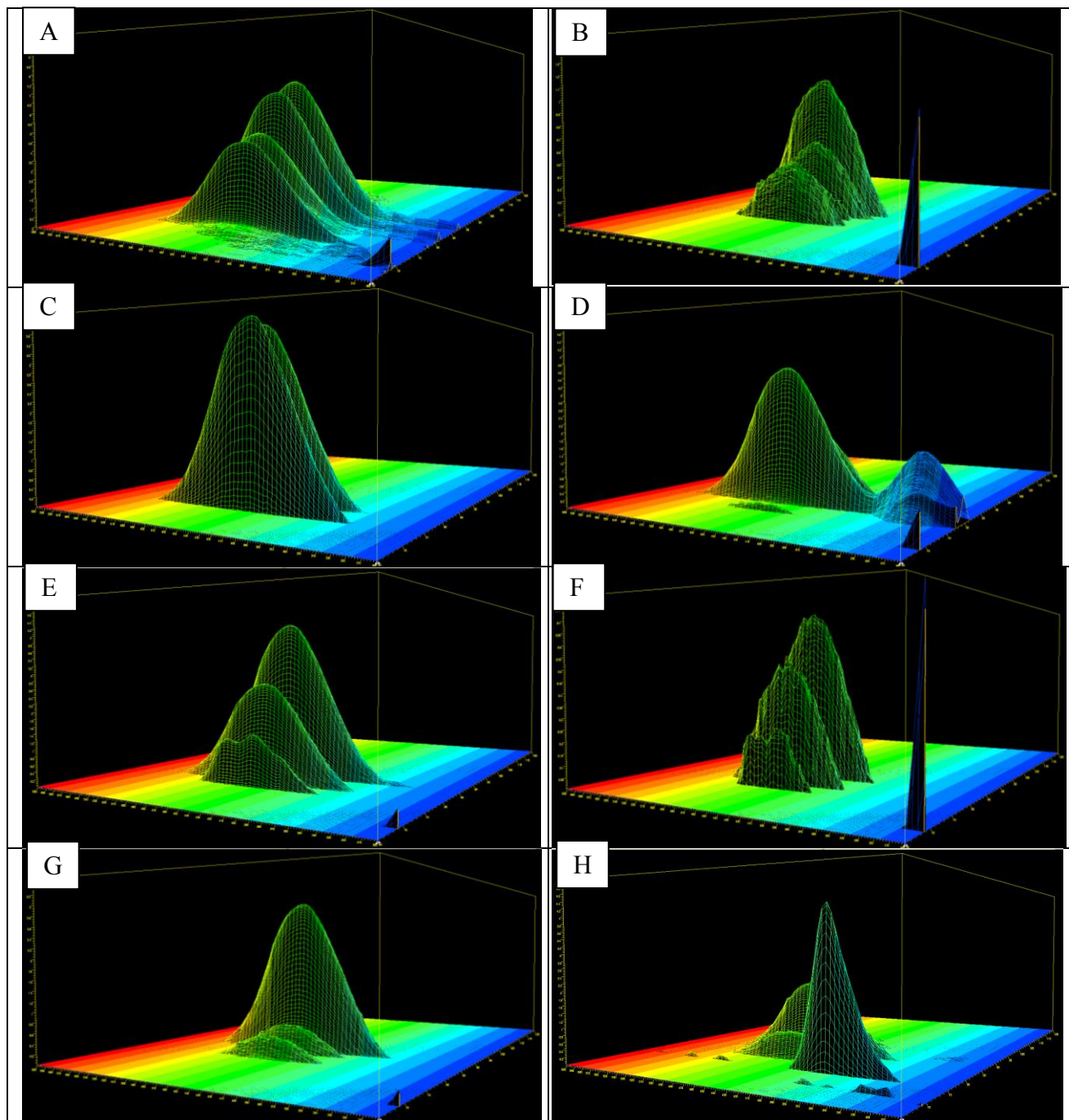


Figure 4.14. Wavelength-views of Analytical HPLC Flexirubin Chromatographs using *Flex29Species_runs_4_1ul*. A., *C. joostei*. B., *C. novum* NRRL B-14798. C., *C. piperi*. D., *C. soli*. E., *C. aquaticum*. F., *C. greenlandense*. G., *C. novum* FH2. H., *C. soldanellicola*.

450nm (Figures 4.14F, 4.14B, 4.14C, and 4.14G, respectively). Uniquely, the peak with the lowest retention time of *C. aquaticum* is not smooth like most of the other peaks present, but rather has three maxima. In addition, *C. soldanellicola* had a very large peak with a maximum absorbance near 400nm (Figure 4.14H). Much variation in the maximum absorbance of the minor peaks was observed for the chromatographs of the *Chryseobacterium*.

The chromatographs of the *Epilithonimonas* species had much variation as well. Minor UV absorbing peaks were found in all three species. *E. lactis* had a few peaks with the four maxima just like the analogous peaks found in *C. shigense*, *C. vrystaatense*, *C. novum* JM1 and *C. angstadtii* (Figure 4.15B compared to Figures 4.13B, 4.13C, 4.13D, and 4.13E, respectively). *E. diehli* had many peaks similar to those found in other species and without a maximum absorbance near 450nm. Specifically, *E. diehli* had a peak with a maximum absorbance near 450 nm with three maxima like *C. aquaticum* and a major peak with a maximum absorbance at 400nm like *C. soldanellicola* (Figure 4.15A compared to Figures 4.14E and 4.14H, respectively).

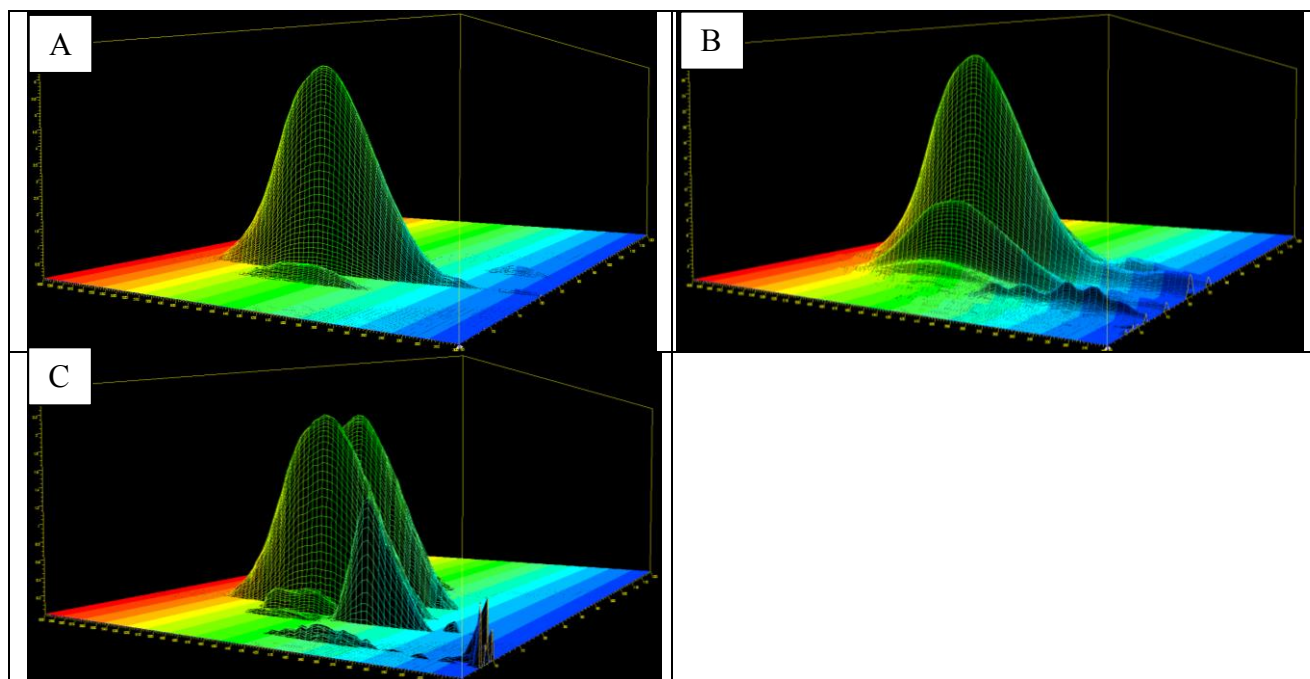


Figure 4.15. Wavelength-views of Analytical HPLC Flexirubin Chromatographs using *Flex29Species runs 4* *lul.M. A., E. tenax. B., E. lactis. C., E. diehli.*

Much like the other genera studied, the chromatographs of the *Flavobacterium* species had much variation as well. UV absorbing peaks were observed in *F. frigidimaris* EED, JRR, and KMA, as well as in *F. granuli*, and *F. novum* KJJ. Minor peaks with multiple maxima as noted before were also seen in *F. frigidimaris* EED, JRR, and KMA and in *F. novum* KJJ. One of the minor peaks of *F. novum* R30-53 has a maximum absorbance at 400 nm as seen in other species (Figure 4.16F).

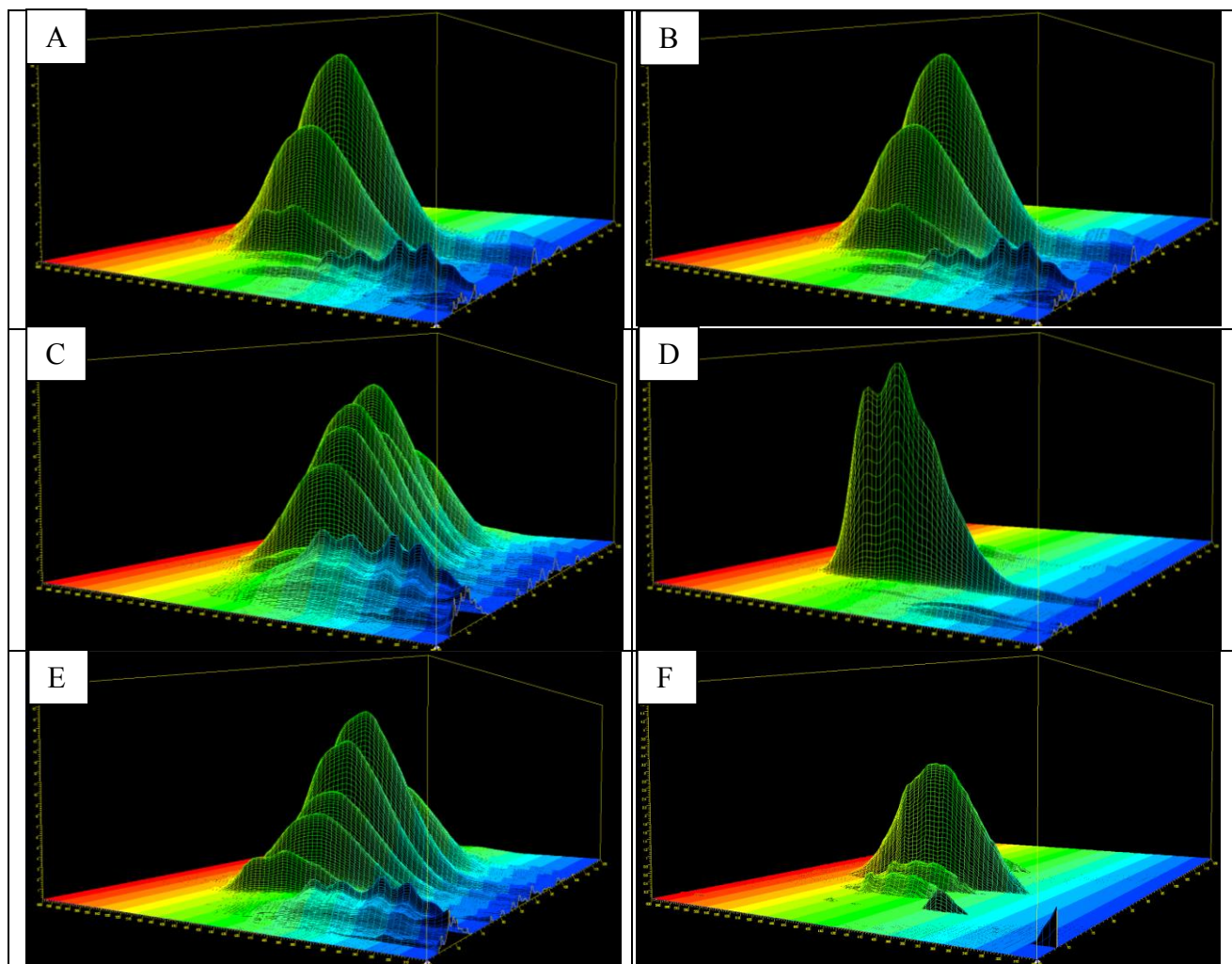
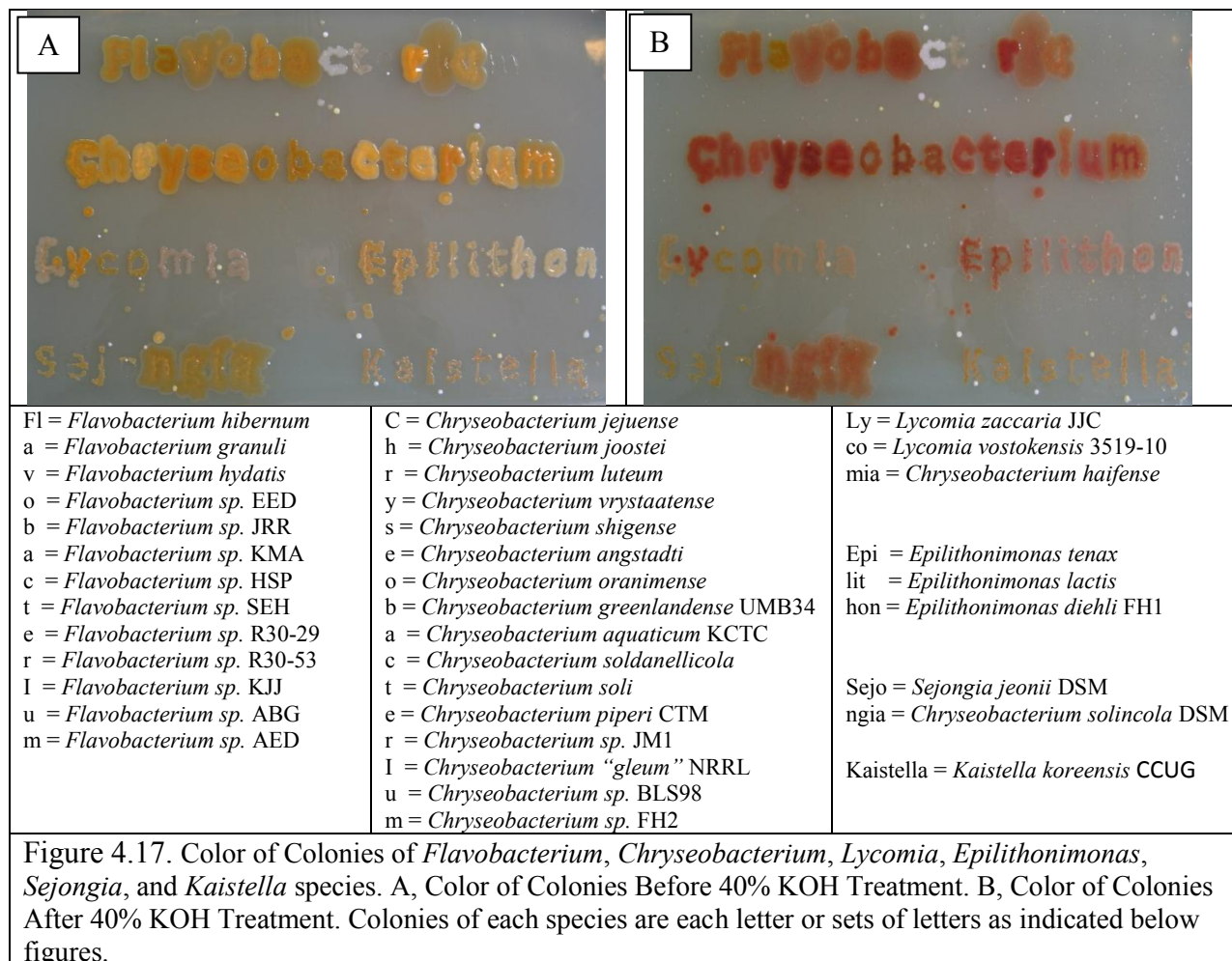


Figure 4.16. Wavelength-views of Analytical HPLC Flexirubin Chromatographs using *Flex29Species_runs_4_1ul.M. A., F. frigidimaris* EED. B., *F. frigidimaris* JRR. C., *F. frigidimaris* KMA. D., *F. granuli*. E., *F. novum* KJJ. F., *F. novum* R30-53.



Similar flexirubin profiles should have similar colors in the image above (Figure 4.17). Indeed, *C. vrystaatense* and *C. novum* JM1 have nearly identical profiles and similar colors. *C. shigense* has a similar profile and similar darker orange color as *C. vrystaatense* and *C. novum* JM1 as well. In addition, the pigment colors of *C. oranimense*, *C. aquaticum*, and *C. greenlandense* are similar and again have similar flexirubin profiles. However, *C. luteum*, *C. soldanellicola*, *C. piperi*, *C. "gleum"* and *C. diehli* have similar yellow-whitish colors, but their profiles do not seem to be as related as the other similar-colored *Chryseobacterium* groups. The profiles of the *Epilithonimonas* have at least similar peaks but in different proportions. They also have different colony colors. Therefore, the amount of each flexirubin peak has just as much

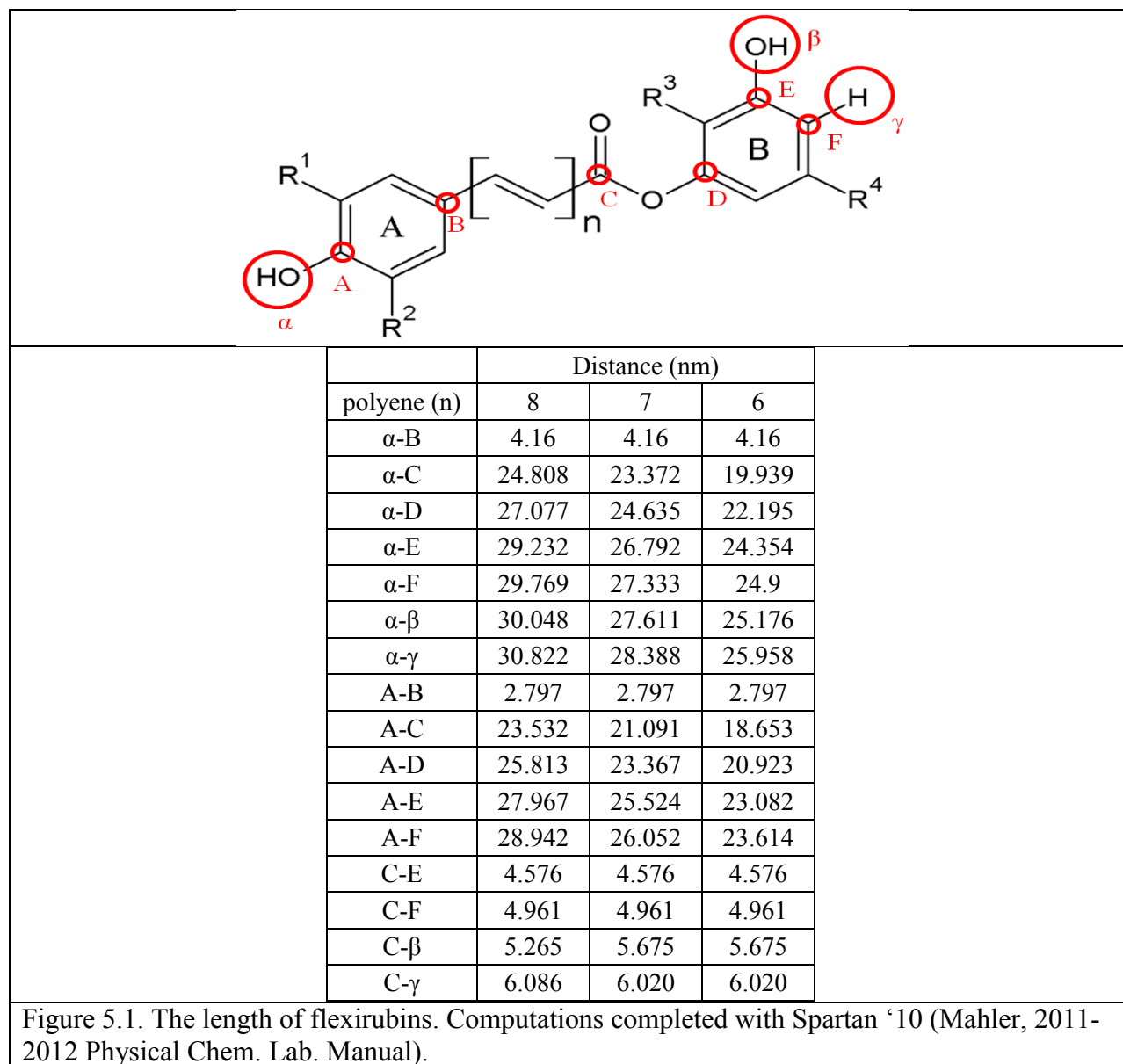
effect on the colony color as the flexirubin peaks present. The correlation of flexirubin profiles and pigment colors also seems to be difficult to determine for the *Flavobacterium*. The three *F. frigidimaris* strains have similar profiles, but only the EED and JRR strains have similar colony pigmentation. Comparing the colonies before and after KOH treatment shows that one particular yellow-colored colony, *F. granuli*, failed due to no observed bathochromatic shift. Interestingly, *F. granuli* has one major peak with three maxima. This peak is found it seems in the other *Flavobacterium* but in much less proportion. Species that do not fail the KOH test have smooth peaks with only one maxima and therefore seem to be peaks representing true flexirubin pigments. Due to its multiple maxima and remaining yellow color with the addition of KOH, the major peak of *F. granuli* seems to be a different pigment. It may be a carotenoid. The major peak of *F. granuli* is about 70% of the total peak area of this species and is also nearly baseline separated even at an eluting methanol percentage of 93%. These two aspects demonstrate that the major peak of *F. granuli* should be targeted for purification and molecular structure determination. If after the *F. granuli* pigment structure is determined and it is not a carotenoid, “flavirubin” is proposed as its name.

Multiple species have well isolated peaks such as *C. luteum*, *E. lactis*, and *E. diehli*. As discussed for the *F. granuli* major peak, it would be easy and very straightforward to optimize preparative runs to collect purified fractions of these major peaks. Likewise, the collection of flexirubin profiles of many species enables the selection of easy to purify peaks. The structural determination of multiple peaks would enable some peaks to be identified by wavelength and retention time. Having a small catalog of these identified peaks would give better understanding to what the flexirubin profiles represent rather than being just analogous to phospholipid analysis with many unknown molecules on TLC plates.

The various peaks with different wavelengths, number of maxima, and retention times indicate many variations in flexirubins present in the *Flavobacterium*, *Chryseobacterium*, and *Epilthonimonas*. Whether or not these variations cluster by genera has yet to be determined. After spectra have been repeated two more times for these 25 species, clustering may be investigated with the data points for each species by principal component analysis (PCA). While the variations of flexirubins may not be as straight forward to use as a technique to cluster related species taxonomically, the flexirubin profile method is another efficient analysis that should be used to characterize flexirubin-producing *Flavobacteriaceae* species.

Ch. 5. Investigated Flexirubin Characteristics

While the optimization of *C. oranimense* preparative HPLC runs were underway, computational studies were completed for insight into the function and outer membrane orientation of flexirubins. While there are at least three possible orientations of flexirubin in the outer membrane, the portion of the molecule that adheres to this orientation can be studied by simply determining the lengths of the some of the flexirubin components (Figure 1.2A).



Likewise, multiple distances between substituents of the flexirubins were calculated using Spartan '10 (Mahler, 2011-2012 Physical Chem. Lab. Manual).

It was originally thought that the flexirubins may be orientated in such a way that the two rings, along with the ester group for the one, are anchored among the hydrophilic heads of each opposite membrane with the polyene bridge spanning the membrane. However, the 15.8 nm, 18.3 nm, or 20.7 nm length, respectively, of the 6, 7, or 8 n polyene flexirubins would not fit in the normal 6 nm membrane thick outer membrane as determined for “*Flexibacter polymorphus*” the genus of which the flexirubin name originates (Ridgway *et al.*, 1975). Therefore, the flexirubins may either localize lengthwise in the outer membrane like lutein or span the two outer membrane leaflets diagonally with the rings and ester group anchored among the hydrophilic heads as previously described and as proposed for zeaxanthin and lutein (Gruszecki and Strzałka, 2005). Further, the distance of α - B of the first ring and of C - β of the second ring and ester group of about 4.2 nm and 5.8 nm, respectively, suggests that they both span and may be anchored by the hydrophilic heads. In addition, the localization of diagonally spanning the membrane should be the more energetically favorable of the two possible orientations by

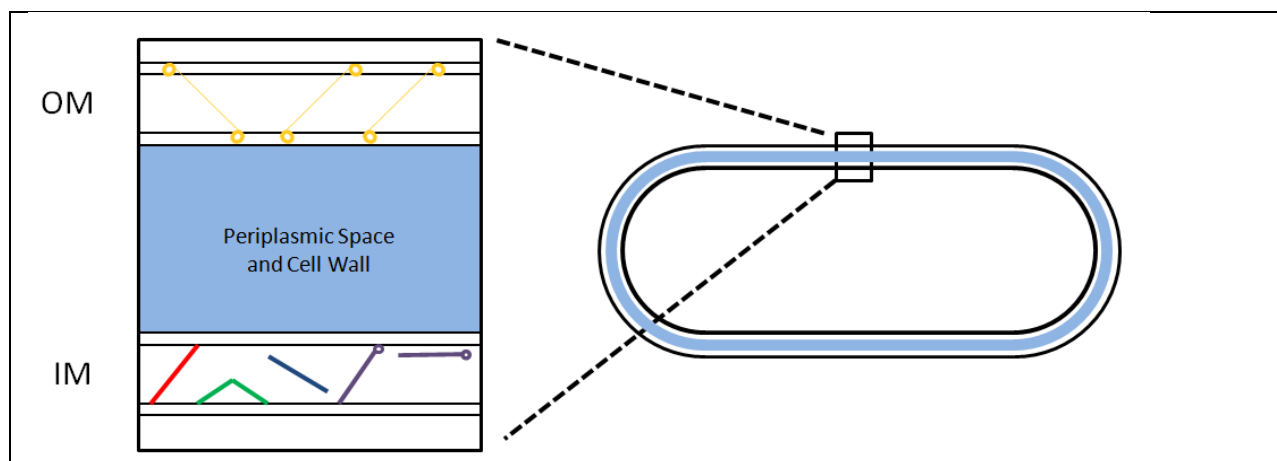
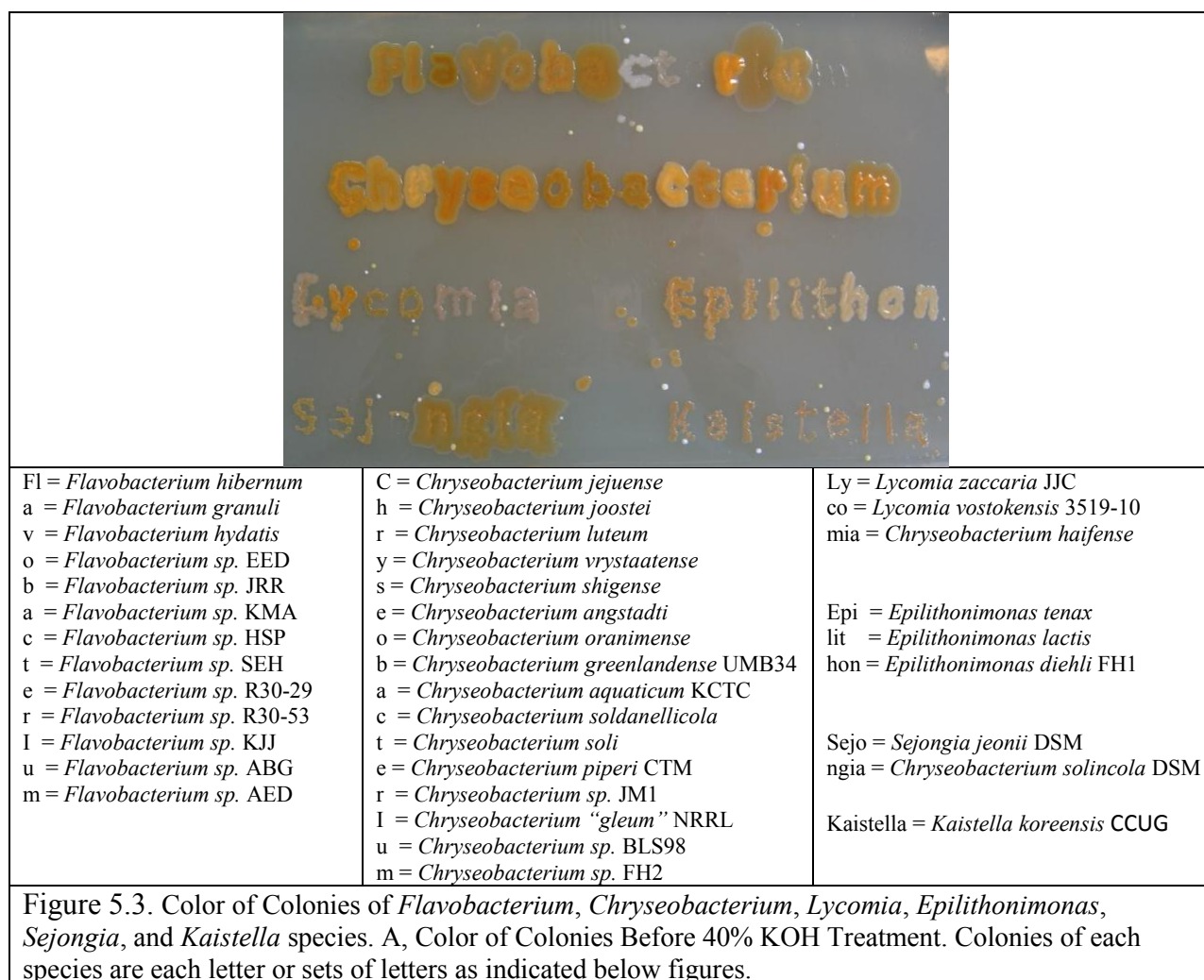


Figure 5.2. Illustration showing the proposed localization of flexirubin by this study in the outer membrane (OM) and carotenoids in the inner membrane (IM) of a microbial cell by another study. The colored structures correspond to the chemical structures in Figure 1.2 (Irschik and Reichenbach, 1978; Gruszecki and Strzałka, 2005).

minimizing any hydrophilic and hydrophobic interactions.

Flexirubins currently have an unknown function, but the proposed orientation suggests roles in membrane maintenance and even flexibility. Flexirubin do have similar structures to avenanthramides and alk(en)ylresorcinols which have both been shown to have antioxidative properties (Mattila *et al.*, 2005). If flexirubins confer flexibility to the outer membrane, then they could promote gliding motility as suggested previously (Reichenbach *et al.*, 1980). An issue that arises with this hypothesis, however, is that *Chryseobacterium* species may not have gliding motility (Bernardet *et al.*, 1996). However, while some *Chryseobacterium* may have lost the ability to glide such as *C. oranimense*, *C. greenlandense*, and *C. aquaticum*, many species appear



to actually have the ability as can be seen especially in the “M” of *Chryseobacterium* or *C. novum* FH2 (Figure 5.3). While determining gliding motility by the observation of movement on an agar plate is not a traditional method, these species appear to have moved more than just from colony growth. Moreover, the species that did not appear to have moved may have been growing sluggishly. Better growth of species that are already growing well in liquid culture when inoculated onto the plate as a letter may resolve this issue.

Future Work

First, a large plate of the different colonies needs to be prepared as presented for Figure 5.3, but with all colonies growing well beforehand in liquid culture. Once this plate has been imaged before and after KOH treatment, the colony colors and motility need to be analyzed for correlation to the presence of flexirubins and to the profiles of the flexirubins as well. A way to determine the amount of motility may be to measure the diameter from the bright color to the edge of the letter where the color seems to be darker (Figure 5.3). Both the distance of motility and color of colonies can be determined with ImageJ (Rasband, 1997-2012). Next, some genomic work could be completed to determine if flexirubin-producing species have gliding motility genes or other shared genotypes.

An initial study was attempted to compare the core genome of flexirubin positive and flexirubin negative *Flavobacteriaceae* using RAST (Aziz *et al.*, 2008). However, the study was not overly conducive and was not completed. Now, with the completed genomes of more bacteria that do and do not have flexirubin synthesis, such a study may be more productive. Specifically, motility genes such as *Gld* and *spr* need to be found to predict gliding motility with an *in silico* experiment (Lee *et al.*, 2011). In addition, it seems that flexirubin producing bacteria have shared fatty acid genes ABC transported genes and at least the *darA* and *darB* genes essential for

flexirubin synthesis; this could also be further investigated as well (McBride et al., 2009).

Another set of key experiments to elucidate possible flexirubin functions would be to test the antioxidant capacity of any purified flexirubin pigments.

There are multiple methods to test antioxidant capacity which are accessible to the Newman Lab. Some methods have been validated using cyclic voltammetry to determine the antioxidant capacity of low-molecular weight antioxidants (LMWAs) (Chevion *et al.*, 2000). Collaboration with Dr. Ramsey's lab of the Chemistry department that specializes in cyclic voltammetry may be a fruitful way to determine if flexirubins indeed may inhibit the oxidation of fatty acids or other molecules in general. Other techniques which may be easier to perform if the reagents are available may be the 1,1-diphenyl-2-picrylhydrazyl radical (DPPH[•]) method. This method is based on the inhibition of the loss of color of the methanol solution of DPPH[•] and a proposed antioxidant and compared to a positive control solution containing a well known antioxidant, such as butylated hydroxyanisole (BHA), both by UV-Vis (Eman *et al.*, 2010; Brand-Williams *et al.*, 1995). Many other DPPH[•] based methods, as well as OH[•] and O₂^{•-} based method could also be attempted (Spranger *et al.*, 2008). The determination of any flexirubin function could be the basis of many possible studies and grant applications past looking at only the profile of this class of natural products in related species.

This study has provided the framework for years of projects on flexirubins. According to current literature, this study presents the first optimized preparative HPLC method to have achieved baseline separation. In addition, this study is the first of its kind to collect flexirubin profiles for many species, let alone 25 species as was completed at least once. Much work has been completed in the past year for this study, but many more questions have yet to be answered. This study was designed in response to questions about flexirubins from years of observation by

myself and fellow Newman lab members, but has only answered a few of those questions. The method of collecting a flexirubin profile based on reverse-phase HPLC will be a great addition to studies of novel species that synthesis flexirubins. With the designed flow chart similar preparative HPLC methods, as optimized for this study, can be designed efficiently and relatively easily for other pigments of species under study in the Newman lab. Such pigments could include the pink pigments of the *Pedobacter* species and the brown pigment possibly unique to *Kaistella koreensis* when grown at 4°C for a few weeks due. As the price of genome sequences decreases, the ability to correlate core genomes between flexirubin producing bacteria and flexirubin profiles will add much to the little knowledge on flexirubin synthesis and biochemistry. Therefore, this project overlaps well with and builds up other Newman lab projects including genome assembly of related species and the publication of novel species.

Appendix 1. Strains, Original Isolation, and Reference for each species used in this study.

Species	Strain	Isolated from	Reference
<i>C. aquaticum</i>	KCTC 12483 ^T	Water reservoir, Buyeo, Korea	Kim <i>et al.</i> , 2008
<i>C. angstadtii</i>	KM	Newt tank	LycoMicro 1998
<i>C. diehli</i>	BLS98	Wastewater Treatment Device	Strahan, 2008
<i>C. "gleum"</i>	NRRL B-14798	High vaginal swab, London, UK	Holmes <i>et al.</i> , 1984
<i>C. greenlandense</i>	UMB34 ^T	deep ice core, Greenland	Loveland-Curtze <i>et al.</i> , 2010
<i>C. jejuense</i>	DSM 19299 ^T	Soil samples, Jeju, Korea	Weon <i>et al.</i> , 2008
<i>C. joostei</i>	LMG 18212 ^T	Raw tanker milk, RSA	Hugo <i>et al.</i> , 2003
<i>C. luteum</i>	DSM 18605 ^T	Phyllosphere of grasses	Behrendt <i>et al.</i> , 2007
<i>C. piperi</i>	CTM ^T	freshwater creek, Loyalsock Creek, PA USA	Strahan <i>et al.</i> , 2011
<i>C. oranimense</i>	LMG 24030 ^T	raw cow's milk, Israel	Hantsis-Zacharov <i>et al.</i> , 2008
<i>C. shigense</i>	DSM 17125 ^T	Lactic acid beverage, Japan	Shimomura <i>et al.</i> , 2005
<i>C. soldanellicola</i>	DSM 17072 ^T	Roots of sand-dune plants, Korea	Park <i>et al.</i> , 2006
<i>C. soli</i>	DSM 19298 ^T	Soil samples, Jeju, Korea	Weon <i>et al.</i> , 2008
<i>C. vrystaatense</i>	LMG 22846 ^T	Raw Chicken, RSA	De Beer <i>et al.</i> , 2005
<i>C. novum</i>	FH2	freshwater creek, Fox Hollow, PA USA	LycoMicro 2011
<i>C. novum</i>	JM1	Jazzman's Café Milk cafe	LycoMicro 2011
<i>E. diehli</i>	FH1	freshwater creek, Fox Hollow, PA USA	LycoMicro 2011
<i>E. lactis</i>	DSM 1922 ^T	raw cow's milk, Israel	Shakéd <i>et al.</i> , 2010
<i>E. tenax</i>	DSM 16811 ^T	epilithon-covered stones from the River Taff, UK	O'Sullivan <i>et al.</i> , 2006
<i>F. granuli</i>	DSM 19729 ^T	anaerobic granules used in the wastewater treatment plant of beer-brewing factory in Kwang-Ju, Republic of Korea	Aslam <i>et al.</i> , 2005
<i>F. frigidimaris</i>	EED	freshwater creek, Loyalsock Creek, PA USA	LycoMicro 2012
<i>F. frigidimaris</i>	JRR	freshwater creek, Loyalsock Creek, PA USA	LycoMicro 2012
<i>F. frigidimaris</i>	KMA	freshwater creek, Loyalsock Creek, PA USA	LycoMicro 2013
<i>F. novum</i>	KJJ	freshwater creek, Loyalsock Creek, PA USA	LycoMicro 2012
<i>F. novum</i>	R30-53	freshwater creek, Larry's Creek, PA USA	LycoMicro 2012

Appendix 2. Species, HPLC Datafile and Method for each figure.

Figure	Species	HPLC Datafile	HPLC Method*
Figure 2.2A	<i>C. oranimense</i>	Coranimense8.D	Flex8.M
Figure 2.2B	<i>C. oranimense</i>	Coranimense8_4A_9.D	Flex9Frac.M
Figure 2.2C	<i>C. oranimense</i>	Coranimense8_4A_10.D	Flex10Frac.M
Figure 2.2D	<i>C. oranimense</i>	Coranimense8_4A_11.D	Flex11Frac.M
Figure 2.2E	<i>C. oranimense</i>	Coranimense8_4A_12.D	Flex12Frac.M
Figure 2.3A	<i>C. oranimense</i>	Coranimense_4A_18B.D	Flex18Frac.M
Figure 2.3B	<i>C. oranimense</i>	Coranimense8_4A_15.D	Flex15Frac.M
Figure 2.3C	<i>C. oranimense</i>	Coranimense_4A_17B.D	Flex17Frac.M
Figure 2.3D	<i>C. oranimense</i>	Coranimense_4A_14B.D	Flex14Frac.M
Figure 2.3E	<i>C. oranimense</i>	Coranimense_4A_16C.D	Flex16Frac.M
Figure 2.4A	<i>C. oranimense</i>	Coranimense_4A_20.D	Flex20Frac.M
Figure 2.4B	<i>C. oranimense</i>	Coranimense_4A_19.D	Flex19Frac.M
Figure 2.5A	<i>C. oranimense</i>	Coranimense_4A_16K.D	Flex16Frac.M
Figure 2.4C	<i>C. oranimense</i>	Coranimense_4A_16_G10.D	Flex16Frac.M
Figure 2.8A	<i>C. oranimense</i>	Coranimense_4A_16K.D	Flex16Frac.M
Figure 2.8B	<i>C. oranimense</i>	Coranimense_16_0013	Flex16Frac.M
Figure 2.9A	<i>C. oranimense</i>	Coranimense_101312_seq_01	Flex16Frac50_6.M
Figure 2.9B	<i>C. oranimense</i>	Coranimense_101312_seq_02	Flex16Frac50_6.M
Figure 2.9C	<i>C. oranimense</i>	Coranimense_101312_seq_03	Flex16Frac50_6.M
Figure 2.10A	<i>C. oranimense</i>	Coranimense_101812_seq_08	Flex16FracSP2_100ul.M
Figure 2.11A	<i>C. oranimense</i>	Coranimense_101812_seq_09	Flex16FracSP2_100ul.M
Figure 2.11B	<i>C. oranimense</i>	Coranimense_111912_seq_25	Flex16FracSP2_100ul.M
Figure 2.12A	Congo Red	Coranimense_122012_indv_2	Flex16FracSP5_5_100ul.M
Figure 2.12B	Congo Red	Coranimense_122012_indv_2	Flex16FracSP5_5_100ul.M
Figure 2.12C	Red Pepper	Coranimense_122012_indv_3	Flex16FracSP5_5_100ul.M
Figure 2.12D	Red Pepper	Coranimense_122012_indv_3	Flex16FracSP5_5_100ul.M
Figure 2.12E	Alizrin Red	Coranimense_122012_indv_4	Flex16FracSP5_5_100ul.M
Figure 2.12F	Alizrin Red	Coranimense_122012_indv_4	Flex16FracSP5_5_100ul.M
Figure 2.13A	<i>C. oranimense</i>	Coranimense_020413_seq_01	Flex16FracSP3_4_100ul.M
Figure 2.13B	<i>C. oranimense</i>	Coranimense_020413_seq_02	Flex16FracSP3_4_100ul.M
Figure 2.13C	<i>C. oranimense</i>	Coranimense_020413_seq_03	Flex16FracSP3_4_100ul.M
Figure 2.13D	<i>C. oranimense</i>	Coranimense_020413_seq_04	Flex16FracSP3_5_100ul.M
Figure 2.13E	<i>C. oranimense</i>	Coranimense_020513_indv_2	Flex16FracSP3_6_100ul.M
Figure 2.14A	<i>C. oranimense</i>	Coranimense_020513_indv_2	Flex16FracSP3_6_100ul.M
Figure 2.14B	<i>C. oranimense</i>	Coranimense_020513_indv_3	Flex16FracSP3_3_100ul.M
Figure 2.14C	<i>C. oranimense</i>	Coranimense_020513_indv_3	Flex16FracSP3_3_100ul.M

Figure 2.14D	<i>C. oranimense</i>	Coranimense_020513_indv_3	Flex16FracSP3_3_100ul.M
Figure 2.14E	<i>C. oranimense</i>	Coranimense_020513_indv_4	Flex16FracSP3_3_100ul.M
Figure 2.14F	<i>C. oranimense</i>	Coranimense_020513_indv_4	Flex16FracSP3_3_100ul.M
Figure 2.14G	<i>C. oranimense</i>	Coranimense_020513_indv_4	Flex16FracSP3_3_100ul.M
Figure 2.15A	<i>C. oranimense</i>	Coranimense_020513_seq_01	Flex16FracSP3_3_100ul.M
Figure 2.15B	<i>C. oranimense</i>	Coranimense_020513_seq_01	Flex16FracSP3_3_100ul.M
Figure 2.15C	<i>C. oranimense</i>	Coranimense_020513_seq_02	Flex16FracSP3_3_100ul.M
Figure 2.15D	<i>C. oranimense</i>	Coranimense_020513_seq_02	Flex16FracSP3_3_100ul.M
Figure 2.16A	<i>C. oranimense</i>	Coranimense_021612_indv_10	Flex16FracSP3_3_100ul.M
Figure 2.16B	<i>C. oranimense</i>	Coranimense_021612_indv_1	Flex16FracSP3_3_100ul_30.M
Figure 2.16C	<i>C. oranimense</i>	Coranimense_021712_indv_2	Flex16FracSP3_3_100ul_10.M
Figure 2.17A	<i>C. oranimense</i>	Coranimense_021912_indv_1	Flex16FracSP3_3_100ul_10.M
Figure 2.17B	<i>C. oranimense</i>	Coranimense_021912_indv_6	Flex16FracSP3_3_100ul_10_AC2.M
Figure 2.17C	<i>C. oranimense</i>	Coranimense_021912_indv_7	Flex16FracSP3_3_100ul_10_AC2.M
Figure 2.17D	<i>C. oranimense</i>	Coranimense_021912_indv_8	Flex16FracSP3_3_100ul_10_AC2.M
Figure 2.18A	<i>C. oranimense</i>	Coranimense_022013_indv_3	Flex16FracSP3_3_100ul.M
Figure 2.18B	<i>C. oranimense</i>	Coranimense_022013_indv_5	Flex16FracSP3_12_100ul.M
Figure 2.18C	<i>C. oranimense</i>	Coranimense_022013_indv_6	Flex16FracSP3_18_100ul_60C.M
Figure 2.18D	<i>C. oranimense</i>	Coranimense_022013_indv_7	Flex16FracSP3_19_100ul_60C.M
Figure 2.18E	<i>C. oranimense</i>	Coranimense_022013_indv_8	Flex16FracSP3_20_100ul_60C.M
Figure 2.19A	<i>C. oranimense</i>	Coranimense_022513_indv_2	Flex16FracSP3_3_100ul_2-PO4.M
Figure 2.19B	<i>C. oranimense</i>	Coranimense_022513_indv_3	Flex16FracSP3_3_100ul_2-PO4.M
Figure 2.19C	<i>C. oranimense</i>	Coranimense_022513_indv_5	Flex16FracSP3_3_100ul_2-PO4.M
Figure 2.19D	<i>C. oranimense</i>	Coranimense_022513_indv_7	Flex16FracSP3_3_100ul_4-PO4.M
Figure 2.19E	<i>C. oranimense</i>	Coranimense_022513_indv_7	Flex16FracSP3_3_100ul_4-PO4.M
Figure 2.20A	<i>C. oranimense</i>	Coranimense_031912_indv_4	Flex16FracSP3_3_100ul.M
Figure 2.20B	<i>C. oranimense</i>	Coranimense_032012_indv_2	Flex16FracSP3_3_100ul.M
Figure 2.21A	<i>C. oranimense</i>	Coranimense_032213_indv_2	Flex18FracSP3_3_100ul.M
Figure 2.21B	<i>C. oranimense</i>	Coranimense_032213_indv_4	Flex19FracSP3_3_100ul.M
Figure 2.21C	<i>C. oranimense</i>	Coranimense_032413_indv_1	Flex20FracSP3_3_100ul.M
Figure 2.21D	<i>C. oranimense</i>	Coranimense_032513_indv_1	Flex21FracSP3_3_100ul.M
Figure 2.21E	<i>C. oranimense</i>	Coranimense_032513_indv_2	Flex22FracSP3_3_100ul.M
Figure 2.22A	<i>C. oranimense</i>	Coranimense_032513_indv_4	Flex25FracSP3_3_100ul.M
Figure 2.22B	<i>C. oranimense</i>	Coranimense_032513_indv_5	Flex26FracSP3_3_100ul.M
Figure 2.22C	<i>C. oranimense</i>	Coranimense_032513_indv_7	Flex27FracSP3_3_100ul.M
Figure 2.2D	<i>C. oranimense</i>	Coranimense_032513_indv_8	Flex27FracSP3_3_30ul.M
Figure 2.22E	<i>C. oranimense</i>	Coranimense_032513_indv_9	Flex28FracSP3_3_30ul.M
Figure 2.23A	<i>C. oranimense</i>	Coranimense_032713_indv_4	Flex29FracFixSP3_3_100ul.M
Figure 3.1A	<i>C. oranimense</i>	Coranimense_032713_indv_4	Flex29FracFixSP3_3_100ul.M

Figure 3.2A	<i>C. oranimense</i>	Coranimense_032713_indv_4	Flex29FracFixSP3_3_100ul.M
Figure 3.2B	<i>C. oranimense</i>	Coranimense_032713_indv_5	Flex29FracFixSP3_3_100ul.M
Figure 3.2C	<i>C. oranimense</i>	Coranimense_032713_indv_6	Flex29FracFixSP3_3_100ul.M
Figure 3.2D	<i>C. oranimense</i>	Coranimense_032713_indv_7	Flex29FracFixSP3_3_100ul.M
Figure 3.2E	<i>C. oranimense</i>	Coranimense_032713_indv_8	Flex29FracFixSP3_3_100ul.M
Figure 3.3A	<i>C. oranimense</i>	Coranimense_032713_indv_9	Flex29FracFixSP3_3_100ul.M
Figure 3.3B	<i>C. oranimense</i>	Coranimense_032713_indv_10	Flex29FracFixSP3_3_100ul.M
Figure 3.3C	<i>C. oranimense</i>	Coranimense_032713_indv_11	Flex29FracFixSP3_3_100ul.M
Figure 3.3D	<i>C. oranimense</i>	Coranimense_040313_indv_2	Flex29FracFixSP3_3_100ul.M
Figure 3.3E	<i>C. oranimense</i>	Coranimense_040313_indv_3	Flex29FracFixSP3_3_100ul.M
Figure 3.4A	<i>C. oranimense</i>	Coranimense_040813_indv_1	Flex29FracFixSP3_3_100ul.M
Figure 3.4B	<i>C. oranimense</i>	Coranimense_040813_indv_2	Flex29FracFixSP3_3_100ul.M
Figure 3.4C	<i>C. oranimense</i>	Coranimense_040813_indv_3	Flex29FracFixSP3_3_100ul.M
Figure 3.6	<i>C. oranimense</i>	Coanimense_041913_indv_14	Flex27FracSP3_3_30ul_short4_M
Figure 4.2A	<i>C. oranimense</i>	Coranimense_033013_indv_1.D	Flex_small species runs_1ul.M
Figure 4.2B	<i>C. oranimense</i>	Coranimense_033013_indv_3.D	Flex_small species runs_3_1ul.M
Figure 4.2C	<i>C. oranimense</i>	Coranimense_033113_indv_1.D	Flex29species_runs_3_100ul.M
Figure 4.3A	<i>C. oranimense</i>	Coranimense_033113_indv_2.D	Flex29species_runs_4_1ul.M
Figure 4.3B	<i>C. oranimense</i>	Coranimense_033113_indv_3.D	Flex29species_runs_4_1ul.M
Figure 4.3C	<i>C. oranimense</i>	Coranimense_033113_indv_4.D	Flex29species_runs_6_1ul.M
Figure 4.3D	<i>C. oranimense</i>	Coranimense_033113_indv_5.D	Flex29species_runs_7_1ul.M
Figure 4.4A	<i>C. luteum</i>	25Speciesrun_09.D	Flex29species_runs_4_1ul.M
Figure 4.4B	<i>C. luteum</i> (380-600 nm)	25Speciesrun_09.D	Flex29species_runs_4_1ul.M
Figure 4.4C	<i>C. shig</i>	25Speciesrun_01.D	Flex29species_runs_4_1ul.M
Figure 4.5A	<i>C. vrystaatense</i>	25Speciesrun_08.D	Flex29species_runs_4_1ul.M
Figure 4.5B	<i>C. novum</i> JMI	25Speciesrun_10.D	Flex29species_runs_4_1ul.M
Figure 4.5C	<i>C. angstadi</i>	25Speciesrun_15.D	Flex29species_runs_4_1ul.M
Figure 4.6A	<i>C. oranimense</i>	Coranimense_033113_indv_2.D	Flex29species_runs_4_1ul.M
Figure 4.6B	<i>C. diehli</i> BLS98	25Speciesrun_06.D	Flex29species_runs_4_1ul.M
Figure 4.6C	<i>C. diehli</i> BLS98 (380-600 nm)	25Speciesrun_06.D	Flex29species_runs_4_1ul.M
Figure 4.7A	<i>C. jejuense</i>	25Speciesrun_16.D	Flex29species_runs_4_1ul.M
Figure 4.7B	<i>C. joostei</i>	25Speciesrun_07.D	Flex29species_runs_4_1ul.M
Figure 4.7C	<i>C. novum</i> NRRL B-14798	25Speciesrun_04.D	Flex29species_runs_4_1ul.M
Figure 4.8A	<i>C. piperi</i>	25Speciesrun_14.D	Flex29species_runs_4_1ul.M
Figure 4.8B	<i>C. soli</i>	25Speciesrun_02.D	Flex29species_runs_4_1ul.M
Figure 4.8C	<i>C. soli</i> (380-600 nm)	25Speciesrun_02.D	Flex29species_runs_4_1ul.M
Figure 4.9A	<i>C. aquaticum</i>	25Speciesrun_13.D	Flex29species_runs_4_1ul.M

Figure 4.9B	<i>C. greenlandense</i>	25Speciesrun_03.D	Flex29species_runs_4_1ul.M
Figure 4.9C	<i>C. novum</i> FH2	25Speciesrun_12.D	Flex29species_runs_4_1ul.M
Figure 4.9D	<i>C. soldanellicola</i>	25Speciesrun_19.D	Flex29species_runs_4_1ul.M
Figure 4.10A	<i>E. tenax</i>	25Speciesrun_17.D	Flex29species_runs_4_1ul.M
Figure 4.10B	<i>E. lactis</i>	25Speciesrun_20.D	Flex29species_runs_4_1ul.M
Figure 4.10C	<i>E. diehli</i> FM1	25Speciesrun_18.D	Flex29species_runs_4_1ul.M
Figure 4.11A	<i>F. frigidimaris</i> JRR	25Speciesrun_21.D	Flex29species_runs_4_1ul.M
Figure 4.11B	<i>F. frigidimaris</i> EED	25Speciesrun_22.D	Flex29species_runs_4_1ul.M
Figure 4.11C	<i>F. frigidimaris</i> KMA	25Speciesrun_23.D	Flex29species_runs_4_1ul.M
Figure 4.12A	<i>F. granuli</i>	25Speciesrun_11.D	Flex29species_runs_4_1ul.M
Figure 4.12B	<i>F. novum</i> KJJ	25Speciesrun_05.D	Flex29species_runs_4_1ul.M
Figure 4.12C	<i>F. novum</i> R30-53	Fnovum_R30-53_040313_indv1	Flex29species_runs_4_1ul.M
Figure 4.13A	<i>C. luteum</i>	25Speciesrun_09.D	Flex29species_runs_4_1ul.M
Figure 4.13B	<i>C. shig</i>	25Speciesrun_01.D	Flex29species_runs_4_1ul.M
Figure 4.13C	<i>C. vrystaatense</i>	25Speciesrun_08.D	Flex29species_runs_4_1ul.M
Figure 4.13D	<i>C. novum</i> JMI	25Speciesrun_10.D	Flex29species_runs_4_1ul.M
Figure 4.13E	<i>C. angstadtii</i>	25Speciesrun_15.D	Flex29species_runs_4_1ul.M
Figure 4.13F	<i>C. oranimense</i>	Coranimense_033113_indv_2.D	Flex29species_runs_4_1ul.M
Figure 4.13G	<i>C. diehli</i> BLS98	25Speciesrun_06.D	Flex29species_runs_4_1ul.M
Figure 4.13H	<i>C. jejuense</i>	25Speciesrun_16.D	Flex29species_runs_4_1ul.M
Figure 4.14A	<i>C. joostei</i>	25Speciesrun_07.D	Flex29species_runs_4_1ul.M
Figure 4.14B	<i>C. novum</i> NRRL B-14798	25Speciesrun_04.D	Flex29species_runs_4_1ul.M
Figure 4.14C	<i>C. piperi</i>	25Speciesrun_14.D	Flex29species_runs_4_1ul.M
Figure 4.14D	<i>C. soli</i>	25Speciesrun_02.D	Flex29species_runs_4_1ul.M
Figure 4.14E	<i>C. aquaticum</i>	25Speciesrun_13.D	Flex29species_runs_4_1ul.M
Figure 4.14F	<i>C. greenlandense</i>	25Speciesrun_03.D	Flex29species_runs_4_1ul.M
Figure 4.14G	<i>C. novum</i> FH2	25Speciesrun_12.D	Flex29species_runs_4_1ul.M
Figure 4.14H	<i>C. soldanellicola</i>	25Speciesrun_19.D	Flex29species_runs_4_1ul.M
Figure 4.15A	<i>E. tenax</i>	25Speciesrun_17.D	Flex29species_runs_4_1ul.M
Figure 4.15B	<i>E. lactis</i>	25Speciesrun_20.D	Flex29species_runs_4_1ul.M
Figure 4.15C	<i>E. diehli</i> FM1	25Speciesrun_18.D	Flex29species_runs_4_1ul.M
Figure 4.16A	<i>F. frigidimaris</i> JRR	25Speciesrun_21.D	Flex29species_runs_4_1ul.M
Figure 4.16B	<i>F. frigidimaris</i> EED	25Speciesrun_22.D	Flex29species_runs_4_1ul.M
Figure 4.16C	<i>F. frigidimaris</i> KMA	25Speciesrun_23.D	Flex29species_runs_4_1ul.M
Figure 4.16D	<i>F. granuli</i>	25Speciesrun_11.D	Flex29species_runs_4_1ul.M
Figure 4.16E	<i>F. novum</i> KJJ	25Speciesrun_05.D	Flex29species_runs_4_1ul.M
Figure 4.16F	<i>F. novum</i> R30-53	Fnovum_R30-53_040313_indv1	Flex29species_runs_4_1ul.M

References

1. Achenbach, H., Bottger-Vetter, A., Fautz, E., and Reichenbach, H. (1982). On the Origin of the Branched Alkyl Substituents on Ring B of Flexirubin-Type Pigments. *Arch. Microbiol.* 132: 241-244.
2. Agilent ZORBAX Column Selection Guide for HPLC. Copyright 2007, Agilent Technologies, Inc.
3. Archenbach, H. (1987). The Pigments of the Flexirubin-Type. A Novel Class of Natural Products. *Chem. Org. Naturst.* 52: 73-111.
4. Archenbach, H., and Kohl, W. (1978). Investigations of the Pigments from *Cytophaga johnsonae* Cyl. *Arch. Microbiol.* 117: 253-257.
5. Asolkar, R., Jensen, P., Kauffman, C., and Fenical, W. (2006). Daryamides A-C, Weakly Cytotoxic Polyketides from a Marine-Derived Actinomycete of the Genus *Streptomyces* Strain CNQ-085. *J. Nat. Prod.* 69: 1756-1759.
6. Aslam, Z., Im, W.-T., Kim, M.K., and Lee, S.-T. (2005). *Flavobacterium granuli* sp. nov., isolated from granules used in a wastewater treatment plant. *IJSEM* 55: 747-751.
7. Aziz, R.K., Bartels, D., Best, A.A., DeJongh, M., Disz, T., Edwards, R.A., Formosa, K., Gerdes, S., Glass, E.M., Kubal, M., Meyer, F., Olsen, G.J., Olson, R., Osterman, A.L., Overbeek, R.A., McNeil, L.K., Paarmann, D., Paczian, T., Parrello, B., Pusch, G.D., Reich, C., Stevens, R., Vassieva, O., Vonstein, V., Wilke, A., and Zagnitko, O. (2008). The RAST Server: rapid annotations using subsystems technology. *BMC Genomics* 9:75. doi: [10.1186/1471-2164-9-75](https://doi.org/10.1186/1471-2164-9-75).
8. Behrendt, U., Ulrich, A., Spröer, C. and Schumann, P. (2007). *Chryseobacterium luteum* sp. nov., associated with the phyllosphere of grasses. *IJSEM* 57: 1881-1885.
9. Bendorf, H. Personal Communication, Concerning bathochromic shift reaction induced by KOH. 12 Sept. 2012.
10. Bernardet, J.F., Segers, P., Vancanneyt, M., Berthe, F., Kersters, K., and Vandamme, P. (1996). Cutting a Gordian Knot: Emended Classification and Description of the Genus *Flavobacterium*, Emended Description of the Family *Flavobacteriaceae*, and Proposal of *Flavobacterium hydatis* nom. nov. (Basonym, *Cytophaga aquatilis* Strohl and Tait 1978). *IJSEM* 46(1): 128-148.
11. Brand-Williams, W., Cuvelier, M.E., and Berset, C. (1995). Use of a Free Radical Method to Evaluate Antioxidant Activity. *Lebensm.-Wiss. U. – Technol.* 28: 25-30.
12. Collins, K., Krebs, J., Kirk, K., Smith, K., Duncan, T., Failor, K.C., and Newman, J. (2011). Characterization of Novel bacterial Species Identified by Undergraduate Students in a General Microbiology Course. Poster presented at the 2011 American Society for Microbiology (ASM) Annual Meeting, New Orleans, LA.
13. Chevion, S., Roberts, M.A., and Chevion, M. (2000). The use of cyclic voltammetry for the evaluation of antioxidant capacity. *Free Radical Bio. Med.* 28(6): 860-870.
14. De Beer, H., Hugo, C.J., Jooste, P.J., Willems, A., Vancanneyt, M., Coenye, T., and Vandamme, P.A.R. (2005). *Chryseobacterium vrystaatense* sp. nov., isolated from raw chicken in a chicken-processing plant. *IJSEM* 55: 2149-2153.
15. Dimberg, L.H., Theander, O., and Lingnert, H. (1993). Avenanthramides – A Group of Phenolic Antioxidants in Oats. *Cereal Chem.* 70(6): 637-641.

16. Emam, A.E., Mohamed, M.A., Diab, Y.M., and Megally, N.Y. (2010). Isolation and structure elucidation of antioxidant compounds from leaves of *Laurus nobilis* and *Emex spinosus*. *Drug Discov. Ther.* 4(3): 202-207.
17. Fautz, E., and Reichenbach, H. (1979). Biosynthesis of Flexirubin: Incorporation of Precursors by the Bacterium *Flexibacter elegans*. *Phytochemistry* 18: 957-959.
18. Fautz, E., and Reichenbach, H. (1980). A Simple Test For Flexirubin-Type Pigments. *FEMS Microbiology Letters* 8:87-91.
19. Gruszecki, W.I. and Strzalka, K. (2005). Carotenoids as modulators of lipid membrane physical properties. *Biochim Et Biophysica Acta* 1740: 108-115.
20. Hantsis-Zacharov, E., Shakéd, T., Senderovich, Y., and Halpern, M. (2008). *Chryseobacterium oranimense* sp. nov., a psychrotolerant, proteolytic and lipolytic bacterium isolated from raw cow's milk. *IJSEM* 58: 2635-2639.
21. Holmes, B., Owen, R.J., Steigerwalt, A.G., and Brenner, D.J. (1984). *Flavobacterium gleum*, a new species found in human clinical specimens. *Int. J. of Syst. Bacteriol.* 34(1): 21-25.
22. Housecraft, C.E., and Sharpe, A.G. Experimental Techniques In *Inorganic Chemistry*, 4th ed., Pearson, 2012; pp. 88-89.
23. Huber, U., and Majors, R.E. Principles in preparative HPLC: A Primer. Copyright 2007, Agilent Technologies, Inc.
24. Hugo, C.J., Segers, P., Hoste, B., Vancanneyt, M., and Kersters, K. (2003). *Chryseobacterium joostei* sp. nov., isolated from the dairy environment. *IJSEM* 53: 771-777.
25. Irschik, H., and Reichenbach, H. (1978). Intracellular Location of Flexirubins in *Flexibacter elegans* (Cytophagales). *Biochimica et Biophysica Acta* 510: 1-10.
26. Johansson, F., Olbe, M., Sommarin, M., and Larsson, C. (1995). Brij 58, a polyoxyethylene acyl ether, creates membrane vesicles of uniform sidedness. A new tool to obtain inside-out (cytoplasmic side-out) plasma membrane vesicles. *Plant J.* 7(1):165-173.
27. Kiemle, D.J.; Silverstein, R.M.; Webster, F.X. Proton NMR Spectrometry In *Spectrometric Identification of Organic Compounds*, 7th ed., John Wiley, Hoboken, NJ, 2005; pp 127-176.
28. Kim, K.K., Lee, K.C., Oh, H.-M. and Lee, J.-S. (2008). *Chryseobacterium aquaticum* sp. nov., isolated from a water reservoir. *IJSEM* 58: 533-537.
29. Kozubek, A. (1987). The Effect of 5-(n-Alk(enyl)resorcinols on Membranes. I. Characterization of the Permeability Increase Induced by 5-(n-Heptadecenyl)resorcinol. *Acta Biochim. Pol.* 34(4): 357-367.
30. Krebs, J., Sampsell, D., McDonald, C., and Newman, J. (2012). Purification and Molecular Structure Determination of Flexirubins from Chryseobacteria. Poster presented at the 2012 Undergraduate Research Symposium in the Chemical and Biological Sciences, University of Maryland, Baltimore County, Baltimore, MD.
31. Krebs, J., Gale, A., and Newman, J. (2013). Purification of Flexirubin Pigments from *Chryseobacterium*. Oral Presentation presented at the 2013 Pennsylvania Academy of Science (PAS) meeting, University of Pittsburgh-Bradford, Bradford, PA.
32. Lee, H., Kang, S., Kwon, K., Lee, J.-H., and Kim, S.-J. (2011). Genome Sequence of the Algicidal Bacterium *Kordia algicida* OT-1. *Journal of Bacteriol.* 198(15): 4031-4032.

33. Liu, L., Zubik, L., Collins, F.W., Marko, M., and Meydani, M. (2004). The antiatherogenic potential of oat phenolic compounds. *Atherosclerosis* 175: 39-49.
34. Loveland-Curtze, J., Miteva, V., and Brenchley, J. (2010). Novel ultramicrobacterial isolates from a deep Greenland ice core represent a proposed new species, *Chryseobacterium greenlandense* sp. nov. *Extremophiles* 14(1): 61-69.
35. Mahler, C. 2011-2012 Physical Chem. Lab. Manual. pp. 71-74.
36. Mattila, P., Pihlava, J.-M., and Hellstrom, J. (2005). Contents of Phenolic Acids, Alkyl- and Alkenylresorcinols, and Avenanthramides in Commercial Grain Products. *J. Agric. Food. Chem.* 53: 8290-8295.
37. McBride, M., Xie, G., Martens, E., Lapidus, A., Henrissat, B., Rhodes, R., Goltsman, E., Wang, W., Xu, J., Hunnicutt, D., Staroscik, A., Hoover, T., Cheng, Y., and Stein, J. (2009). Novel Features of the Polysaccharide-Digesting Gliding Bacterium *Flavobacterium johnsoniae* as Revealed by Genome Sequence Analysis. *App. and Env. Microbiol.* 75(21): 6864-6875.
38. McDonald, C. Personal Communication, Concerning sample requirements for NMR. May. 2012.
39. McDonald, C. Spectroscopy and Molecular Structure Class. Spring 2012.
40. Miyagawa, H., Ishihara, A., Nishimoto, T., Ueno, T., and Mayama, S. (1995). Induction of Avenanthramides in Oat Leaves Inoculated with Crown Rust Fungus, *Puccinia coronata* f. sp. *avenae*. *Biosci. Biotech. Biochem.* 59(12): 2305-2306.
41. Mojib, N., Philpott, R., Huang, J., Niederweis, M., and Bej, A. (2010). Antimycobacterial activity in vitro of pigment isolated from Antarctic Bacteria. *Antonie van Leewenhoek* 98: 531-540.
42. Nowak-Thompson, B., Hammer, P., Hill, D., Stafford, J., Torkewitz, N., Gaffney, T., Lam, S., Molnar, I., and Ligon, J. (2003). 2,5-Dialkylresorcinol Biosynthesis in *Pseudomonas aurantiaca*: Novel Head-to Head condensation of Two Fatty Acid-Derived Precursors. *Journal of Bacteriol.* 185(3):860-869.
43. O'Sullivan, L.A., Rinna, J., Humphreys, G., Weightman, A.J., and Fry, J.C. (2006). Culturable phylogenetic diversity of the phylum 'Bacteroidetes' from river epilithon and coastal water and description of novel members of the family *Flavobacteriaceae*: *Epilithonimonas tenax* gen. nov., sp. nov. and *Persicivirga xylanidelens* gen. nov., sp. nov. *IJSEM* 56: 169-180.
44. Park, M.S., Jung, S.R., Lee, K.H., Lee, M.-S., Do, J.O., Kim S.B., and Bae, K.S. (2006). *Chryseobacterium soldanellicola* sp. nov. and *Chryseobacterium taeanense* sp. nov., isolated from roots of sand-dune plants. *IJSEM* 56: 433-438.
45. Rasband, W.S. ImageJ, U. S. National Institutes of Health, Bethesda, Maryland, USA, <http://imagej.nih.gov/ij/>, 1997-2012.
46. Reichenbach, H., Kleinig, H., and Archenbach, H. (1974). The Pigments of *Flexibacter elegans*: Novel and Chemosystematically Useful Compounds. *Arch. Microbiol.* 101: 131-144.
47. Reichenbach, H., Kohl, W., Bottger-Vetter, A., and Archenbach, H. (1980). Flexirubin-Type Pigments in *Flavobacterium*. *Arch Microbiol.* 126:291-293.
48. Ridgway, H.F., Wagner, R.M., Dawsey, W.T., and Lewin, R.A. (1975). Fine structure of the cell envelope layers of *Flexibacter polymorphus*. *Can J. Microbiol.* 21: 1733-1750.

49. Samappito, S., Page, J.E., Schmidt, J., De-Eknamkul, W., and Kutchan, T.M. (2003). Aromatic and pyrone polyketides synthesized by a stilbene synthase from *Rheum tataricum*. *Phytochemistry*. 62: 313-323.
50. Scientific Instruments and Consumables. Varian, Inc. Scientific Instruments. Accessed Feb 2013. <http://pdf.directindustry.com/pdf/agilent-technologies-life-sciences-and-chemical/scientific-instruments-and-consumables/32598-159226-_166.html>.
51. Shakéd, T., Hantsis-Zacharov, E., and Halpern, M. (2010). *Epilithonimonas lactis* sp. nov., isolated from raw cow's milk. *IJSEM* 60: 675-679.
52. Shimomura, K., Kaji, K., and Hiraishi, A. (2005). *Chryseobacterium shigense* sp. nov., a yellow pigmented, aerobic bacterium isolated from a lactic acid beverage. *IJSEM* 55: 1903-1906.
53. Spranger, I., Sun, B., Mateus, A.M., Freitas, V.d., Ricardo-da-Silva, J.M. (2008). Chemical characterization and antioxidant activities of oligomeric and polymeric procyanidin fraction from grape seeds. *Food Chem.* 108: 519-532.
54. Strahan, B. (2008). "Analysis of the Continually Diversifying Microbial Community in a Wastewater Sequencing Batch Reactor". Honors Thesis, Spring 2008, Biology Dept., Lycoming College.
55. Strahan, B.L., Failor, K.C., Batties, A.M., Hayes, P.S., Cicconi, K.M., Mason, C.T., and Newman, J.D. (2011). *Chryseobacterium piperi* sp. nov., isolated from a freshwater creek. *IJSEM* 61: 2162-2166.
56. Tamura, K., Peterson, D., Peterson, N., Stecher, G., Nei, M., and Kumar, S. (2011). MEGA5: Molecular Evolutionary Genetics Analysis using Maximum Likelihood, Evolutionary Distance, and Maximum Parsimony Methods. *Mol. Biol. Evol.* 28: 2731-2739.
57. Tindall, B.J., Rosselló-Móra, R., Busse, H.J., Ludwig, W., and Kampf, P. (2010). Notes on the characterization of prokaryote strains for taxonomic purposes. *IJSEM*. 60(1): 249-266.
58. Weon, H.-Y., Kim, B.-Y., Yoo, S.-H., Kwon, S.-W., Stackebrandt, E., and Go, S.-J. (2008). *Chryseobacterium soli* sp. nov. and *Chryseobacterium jejuense* sp. nov., isolated from soil samples from Jeju, Korea. *IJSEM* 58: 470-473.
59. Zophel, A., Kennedy, M., Beinert, H., and Kroneck, P (1991). Investigations on microbial sulfur respiration: Isolation, purification, and characterization of cellular components from *Spirillum* 5175. *Eur. J. Biochem.* 195: 849-856.